EmBIOSysTech
Environmental BIOlogical Systems Technology,
Laboratory of Environmental Biotechnology

University of Cyprus
Faculty of Engineering
Department of Civil and
Environmental Engineering

Microbially Induced Calcium Carbonate Precipitation for Stone Heritage Consolidation

May 2024

Master of Science Thesis (MSc) in

Environmental Engineering

Panagiotis Persianis

Abstract

Microbially induced calcium carbonate precipitation (MICP) is a promising technology for the conservation of natural building and decorative stone. Thus, the initial objective of the project was to identify new strains suitable for the bio-consolidation of heritage buildings in Cyprus, which are significantly impacted by stone decay primarily driven by biochemical and physical factors. The project is divided into three main phases: Identification, Evaluation, and Optimization.

In the Identification phase, 11 different bacterial strains were isolated from marine sediments originating from two distinct areas in Cyprus. These strains were initially assessed for urease activity since urea hydrolysis was identified in the literature review as the most likely pathway to precipitate $CaCO_3$ crystals for consolidation. Concurrently, evaluation of calcium carbonate solubilization was performed to ensure that the strains do not contribute to stone decay. All tested strains showed no solubilization while *Arthrobacter crystallopoietes* DSM 20117 showed the highest urease activity. Subsequently, after identifying the strains and establishing microbial growth curves, the precipitant with calcium carbonate precipitation (CCP) medium was collected. The highest $CaCO_3$ amount produced was 2286 mg/L by *A. crystallopoietes* DSM 20117. The precipitated $CaCO_3$ of *A. crystallopoietes* DSM 20117, *Bacillus licheniformis* PP1 and *Micrococcus* sp. DSM 105846 was analyzed using X-Ray Diffraction (XRD) for product identification, purity assessment, and validation of its effectiveness. The results showed that *A. crystallopoietes* DSM 20117, *B. licheniformis* and *Micrococcus* sp. produce mainly calcite, vaterite and hydroxyapatite, respectively. Scanning Electron Microscopy (SEM) revealed the difference in the precipitation formed by *A. crystallopoietes* DSM 20117 and *B. licheniformis*, where the former produced sharp crystals identified as calcite and the second produced sphere crystals identified as vaterite.

Following these tests, the strain of *A. crystallopoietes* DSM 20117 using CCP medium was selected for the Evaluation phase. During this phase, the selected strain was applied to building stones (Lympia, LYM and Gerolakkos, GER) *in-vitro* to assess the consolidation treatment. The conducted tests included: Karsten tube and contact angle tests to evaluate water absorption and surface hydrophobicity, respectively; Drilling

Resistance Measurements (DRMS) followed by Scratch tests on the stone surface to assess compressive strength and the depth of biological treatment; and SEM analysis to observe the effect of the product on the stone microstructure. Water absorption was lower in the treated area of LYM and GER, compared to the control area. Drilling resistance was higher in treated GER, compared to the control area, whereas in LYM treated area it was higher close to the surface (up to 500 μm), compared to the control area. However, it is noteworthy to mention that the high porosity and large grain size of GER might have affected the results of the treatment.

Subsequently, the Optimization phase involved testing the growth of *A. crystallopoietes* DSM 20117 (L1), *A. crystallopoietes* P21 (P3) and *Micrococcus* sp. DSM 105846 (P4) in four different media: B4, B4+Urea, Yeast Extract (YE)+Urea, and YE+Ammonium sulfate, followed by biological treatment of the LYM and GER stones using these strains.

In B4 medium, *A. crystallopoietes* DSM 20117 produced a substantial amount of weddellite, although the specific pathway remains unknown. Although, *A. crystallopoietes* P-21 (P3) did not yield high crystal amounts in CCP medium, it showed significant calcite production of 2645 mg/L in B4 medium. Similarly to *A. crystallopoietes* P-21 (P3), *Micrococcus* sp. 105846 DSM (P4) did not yield high crystal amounts in CCP medium, but in B4 + Urea, it exhibited distinct crystals of vaterite and hydroxyapatite.

In the optimization biological treatment, *A. crystallopoietes* DSM 20117 and P-21 grew with B4 medium, while *Micrococcus* sp. 105846 DSM (P4) grew in B4 + Urea. *A. crystallopoietes* P-21 (P3) proved the most effective, reducing water absorption rates from 0.227 ml/min to 0.007 ml/min for LYM stone and from 2.37 ml/min to 0.33 ml/min for GER stone. Moreover, in the DRMS test, the area treated with *A. crystallopoietes* DSM 20117 (L1) demonstrated superior effectiveness compared to the treatment with the other strains. Cost analysis underlined that production of calcite by *A. crystallopoietes* DSM 20117 is the most cost effective.

The overall results demonstrated the potential of *A. crystallopoietes* DSM 20117 and P-21 to be used as alternative environmental-friendly means for the conservation of architectural stone heritage. At the same time, the aforementioned strains show significant potential for application in other fields, such as in the bioremediation and

self-healing of concrete, due to their high urease activity, and production of calcite and vaterite, when the appropriate medium is used.

Περίληψη

Η μικροβιακά επαγόμενη καταβύθιση ανθρακικού ασβεστίου (MICP) είναι μια πολλά υποσχόμενη τεχνολογία για την προστασία του δομικού και διακοσμητικού λίθου. Επομένως, ο αρχικός στόχος του έργου ήταν ο εντοπισμός νέων στελεχών, κατάλληλων για τη βιοσυσσωμάτωση κτιρίων πολιτιστικής κληρονομιάς στην Κύπρο, τα οποία επηρεάζονται σημαντικά από τη φθορά της πέτρας που οφείλεται κυρίως σε βιοχημικούς και φυσικούς παράγοντες. Το έργο χωρίζεται σε τρεις κύριες φάσεις: ταυτοποίηση, αξιολόγηση και βελτιστοποίηση.

Στη φάση της Ταυτοποίησης, απομονώθηκαν 11 διαφορετικά βακτηριακά στελέχη από θαλάσσια ιζήματα που προέρχονταν από δύο διαφορετικές περιοχές της Κύπρου. Τα στελέχη αυτά αξιολογήθηκαν αρχικά ως προς τη δραστικότητα ουρεάσης, καθώς η υδρόλυση της ουρίας προσδιορίστηκε στη βιβλιογραφική ανασκόπηση ως η πιο πιθανή οδός για την καταβύθιση κρυστάλλων $CaCO_3$ για σταθεροποίηση. Ταυτόχρονα, πραγματοποιήθηκε αξιολόγηση της διαλυτοποίησης του ανθρακικού ασβεστίου για να διασφαλιστεί ότι τα στελέχη δεν συμβάλλουν στην αποσάθρωση των λίθων. Όλα τα στελέχη που εξετάστηκαν δεν παρουσίασαν διαλυτοποίηση, ενώ το *A. crystallopoietes* DSM 20117 παρουσίασε την υψηλότερη δραστικότητα ουρεάσης. Στη συνέχεια, αφού ταυτοποιήθηκαν τα στελέχη και καταρτίστηκαν καμπύλες μικροβιακής ανάπτυξης, συλλέχθηκε το κατακρημνιστικό με μέσο καταβύθισης ανθρακικού ασβεστίου (CCP). Η υψηλότερη ποσότητα $CaCO_3$ που παρήχθη ήταν 2286 mg/L από το *A. crystallopoietes* DSM 20117. Το κατακρημνισμένο $CaCO_3$ των *A. crystallopoietes* DSM 20117, *B. licheniformis* PP1 και *Micrococcus* sp. DSM 105846 αναλύθηκε με τη χρήση περίθλασης ακτίνων Χ (XRD) για την ταυτοποίηση του προϊόντος, την αξιολόγηση της καθαρότητας και την επικύρωση της αποτελεσματικότητάς του. Τα αποτελέσματα έδειξαν ότι οι *A. crystallopoietes* DSM 20117, *B. licheniformis* και *Micrococcus* sp. παράγουν κυρίως ασβεστίτη, βατερίτη και υδροξυαπατίτη, αντίστοιχα. Η ηλεκτρονική μικροσκοπία σάρωσης (SEM) αποκάλυψε τη διαφορά στο ίζημα που σχηματίζεται από το *A. crystallopoietes* DSM 20117 και το *B. licheniformis*, όπου το πρώτο παρήγαγε αιχμηρούς κρυστάλλους που αναγνωρίστηκαν ως ασβεστίτης και το δεύτερο σφαιρικούς κρυστάλλους που αναγνωρίστηκαν ως βατερίτης.

Μετά από τις δοκιμές, επιλέχθηκε το στέλεχος *A. crystallopoietes* DSM 20117 που μεγάλωνε σε μέσο CCP για τη φάση Αξιολόγησης. Κατά τη διάρκεια αυτής της φάσης, το επιλεγμένο στέλεχος εφαρμόστηκε σε οικοδομικούς λίθους (Πέτρα Λυμπιών, LYM και Γερολάκκου, GER) *σε συνθήκες εργαστηρίου* για την αξιολόγηση της επεξεργασίας σταθεροποίησης. Οι δοκιμές που διεξήχθησαν περιλάμβαναν: Δοκιμές σωλήνα Karsten και γωνίας επαφής για την αξιολόγηση της απορρόφησης νερού και της επιφανειακής υδροφοβικότητας, μέτρηση της αντίστασης σε διάτρηση (DRMS), ακολουθούμενη από δοκιμή χαραγής στην επιφάνεια του λίθου για την αξιολόγηση της θλιπτικής αντοχής και του βάθους της βιολογικής επεξεργασίας και ανάλυση SEM για την παρατήρηση της επίδρασης του προϊόντος στη μικροδομή του λίθου. Η απορρόφηση νερού ήταν χαμηλότερη στην επεξεργασμένη περιοχή του LYM και του GER, σε σύγκριση με την περιοχή ελέγχου. Η αντοχή στη διάτρηση ήταν υψηλότερη στην επεξεργασμένη περιοχή GER, σε σύγκριση με την περιοχή ελέγχου, ενώ στην περιοχή LYM που υποβλήθηκε σε επεξεργασία ήταν υψηλότερη κοντά στην επιφάνεια (έως 500 μm), σε σύγκριση με την περιοχή ελέγχου. Ωστόσο, αξίζει να αναφερθεί ότι το ψηλό πορώδες και οι μεγάλοι σε μέγεθος κόκκοι της πέτρας GER μπορεί να επηρέασαν τα αποτελέσματα της επεξεργασίας

Στη συνέχεια, η φάση Βελτιστοποίησης περιελάμβανε τη δοκιμή της ανάπτυξης των *A. crystallopoietes* DSM 20117 (L1), *A. crystallopoietes* P21 (P3) και *Micrococcus* sp. DSM 105846 (P4) σε τέσσερα διαφορετικά μέσα. Ακολούθησε βιολογική επεξεργασία των λίθων LYM και GER με τη χρήση αυτών των στελεχών.

Στο μέσο B4, το *A. crystallopoietes* DSM 20117 παρήγαγε σημαντική ποσότητα weddellite, αν και η συγκεκριμένη μεταβολική οδός παραμένει άγνωστη. Το *A. crystallopoietes* P-21 (P3) δεν παρήγαγε μεγάλες ποσότητες κρυστάλλων σε μέσο CCP, αλλά παρουσίασε σημαντική παραγωγή ασβεστίτη 2645 mg/L σε μέσο B4. Ομοίως με το *A. crystallopoietes* P-21 (P3), το *Micrococcus* sp. 105846 DSM (P4) δεν παρήγαγε υψηλές ποσότητες κρυστάλλων σε μέσο CCP, αλλά σε μέσο B4 + Urea, παρουσίασε διακριτούς κρυστάλλους βατερίτη και υδροξυαπατίτη.

Στη βελτιστοποιημένη επεξεργασία, τα *A. crystallopoietes* DSM 20117 και P-21 αναπτύχθηκαν με μέσο B4, ενώ το *Micrococcus* sp. 105846 DSM (P4) αναπτύχθηκε σε B4 + ουρία. Το *A. crystallopoietes* P-21 (P3) αποδείχθηκε πιο αποτελεσματικό,

μειώνοντας τους ρυθμούς απορρόφησης νερού από 0,227 ml/min σε 0,007 ml/min για τον λίθο LYM και από 2,37 ml/min σε 0,33 ml/min για τον λίθο GER. Επιπλέον, στη δοκιμή DRMS, η περιοχή που υποβλήθηκε σε επεξεργασία με το *A. crystallopoietes* DSM 20117 (L1) επέδειξε ανώτερη αποτελεσματικότητα σε σύγκριση με την επεξεργασία με τα άλλα στελέχη. Η ανάλυση κόστους υπογράμμισε ότι η παραγωγή ασβεστίτη από το *A. crystallopoietes* DSM 20117 είναι η πιο οικονομική.

Τα συνολικά αποτελέσματα κατέδειξαν τη δυνατότητα των *A. crystallopoietes* DSM 20117 και P-21 να χρησιμοποιηθούν ως εναλλακτικά φιλικά προς το περιβάλλον μέσα για τη διατήρηση της αρχιτεκτονικής κληρονομιάς από πέτρα. Παράλληλα, τα προαναφερθέντα στελέχη παρουσιάζουν σημαντικές δυνατότητες εφαρμογής σε άλλους τομείς, όπως στη βιοεξυγίανση και την αυτό-ίαση του σκυροδέματος, λόγω της υψηλής δραστικότητας ουρεάσης, και της παραγωγής ασβεστίτη και βατερίτη όταν χρησιμοποιείται το κατάλληλο μέσο.

Table of Contents

Chapter 1: Literature review

1.1 Introduction

Recently, the international community has recognized the need to protect and safeguard the world's cultural and architectural heritage, as one of the targets of the United Nations Sustainable Development Goals (SDG 11.4). Many of the most important cultural heritage monuments worldwide are built with carbonated stones. Most of them are facing permanent damage, thus leading to considerable loss of historical authenticity and cultural importance. Carbonate stones are subject to weathering due to several physicochemical and biological factors [1]. These frequently lead to calcite leaching, because of the induction of a progressive mineral matrix dissolution, which increases the stone's porosity, decreases its mechanical strength, and accelerates deterioration [2]. Particularly, organic and inorganic atmospheric pollutants can cause acid rain-mediated mineral dissolution and sulfate crust development, which together with salt crystallization and freeze-thaw damage, are among the major causes of stone deterioration.

Biologically-based and microbially induced calcium carbonate ($CaCO_3$) precipitation (MICP) is an eco-friendly method for the sustainable protection of carbonate stone monuments [3–5]. Moreover, MICP is an evolving technique with applications in various other industries, such as in the remediation of heavy metals from polluted soils and waters [6–8], soil strengthening and sand consolidation [9–11], microbial enhanced oil recovery (MEOR) [12–14], carbon dioxide sequestration [15–17] and concrete self-healing [18,19].

MICP is governed mainly by the concentration of non-precipitated calcium, total inorganic carbon, pH, and the availability of nucleation sites for $CaCO_3$ formation [20–22]. It occurs naturally in marine water, freshwater, soils, aquifers, caves, and hypersaline habitats [23]. Depending on the surrounding conditions, microorganisms follow different metabolic pathways producing $CaCO_3$. Such pathways are photosynthesis, ureolysis, ammonification, denitrification, sulfate reduction, anaerobic sulfate oxidation, and methane oxidation [22–24].

In the construction industry, the bio-deposition of $CaCO_3$ can cope with deficiencies associated with construction materials by forming calcite crystals and enhancing the

cementation of both natural and composite materials. Concrete, for example, is susceptible to cracking, thus providing easy access to water, chlorides and other aggressive elements to its matrix [26]. MICP can act as a barrier against the penetration of these substances, hence increasing the material's lifespan. Furthermore, reports have shown that carbonatogenic bacteria can successfully protect archeological and historical sites and structures from erosion [27,28]. Different species of bacteria have been tested for the consolidation of stone, including *Bacillus* spp, *Myxococcus* spp, *Sporosarcina* spp [31–33]. *Myxococcus xanthus* is an abundant gram-negative, non-pathogenic aerobic soil bacterium. It can precipitate $CaCO_3$ and other substances to protect and consolidate stone. *Sporosarcina pasteurii*, formerly referred to as *Bacillus pasteurii*, is the most frequently used microorganism for MICP due to high urease activity [34,35].

MICP treatment for the consolidation of stone and other building materials has been applied in various ways, such as brushing, immersion, spraying and injection [32]. Liu et al. studied the repetitive brushing of *B. pasteurii* DSM 33 to create an anti-erosion layer over clay samples left in steady-state conditions at 30 ◦C for 7 days [36], showing promising results. Rodriguez-Navaro et al. [33] presented the potential of MICP by *M. xanthus* species to protect and consolidate porous ornaments, through immersion of the samples in growth media containing the microorganism, under shaking and static conditions. Immersion was also applied to black crust samples in growth media containing *Bacillus* and *Micrococcus* species, for 15 days under steady-state conditions [3].

1.2 Biomineralization

Biomineralization is the process where living organisms convert elements from their local environment into minerals. Minerals can offer (1) physical and chemical protection; (2) provide nutrients to support microbial growth and metabolism, including (a) bio-essential elements and (b) trace metals; (3) provide energy to support microbial growth by serving as (a) electron acceptors/donors, and (b) electrical conductors to facilitate extracellular electron transfer (EET) [37].

One fundamental role of minerals is to offer physical protection to microbes. Fractures, fissures and pores within minerals protect microbes from harsh conditions, such as UV

irradiation, physical abrasion, and thermal fluctuation. These protective functions of minerals are essential to microbial survival in extreme environments, such as deserts, where ecosystems are almost entirely composed of microbial communities in chasmolithic (crevices on rock surfaces), hypolithic (underneath rocks), and endolithic (inside cracks and fissures of rocks) habitats [38,39]. Likewise, minerals, such as skeletal biominerals, offer support and protection to organisms. Skeletal biominerals are separated in three principal classes:(1) calcium carbonates, (2) silica, and (3) calcium phosphates [37]. Calcium carbonate is the most abundant and widespread biogenic mineral, and it is composed of six different structures: calcite, aragonite, vaterite, calcium carbonate monohydrate, calcium carbonate hexahydrate, and amorphous calcium carbonate [29]. The molluscan shells are an example of a fully controlled biomineralization process. The shells are usually in the form of calcite and aragonite, in which calcium carbonate accounts for 95 to 99% per weight. Bird eggshells also consist mainly of calcium carbonate; hen eggshells contain about 95% calcium carbonate [40]. Minerals also offer chemical protection by creating specific micro-environments to favor certain microbial populations by colonizing on alkaline or acidic habitats of mineral surfaces. For example, in serpentinizing peridotite, the mineral surface pH becomes alkaline, and alkaliphilic microorganisms thrive in these habitats. In contrast, the oxidation of metal sulfides creates acidic pH, where acidophilic microbes flourish. Certain minerals with a pH buffering capacity, such as carbonates, can harbor neutrophilic sulfur-oxidizing microorganisms, because acidity created by sulfur oxidation can be neutralized by carbonate minerals [41]. Minerals and rocks not only provide protection to microbes, but also supply nutrients to support their metabolism. A common strategy for microorganisms to extract bio-essential elements from minerals and rocks is through the production of metabolites to enhance mineral dissolution.

During dissolution, a passive layer may form at the surface of a mineral to slow down the rate of dissolution [37]; this layer may be beneficial to the microbes due to less depletion of bio-essential elements by a chemical process such as fluid transport. The importance of minerals as a nutrient source is evidenced by their impact on microbial community structure and functions. Laboratory and field studies show that microbial communities vary in relation to the elemental composition of minerals, especially Fe and P [42]. Other elements, including Na, Si, Mn, S, Mg, Ca and K, are also important.

Furthermore, through redox reactions of elements, especially Fe, S, and Mn, minerals serve the vital role of supplying energy to bacteria. Redox-active minerals can aid in the growth of microorganisms by acting as an electron source or sink, an electrical conductor to enable extracellular electron transfer, an environmental battery photocatalyst to promote photosynthesis, and more [43]. Microbial populations are able to use the energy released during Fe redox reactions because Fe-containing minerals are so common in the environment. Both Fe(III)-reducing heterotrophs and Fe(II)-oxidizing autotrophs are among these microorganisms [43]. Sulfur redox reactions can also provide energy to microbes. Energy can be produced by certain bacteria by the oxidation of sulfide minerals and the reduction of sulfate minerals [44]. Despite the abundance of Mn-bearing minerals and Mn(II)-oxidizing microbes in nature, most biological Mn oxidation does not produce much energy, unlike Fe and S [45]. Similar to this, only a small number of scientists found cell proliferation, when Mn(IV) served as the lone electron acceptor [45]. Some metal sulfides and oxides have long been recognized as electrical conductors that aid in electron transport. Numerous minerals containing iron facilitate the passage of electrons between microorganisms of the same or different species [46]. For instance, by serving as a conduit between methanogen and Fe(III)-reducing species, iron sulfides, magnetite, and hematite all display the ability to enhance methanogenesis. Similar findings have been observed in investigations where the presence of these minerals causes syntropy between Fe-reducing bacteria and nitrate- or sulfate-reducing bacteria. For some microbes that are unable to use sunlight directly, light-sensitive and semi-conductive minerals can use sunlight as an energy source to transfer electrons to these microbes for energy acquisition. Thus, some non-phototrophic microbes can obtain energy from the photoelectrons generated by solar irradiation of semi-conductive metal sulfides and oxides. These examples highlight a wide range of strategies that microbes employ to harness energy from minerals.

1.3 Metabolic Pathways / Enzymes used for MICP

During Earth's history, precipitation of calcium carbonate by heterotrophic microbes has substantially contributed to the genesis of copious amounts of carbonate sediment and its subsequent lithification [74]. The formation and burial of carbonate-bearing rocks is by far the most important mechanism for carbon removal and storage on Earth. Carbonate deposits account for about one-sixth of the global sedimentary rocks,

representing a major fraction of the global carbon storage. A significant fraction of this carbonate stock is of microbial origin. To date, a number of microbial metabolic processes, such as photosynthesis and redox reactions using nitrogen and sulfur compounds, have been identified as potentially controlling the formation of microbial carbonate minerals. Microbial sulfate reduction is suspected to be largely responsible for the formation of authigenic carbonate minerals in marine sediments and stromatolites, acting as an alkalinity driver. Metabolic activities, such as sulfate reduction, iron reduction, urea hydrolysis, denitrification, methane oxidation and photosynthesis, are known to promote microbially induced calcium carbonate ($CaCO_3$) precipitation (MICP) [75]. Boquet et al. [76] stated that $CaCO_3$ precipitation is a common as well as a circumstantial behavior in the bacterial world, where most of the bacteria are able to precipitate $CaCO_3$ under proper conditions. For MICP, bacteria create substantial alkaline pH conditions and produce dissolved inorganic carbon. Furthermore, bacterial cells act as ideal nucleation sites for formation of $CaCO_3$ crystals.

1.4 Ammonification

Bacterial ammonification plays a critical role in the cycling of nitrogen through ecosystems and it is important for maintaining soil fertility and water quality. It is the process by which bacteria break down organic nitrogen compounds, such as amino acids and nucleotides, into ammonium (NH_4^+) ions. This process is typically carried out by a diverse group of bacteria known as ammonifiers or ammonifying bacteria, which are widely distributed in soils and aquatic environments. The process of bacterial ammonification involves several steps showed in **Error! Reference source not found.**. First, the organic nitrogen compounds are taken up by the bacteria and hydrolyzed into their constituent amino acids and nucleotides. Next, the amino acids are deaminated, a process that removes the amino group (NH_2) from the amino acid molecule and releases ammonia (NH_3) as a byproduct together with carbon dioxide (CO_2) and water (H_2O). This ammonia can then be further protonated to form ammonium ions (NH_4^+) and hydroxide (OH^-). Hydroxide then reacts with carbon dioxide creating bicarbonate

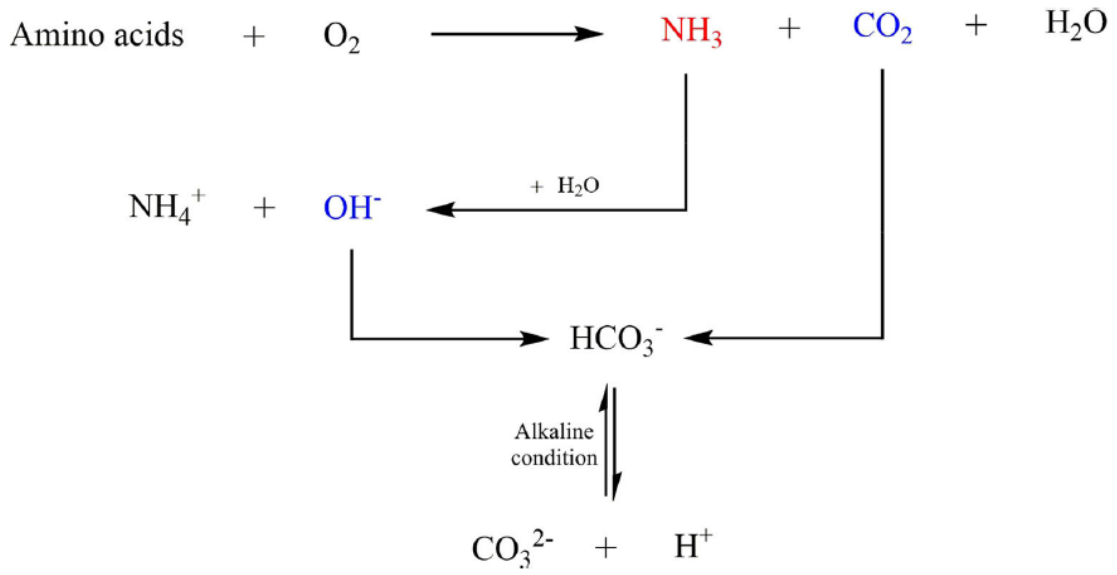

Figure 1: Metabolic pathway of bacterial ammonification.

(HCO_3^-), which, together with an alkaline micro-environment around the cell formed by the ammonium are in favor of calcium carbonate precipitation [47].

Amino acids formed by the hydrolysis of proteins, peptides, and certain amides, may participate further in a variety of reactions, including transamination, decarboxylation (to form amines), racemization and deamination. Oxidative deamination of amino acids, catalyzed by amino acid dehydrogenases or amino acid oxidases to yield a-OXO acids and NH_4^+. The nature of these reactions is indicated in Figure 2, respectively [47].

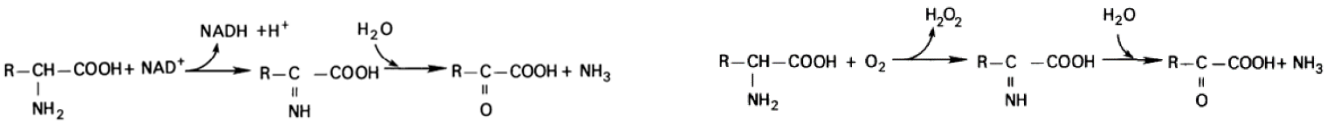

Figure 2: Dehydrogenases and amino acid oxidases.

Both reaction mechanisms involve an initial oxidation of the amino acid and the formation of an imino acid as intermediate. Dehydrogenases utilize nicotinamide-adenine dinucleotide (NAD^+) as an H-accepting coenzyme, whereas the amino acid oxidases are flavoproteins, in which flavinadenine dinucleotide (FAD) is reduced initially and then reoxidized directly by O_2, with the formation of H_2O_2. Dehydrogenases, active essentially towards specific amino acids only, have been purified from plant, animal, and microbial sources. In addition, an L-amino acid dehydrogenase of broader specificity acting on aliphatic amino acids has been

characterized. The equilibria of the reactions catalyzed by amino acid dehydrogenases strongly favor production of amino acids from the respective a-OXO acids and reduced NAD [48].

1.5 Denitrification

Various bacteria can induce calcium carbonate precipitation by producing dissolved inorganic carbon (DIC) through their metabolism in environment that has available nucleation sites, suitable pH, and sufficient supply of dissolved calcium. Dissimilatory nitrate reduction to dinitrogen gas, named denitrification, is one of these MICP processes [49]. Denitrification consists of four sequential reduction steps from nitrate

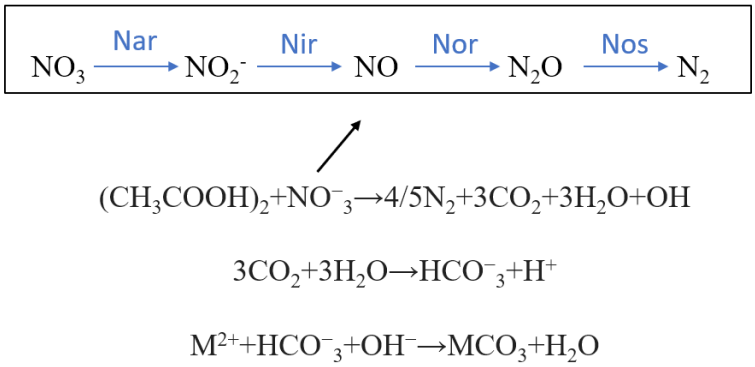

Figure 3: Denitrification Pathway.

as shown in reactions (1) and (2) (Figure 3): (NO_3^-) to (di)nitrogen gas (N_2) through nitrite (NO_2^-), nitric oxide (NO), nitrous oxide (N_2O). In the first reaction each step in the metabolic pathway is carried out by a different enzyme [51]: Nar nitrate reductases are membrane-bound enzymes in which the catalytic subunit faces the cytoplasm and catalyzes the reduction of nitrate into nitrite for energy production [52]. Nitrite reductase (NiR) is a stromal enzyme that catalyses a six-electron step reduction of nitrite to ammonium using reduced Fd as electron donor. The holoenzyme is encoded by a single gene clustered with other nitrate assimilation genes [53]. Nitric oxide reductase (Nor) enzyme catalyzes the reduction of nitric oxide (NO) to nitrous oxide (N_2O). (Nor) also participates in nitrogen metabolism and in the microbial defense against nitric oxide toxicity [55].

M^{2+} indicates the cation present and MCO_3 is the carbonate biomineral formed. Different polymorphs of calcium carbonate (calcite, vaterite, and aragonite) are forming throughout the MICP process, and also some other biominerals such as dolomite

($CaMg(CO_3)_2$), magnesite ($MgCO_3$), strontianite ($SrCO_3$), rhodochrosite (Mn, Fe, Mg) [54].

Denitrification has significant potential for consolidation improvement through biogenic gas production and MICP. However, the demonstrated reaction rate of this process is low compared with urea hydrolysis [56,57]. Also, too much nitrate may lead to the accumulation of intermediate compounds, which can be toxic for the bacteria and inhibit growth [58], or increased emissions of nitrous oxide, which is a dangerous greenhouse gas (GHG) [59,60].

1.6 Dissimilatory Sulfate Reduction

Sulfate reduction in conjunction with sulfur disproportionation may be an early evolved microbial metabolism, providing that biological fractionation of sulfur isotopes started around 3.5 billion years ago [62], and it remains an important energy metabolism for anaerobic life [63]. Sulfate reduction is also a primary driver in the carbon cycle, and it is responsible for a large part of the organic carbon flux to CO_2 in marine sedimentary environments [64] and in wetlands [65]. It happens through sulfate-reducing bacteria that produce bicarbonate ions and hydrogen sulfide under anoxic and anaerobic conditions.

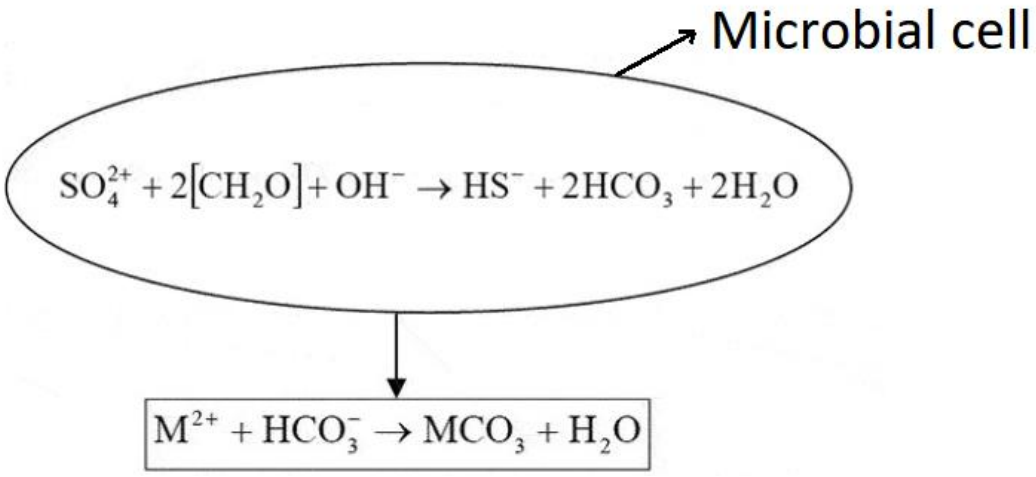

Figure 4:Dissimilatory Sulfate Reduction Pathway

The generation of carbonate ions assists carbonate biomineral formation, and it largely depends on the behavior of hydrogen sulfide since it affects the pH of the environment. The degassing of H_2S and oxidation of sulfide to sulfur by anoxygenic sulfide phototrophic bacteria raises the pH in the system and subsequently favors biomineral formation [61]. On the other hand, H_2S can be oxidized to sulfate ions and produces

sulfuric acid by autotrophic aerobic sulfide-oxidizing bacteria. Sulfuric acid decreases the pH and inhibits biomineral precipitation. The biomineralization or MICP via the sulfur cycle is not possible for engineering applications because relentless maintenance of the anaerobic condition is inefficient. Also, the odorous hydrogen sulfide gas is highly toxic to the environment.

The microbial pathway for dissimilatory sulfate reduction involves the initial reduction of sulfate to sulfite by a combination of sulfate adenylyltransferase (Sat) and adenylyl-sulfate reductase (AprBA) followed by reduction of sulfite by sulfite reductases. Sulfite reductases express the rate-limiting steps in the global sulfur cycle [65] and confer bacteria and archaea the ability to grow via reduction of sulfite, and can function in reverse in some organisms that disproportionate or oxidize elemental sulfur [66,67,68]. Four different groups of sulfite reductases function in dissimilatory sulfur metabolism. Of these, siroheme-dependent dissimilatory sulfite reductase (dsr), siroheme-dependent anaerobic sulfite reductase (asr), and octaheme cytochrome c sulfite reductase (MccA) catalyze the reduction of sulfite to sulfide, while reverse dissimilatory sulfite reductase genes (rdsr) are involved in sulfur oxidation. All of these sulfite reductases, except for mccA, constitute an ancient lineage of enzymes that may predate the separation of Bacteria and Archaea [69].

The taxonomic distribution of dissimilatory sulfite reductases has been considered to be restricted to organisms from selected bacterial and archaeal phyla [70]. Only organisms from nine microbial phylum-level lineages, namely Deltaproteobacteria, Firmicutes, Thermodesulfobacteria, Actinobacteria, Nitrospirae, Caldiserica, Euryarchaeota, Crenarcheota, and Aigarchaeota are known to possess the genetic capacity to reduce sulfite to sulfide using the *dsr* system. The asr enzymes have a far more limited distribution and are known to be present only in organisms from four phylum-level lineages, Gammaproteobacteria, Firmicutes, Spirochaetes, and Fusobacteria. The distribution of MccA enzymes is restricted to organisms from Epsilonproteobacteria [71] and Gammaproteobacteria [72]. Finally, the Rdsr enzyme complex for sulfur oxidation is associated with organisms from five phylum-level lineages including Alphaproteobacteria, Betaproteobacteria, Gammaproteobacteria, Deltaproteobacteria, and Chlorobi. This diversification of sulfite reductases was likely driven by speciation and functional divergence, and to a lesser extent, lateral gene transfer (LGT) [73].

1.7 Photosynthesis

Cyanobacteria are among the most important organisms on Earth, both evolutionarily and ecologically. They are ultimately responsible for the oxygenation of the atmosphere [77] and the consequent evolution of the Earth's lithosphere. Thus, cyanobacteria are the only organisms that use the water molecule, H_2O, as an electron donor for photosynthesis; they are now responsible for fixing most of the inorganic carbon that enters the biosphere, and cyanobacterial plankton is responsible for much of the biological productivity in the oceans [78].

In the photosynthetic cycle, the alkalinity across the microbial cell increases during the exchange of HCO^{3-}/OH^{-} ions. Here, the microbes utilize gaseous or dissolved CO_2 to form organic matter via photosynthesis. Simultaneously, bicarbonate is converted into CO_2 and OH^{-}, eventually forming a carbonate mineral [79]. The photosynthetic microbes that are mainly responsible for carbonate mineral precipitations are cyanobacteria, purple photosynthetic bacteria, and microalgae. Nearly 70% of carbonate rocks on earth were formed due to cyanobacteria. Different forms of carbonate minerals were found in diverse environments, such as freshwater, marine water, hot springs, and terrestrial areas, in which most are formed via the microbial photosynthesis process [80]. However, applying this process for engineering or building material application is still a question because of the need for constant sunlight and inorganic carbon during photosynthesis and carbonate biomineral precipitation [81].

Compared to most other calcifying organisms, cyanobacterial calcification is only

Equation 1

$$2HCO^{-}_3 + Ca^{2+} \longrightarrow CaCO_3 + CO_2 + H_2O$$

weakly controlled by an organic substrate and the precipitated $CaCO_3$ generally has a low level of organization [82]. No intracellular structures have been found that store the precursors to mineralization in cyanobacteria and precipitation is exclusively extracellular. In this regard, photosynthetic fixation of CO_2 from a bicarbonate solution will result in an increase in carbonate ions: (equation 1)

thereby locally increasing the carbonate concentration. Photosynthetic activity may thus lead to pH increases as high as 9.5 or more around the cells in marine

cyanobacterial mats and the resulting increase in carbonate alkalinity may directly or indirectly drive carbonate. Calcification reduces the depletion of dissolved molecular CO_2 around the cells, and buffers against a large rise in pH.

HCO^-_3 results mainly by carbonic anhydrase action. Carbonic anhydrase, an enzyme that catalyzes the reversible hydration of CO_2, is a major protein component of most photosynthetic microorganisms and higher plant tissues. Once thought to be represented in plants by a single enzyme type, it is now apparent that DNA sequences and/or the encoded proteins for the evolutionarily distinct α, β, and γ forms of carbonic anhydrase are present in cyanobacteria, green algae, and higher plants. While exhibiting a wide range in structure, localization, and regulation of expression, some progress has been made in the establishment of roles for these various enzyme forms. The primary role of many of the α and β isoforms is the establishment of inorganic carbon species equilibration. As a result of this activity, enzymes or transport systems which require either CO_2 or HCO^-_3 are not limited by the slow, uncatalyzed rate of CO_2/HCO^-_3 interconversion [83].

1.8 Urea hydrolysis

Urea hydrolysis is one of the most efficient ways to induce MICP and the most widespread one for applications in geotechnical and structural engineering. A series of reactions in urea hydrolysis are driven by urease and carbonic anhydrase enzymes [84]. Based on the following chemical equation, ammonium and carbonate ions are produced: (equation 2)

Equation 2

$$CO(NH_2)_2 + 2H_2O \rightarrow 2NH_4^+ + CO_3^{-2}$$

The aforementioned reaction raises the alkalinity of the solution and the concentration of dissolved inorganic carbon (DIC), thereby increasing the concentration of CO_3^{2-}. $CaCO_3$ precipitates into a solid form in the presence of Ca^{2+} [85], as follows (equation 3):

Equation 3

$$Ca_2^+ + CO_3^{2-} \rightarrow CaCO_3$$

Urease and carbonic anhydrase (CA) are key enzymes in the chemical reaction of living organisms and have been found to be associated with calcification in a number of microorganisms and invertebrates. Urease is a kind of amidohydrolases and leads to production of CO_2 and ammonia [86]. Urease is widely distributed in nature, the predominant sources of urease in rhizosphere are plants, fungi, and bacteria.

Urea, the substrate for urease, is a remarkably stable molecule. Its halflife for spontaneous degradation in water is 3.6 years at 38 ^oC and the products are ammonia and cyanic acid (equation 4):

Equation 4

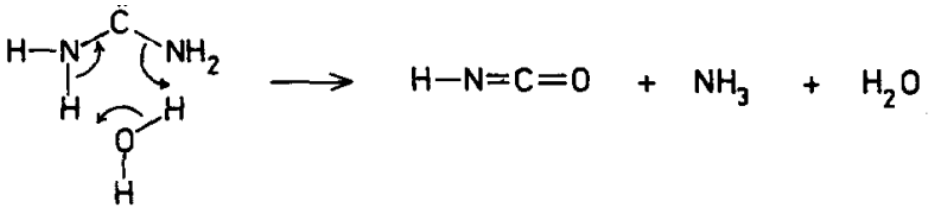

In contrast, urease catalyzes the hydrolysis of urea to form carbamate ion (equation 5):

At pH 7.0 and 38 ^oC, the urease-catalyzed hydrolysis of urea must be at least 10^{14} times as fast as the spontaneous hydrolysis which has never been observed [87].

Equation 5

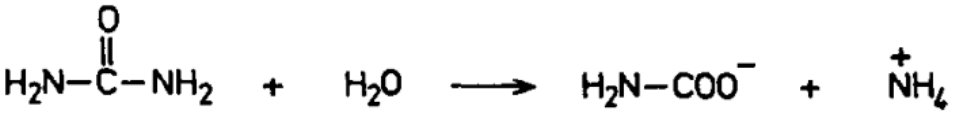

The common urease is a macromolecule composed of three of the above trimers with a three-dimensional structure of curved edges and triangles found the presence of Ni ion in urease macromolecules plays a key role in catalyzing urea decomposition. An amino acid sequence in UreC (residues 308 to 327: TVDELDMLMVMVCHLDPSIP) is highly conserved for each urease detected to-date. It is believed to be located within the enzyme's active site, where histidine residues play a catalytic role by coordinating Ni^{2+} ions. Four auxiliary proteins (UreD, UreE, UreF, and UreG) are involved in the catalytic hydrolysis of urea. UreD may be important for urease supplementation. Significant homo-polymeric associations exist between these helper proteins, while the role of other concentrated helper proteins is under investigation [90].

Urea hydrolysis is the most easily controlled of the carbonate generating reactions, with the potential to produce high concentrations of carbonate within a short time. But there

is another enzyme named carbonic anhydrase whose role is not significantly defined with respect to calcite precipitation. Carbonic anhydrase (CA) is a zinc containing enzyme that facilitates the interconversion of CO_2 and HCO_3^- [88] (equation 6).

Equation 6

$$H_2O + CO_2 \rightarrow HCO_3^-$$

CAs have a wide distribution and participate in all physiological processes that deal with CO_2 and HCO_3 handling, such as cellular pH regulation, and acid and ion transport. Carbonic anhydrase is ubiquitously distributed in organisms and is fundamental to many eukaryotic biological processes such as photosynthesis, respiration, CO_2 and ion transport, calcification and acid base balance [89]. Research on the role of biological CA in calcification or biomineralization is now focusing on biological calcification in marine invertebrates (mollusks) or biomineralization of fish otolith. Although ubiquitous in highly evolved organisms from the eukarya domain, the enzyme carbonic anhydrase has received scant attention in prokaryotes from the bacteria and archaea domains and has been purified from only five species since it was first identified in *Nisseria sicca* [89]. Recent evidence suggests that CA is widespread in metabolically diverse species from bacteria and archaea domain indicating that the enzyme has a more extensive and fundamental role in the prokaryotic physiology than previously recognized.

The six main steps of MICP driven by urea hydrolysis are: First, urease excreted by bacteria catalyses the hydrolysis of urea into ammonia and carbamic acid. The latter spontaneously hydrolyses to produce carbon dioxide and additional ammonia. The carbon dioxide equilibrates with water into carbonic acid, bicarbonate ions and carbonate ions in a pH-dependent manner. The ammonia also equilibrates with water, forming ammonium and hydroxide ions, which increases the pH of the environment and shifts the bicarbonate equilibrium into the formation of excessive carbonate ions. In the presence of a soluble calcium source, $CaCO_3$ precipitation is favoured in the created alkaline environment.

In addition to providing urease, another observed role of bacteria is acting as nucleation sites for crystallization. This has been attributed to the high surface-to-volume ratio of the bacterial cell and the functional groups (e.g., carboxyl, phosphate and amine) on the

cell surface. These functional groups enable the cell to be negatively charged, prompting the attachment of calcium ions and thereby favouring crystal nucleation.

1.9 MICP Applications

1.9.1 Soil Stabilization

The performance of foundation of civil engineering structures lies in the soil. The presence of hydrophilic and reactive minerals, such as kaolinite, montmorillonite, and illite make the soil expansive and sternly impacts its performance due to high upward swelling pressures, causing differential movements that affect the lightweight structures constructed over it. This can cause various damages, such as cracks in the walls of the building, lifting of structure, damage to basement, uneven settlement. Thus, geotechnical engineers and practitioners are intensively seeking to create sustainable ground improvement strategies to mitigate the adverse effect of expansive soils. Problematic soil covers almost one-fifth of the total area of India and the United States and can also be found in several other countries [91]. Approximately $ 7–9 billion per year in economic losses have been reported in the United States alone [92].

Mechanical stabilization involves densifying the mass of the soil by expelling air voids, whereas physical stabilization uses reinforcing bars, fibers, strips, grids, and sheets to achieve more strength and reduce soil settlement [93]. On the contrary, chemical stabilization depends mainly on inducing reactions between the soil particles and the applied stabilizer, such as portland cement, asphalt, fly ash, lime, slag, xanthan gum, and many others [94]. Traditional methods employed to address soil complications have proven to have several disadvantages. Among these, single performance, high energy consumption, and secondary pollution were evidenced [95]. In the same context, [96] it was reported that although cement utilization has led to recognizable engineering development, it is well known that its production is energy-consuming and is regrettably responsible for releasing greenhouse gases such as carbon dioxide (about 5% of global emissions). On the other hand, chemicals used as grouts and stabilizers are often cost-prohibitive and require many digging wells for injecting large volumes, thus rendering the treatment unfeasible. These chemicals may also hinder natural groundwater flow and impact the environmental balance due to the presence of toxic compounds, such as polyurethanes, silicates, acrylamides, phenoplasts, epoxy, and lignosulfonates [97]. The inevitable demand for novel techniques that can improve soil

stabilization with a minimal carbon footprint has compelled researchers to seek non-conventional methods to meet infrastructural needs, while taking into consideration environmental concerns. Recently, microbiologists, geotechnical engineers, and chemists have proposed a new multidisciplinary research branch termed microbially induced carbonate precipitation (MICP), which can induce in situ soil strengthening and provide a sustainable and green alternative to traditional methods [98].

Bio-cementation refers to the consolidation of the soil matrix using bacteria and chemical reagents that produce minerals such as $CaCO_3$. Bacteria and reagents are generally present in soil in aqueous solutions. Bacteria will undergo two processes simultaneously when added to soil: advection and diffusion, which means bacterial transport in soil pores, and bacterial adsorption onto soil particles [99]. Several factors can affect these two processes, including the geometry of soil pores, bacterial cell features, such as shape, surface charge, hydrophobicity, and apanages [100], soil particle characteristics, such as surface roughness and mineralogy [101], and properties of pore fluids, such as temperature, chemistry and flow regime [102]. To achieve MICP treatment, soil bacteria are added together with chemical reagents. Bacteria, through their metabolism, excrete specialized enzymes that interact with the chemical reagents and form a biochemical reaction network that favors the precipitation of $CaCO_3$ minerals. Bio-augmentation is when the MICP treatment employs pre-cultured exogenous bacteria [103]. While this continues to be the preferred approach [104], other treatment approaches have also emerged gaining research interest. For example, bio-stimulation refers to modifying the soil environment (e.g., providing nutrients, altering pH, etc.) to stimulate and enrich indigenous bacterial communities [105]. Extracted enzymes, instead of whole bacterial cells, have also been found capable of precipitating $CaCO_3$ minerals in soils, termed enzymatically induced carbonate precipitation (EICP) [106]. The principal difference between these approaches is the microbial source utilized. Each approach has merits and shortcomings, and the selection is case-specific [107].

Successful soil stabilization also depends on the method for introducing bacterial suspension and cementation reagents into the soil column. The selected method provides a homogeneous distribution of $CaCO_3$ crystals among the soil particles and prevents system clogging at the inlet point [108].

1.9.1.1 Injection method

This method has frequently been used for soil stabilization. However, some drawbacks were reported. It is relatively complex and needs separate rooms to control the flow of pressure and the hydraulic gradient; injection from both directions (vertical and horizontal) is also required [109]. In most cases, clogging occurs around the injection points, which prevents the smooth distribution of bacterial and cementation solutions, causing a non-homogenous distribution of $CaCO_3$ [110]. Recently, a single-phase under low pH injection method was proposed to replace the existing multiple injection. This approach prevented the bio-clogging problem and reduced the generated NH_3 gas by 90% [111].

1.9.1.2 Surface percolation method

It is considered one of the most preferable methods in MICP applications for soil consolidation and stabilization. It is technologically simple, does not require heavy machinery, and offers a relatively cost-effective path for soil improvement, compared to other methods [112]. The bacterial suspension is vertically introduced into the sand column, followed by the cementation solution, in which the bacteria move freely and self-adjust by gravity and capillary.

Cheng and Cord-Ruwisch [113] treated a 2 m column of coarse sand using the surface percolation method and successfully achieved unconfined compressive strength (UCS) values of 850-2067 kPa. Similarly, a 0.6 m sand column (fine and coarse) was treated using the same method. The UCS reached 920-1250 kPa (coarse sand) compared to 410-570 kPa (fine sand). Similar levels of $CaCO_3$ were precipitated in both tests [114]. Although this method has proven remarkably successful, some limitations regarding the treatment of very fine-grained soils have been recorded, most probably due to the lower infiltration rate and permeability.

1.9.1.4 Premixing method

This method was suggested to overcome the problem of non-homogenous distribution of formed $CaCO_3$ crystals. In this method, the bacterial suspension is mechanically premixed with soil to guarantee uniform homogeneity. Limitations of this method are presented in the disturbance of local soil due to repeated mechanical mixing, which causes the development of pseudo-stress in treated soil and eventually creates problems

during the assessment of engineering properties [109]. Moreover, the resulting UCS of cemented soil is relatively low compared to other methods.

The optimum performance of this method should be evaluated to ensure that the product can meet the required application. Numerous tests have been mentioned in different research studies, some of which monitor the conditions governing the process progress, such as urease activity, biomass concentration, pH measurement, and $CaCO_3$ content [115]. Others measure some important engineering properties such as UCS, stiffness, liquefaction resistance, hydraulic conductivity (permeability), bulk density, shear strength, and slake durability index [103].

1.9.2 Geologic CO_2 sequestration

Geologic CO_2 sequestration, also termed carbon capture and storage, is a process aimed at mitigating the release of CO_2 into the atmosphere to resolve the contribution of fossil fuel emissions to global warming and ocean acidification [116,117,118]. The procedure involves capturing waste CO_2 from significant point sources, such as fossil fuel power plants, compressing it to a supercritical fluid, and then moving it to a storage location. There, it is injected underground, typically about a kilometer deep, into formations like depleted oil and gas reservoirs, saline aquifers, or un-minable coal beds, where it is trapped in the pores and spaces of the rock structure. Ideally, the site chosen for CO_2 storage should have a structure with high porosity and permeability; however, to prevent the leakage of CO_2, it must be capped by a layer with low permeability (cap rock), which acts as a seal. Also, the cementing ingredients and the installations must be gas-tight. In this context, the *in situ* use of ureolysis-driven $CaCO_3$ precipitation as a sealant for treating cracks and high permeability regions in cap rocks, well-bore cement, and installations has been proposed and studied [116, 118]. This is seen as a potential means to enhance the durability of CO_2 storage by inducing the transformation of CO_2 into a solid carbonate phase [117]. Importantly for this application, it was shown that neither *Sporosarcina pasteurii* [119] nor the free enzyme [120] had their activities incapacitated by the pressure and temperature conditions corresponding to the CO_2 storage sites (P > 8.9 MPa, T 32 ºC) [120,121]. Another notable application of $CaCO_3$ bio-precipitation in managing geological formations is the selective plugging of oil reservoir bedrocks. The plugging is done to enhance secondary oil recovery [122]. This is because the secondary oil recovery is performed with water flooding, and to enable

water to reach oil in the tiny pores of bedrocks, the bigger ones, from which oil has been already recovered by primary oil production, have to be blocked.

1.9.3 Remediation

Since MICP involves the wider natural distribution of urease-producing microorganisms and cheaper chemical consumption, it has been frequently used by researchers for heavy metal remediation [123,124,125], making it an economical and efficient method [126]. MICP process involve microbial metabolism to produce carbonate, with which the metal ions in the environment react to form carbonate minerals that get precipitated [127]. As mentioned, the mechanisms of microorganisms that can induce carbonate precipitation include ammonification, denitrification, sulfate reduction, photosynthesis, andurea hydrolysis. Among them, *Sporosarcina pasteurii*, a urease-producing microbe, demonstrated the best mineralization efficiency and has frequently been employed to remedy heavy metal pollution [128]. Some researchers discovered that under suitable conditions, MICP bacterial strain can hydrolyze urea into CO_3^{2-} via the urease produced by its metabolic activities and then immobilize the metal ions such as Cu^{2+}, Pb^{2+} Zn^{2+}, Cd^{2+} in the surrounding environment in the form of precipitates [129]. This process can prevent the migration of heavy metals and reduce their toxicity threat. Wang et al. (2023) converted microbial-induced calcite to less soluble hydroxyapatite and investigated the phase and morphology evolutions of the solids, along with the distribution and release of Cd; they found that the conversion of calcite to hydroxyapatite enhanced the removal efficiency of Cd [130]. Kumari et al. (2016) used *Exiguobacterium undae* YR10 to conduct MICP remediation on Cd-contaminated soil at 10°C. The applied potential of MICP technology in the remediation of heavy metal-contaminated soil at low temperatures was verified [131]. MICP can also increase the environment's pH and enhance the mineral crystallization driving force. Studies on the mineralized mechanism of MICP showed that the bacteria act as a crystallographic site, the extracellular polymeric substance (EPS) produced in mineralized metabolism regulates the nucleation of inorganic crystals, and bacterial strain plays a role in structural assembly and bonding [132].

Although MICP method is efficient, durable, economic, and eco-friendly at a low concentration of pollutants, high pollutant concentration or extreme pH (alkaline medium) lead to microbial inactivation [133]. Adsorption materials are not a proper

solution for this problem, because most of them can absorb high concentrations of pollutants [134]. Therefore, in recent years, the method of absorbing materials loaded with microorganisms has emerged to treat pollutants (especially pollutants having high concentrations), and the combination of the two has many advantages. Remediation materials can provide a good shielding environment for microbial communities and reduce their exposure area to pollutants, thus improving their survival rate, enzyme activity, and biodegradation ability in the environment [135]. Currently, studies have confirmed the effectiveness of adsorbent-supported urease microorganisms in the treatment of heavy metals in wastewater and terrestrial soil [136] successfully immobilized urease enzymes in wastewater using eggshell membranes and found good operational and storage stability [137]. Significantly reduced exchanged-state Cd content in soil by corn cob-loaded urease microorganisms. [138] found that the restoration of heavy metals can be achieved by scoria and urease microorganisms and can be completed in four stages: i) material adsorption stage, ii) platform stage, iii) microbial remediation stage and iv) equilibrium stage.

1.9.4 Conservation of natural stone

Microbes appear also to be able to consolidate stone heritage structures and protect them from weathering. Stone decay can be driven by chemical, physical, and biological factors and usually by their combined action. Water plays a significant part as a weathering agent. Rainwater can solubilize calcium carbonate, with the extent of dissolution depending on the acidity of the solution [139], which is caused by the presence of inorganic ions such as NH_4^+, SO_4^{2-}, Cl^-, Na^+, NO_3^-, Ca^{2+}, and K^+ all observed in areas of high air pollution [140].

Additionally, water can transport salts onto the stone surface or within its porous structure. It is known that soluble salts greatly limit the durability of porous building materials. Crystallization pressure in porous materials relies on their pore structure, saturation capacity, and the energy dissimilarity between the crystal and the pore wall. It is well known that crystallization pressure is lower in larger pores [141], whilst high degrees of saturation lead to high crystallization pressures [142].

Moreover, salt damage depends on the environment in which precipitation occurs. Salt crystallization in porous stones takes place either on their surface (efflorescence) or within their pores (sub-florescence). Salt sub-florescence produces considerably more

decay in porous stone than efflorescence, due to the lack of an escape route and the release of the pressure of salt crystallization [143].

Furthermore, water promotes biological decay favoring the suitability of nutrients for microorganisms. This occurs when it combines with compounds from the stone substrate (i.e., carbonatic ones) or with the NOx pollutants from the atmosphere. Biodeterioration can alter the mechanical properties (by breakage and loss of cohesion of the substrate), induce chemical alteration (due to excretion of metabolites), lead to aesthetic damages (through the formation of patinas and crusts). Such damages and alterations highly depend on the colonizing organisms (varying from bacteria, to fungi, lichens, mosses, and higher plants), which are variably favored by micro- and macro-environmental conditions [144].

Indirect control methods are known to be able to reduce the bio-deterioration phenomena through the identification of environmental conditions unfavorable to biological growth, and certainly stand out as the leading choice for long-lasting results. However, the use of indirect methods is not always possible in hypogea, and outdoor monuments, where the reduction of humidity, which is the main factor affecting bio-deterioration [145], but also temperature and nutrients are inhibited. To counteract natural degradation, stones should be treated with products able to improve their resistance against decay, through the use of formulations with consolidating, water-repellent, and biocidal properties. Once the weathering has begun, these materials should ensure good adhesion and intergranular cohesion within the lithic matrix, as well as the preservation of the stone against the destructive action of water, atmospheric pollutants, particulate matter, and thermal stress [146]. Among the most common organic polymers used in conservation are acrylic polymers, epoxy resins, polyurethanes, and perfluoropolyether [147]. They display good hydrophobic properties and, some of them, also have consolidating capability. However, in the long term, their thermal and photochemical fluctuation causes chromatic and mechanical alterations [148]. In contrast, silica-based materials obtained from alkoxysilanes and alkyl alkoxysilanes *in situ* sol-gel reactions solve the above disadvantages, although they often display cracking upon drying, thus reducing the consolidation efficiency; furthermore, due to their structural rigidity, they show mechanical properties that are not compatible with the weathered stones; in addition, the low molecular weight starting

compounds are prone to evaporation before the polymerization process occurs inside the stone substrate [149].

The design of advanced conservation products requires compliance with eco-sustainability criteria. This topic is crucial, not only to respect health and the environment, but also to avoid the drawbacks originating from the use of non-tested materials, as has been indeed the case for several products used in the past for restoration works. Different conservation materials have been employed, which partially fulfill the above conditions, and recent conservation techniques have been developed (among them bacterial biomineralization as one of the most promising approaches) to achieve performing and eco-friendly solutions,.

Biomineralization could mitigate the negative impacts of weathering on stone objects inducing the formation of calcium carbonate (CaCO3), resulting in a highly coherent and effective protective layer on degraded substrates [149]. As a promising emerging material, MICP technology has found successful applications in cultural relic restoration. In the 1990s, Le Metayer-Levrel [150] led microbial mineralization treatments on the surface of the Southeast Tower of the Saint-Médard Church, resulting in the development of a population of carbonate bacteria that discouraged the growth of native acid-producing bacteria. This treatment effectively maintained the appearance of the tower for 3.5 years without significant changes. These biogenic calcium carbonates provide a protective layer on stone artifacts, reducing water absorption while providing breathability. Later, Minto et al. [151] used *Sporosarcina pasteurii* to solidify marble and concrete, indicating that bacteria-induced mineralization coatings could effectively bond with substrates. In the study by Mu et al. (2021) [152], *Bacillus pasteurii* was used to perform repair experiments on blocks and beams made of white marble stone. The results revealed that after MICP repair, the bending strength of white marble stone beams approached that of the intact samples. Besides, Liu et al. (2020) [153] used a method involving the extraction and injection of urease or bacterial liquid along with mineral precipitates formed by a reaction into cracks in ancient architectural bricks and stones. After cyclic injections, this method effectively filled the cracks in the ancient architectural bricks and stones. Although the MICP technology has been successfully applied to the conservation of cultural relics, the efficiency and the impact of soluble salts on MICP technology is still a challenge for the conservation of cultural

relics, whilst repeated treatment is always required to achieve acceptable performance (Fernandes, 2006) [154].

Yang et al. (2021) [155] have proposed a biocarbonation method of reactive magnesia to form microbially induced inorganic heavy mineral concertrate (HMC) for soil improvement. This method has found applications in various areas. For example, Chen et al. (2021)[156] used the biocarbonation method of reactive magnesia to maintain electrolytic manganese residue, which increased the dry density and reduced the moisture content of the residue, improving its strength. Wang et al. (2023) [157] applied the biocarbonation method of reactive magnesia to stabilize dredged sludge, enhancing the physical and mechanical properties of the sludge. Dong et al. (2023) [158] used microbial carbonation of reactive magnesia to reinforce weathered rock cracks effectively, offering an efficient method for stabilizing surface weathered rock cracks. Wang et al. (2022) [159] utilized microbial carbonation of reactive magnesia cement to stabilize construction and demolition waste in underwater engineering, demonstrating its ability to stabilize underwater environmental engineering structures and demolition waste particles.

1.10 Originality and aims of the present thesis

The originality of the present thesis lies on two main aspects: (1) the bio-consolidation of the architectural heritage of Cyprus built with porous materials, using native strains, which can act as a biological ecofriendly preservation method with enhanced applicability at local level; (2) the investigation of novel, less studied bacterial species with enhanced MICP properties using the best medium, which can potentially be applied in various sectors.

Therefore, this master thesis **aims** to discover new local bacterial strains that can produce high amounts of calcium carbonate, which will be resistant in extreme conditions. The most promising bacteria will be tested *in-vitro*, for bio-consolidation, using local stones and the changes in their mechanical properties will be recorded. Also, this thesis **aims** to test the most used media based on the bibliography in order to find the most efficient one in terms of cost/production to be used in bio-consolidation.

Chapter 2: Materials and Methods

2.1 Sampling Sites and Isolation

The marine sediment samples were collected from two different locations in Cyprus: (1) Protaras (35°00'51.7"N 34°03'29.5"E) and (2) Larnaca (34°56'50.8"N 33°39'49.4"E). The aforementioned marine sites were chosen based on differences in the origin of the sand. Specifically, Protaras coasts comprise of Pleistocene age medium-grain calcarenite sand, while Larnaca has fine calcarenite sand with some accessory minerals originating from the small igneous Troulli Massif and Eastern Troodos [160]. The specimens were collected at least 50 meters away from the coast to avoid bacteria related to human activities.

The samples were suspended in sterilized saline solution (85% NaCl) and filtered. Fragments of filtered and unfiltered sand and water were first cultured in calcium carbonate precipitation (CCP) agar media. CCP media contain 20 g of Urea, 2.12 g $NaHCO_3$, 10 g NH_4Cl, 3 g of Nutrient broth, 4.5 g $CaCl_2 \cdot 2H_2O$, 20 g Agar per liter of distilled water at pH 8.5 [161]. The incubation period was 5 days at 28 °C with constant agitation at 120 rpm (Shaking Orbital Incubator SI50, Stuart). Each microbial culture was then replated in CCP agar media until single bacterial colonies were fully isolated.

2.2 Calcium Carbonate Solubilization and Urease Activity

Since microorganisms can have an impact on the deterioration of limestone by solubilizing $CaCO_3$, the carbonate solubilization capability of each isolate was analysed [20]. Calcium carbonate solubilization (CCS) media contained: 10 g of dextrose, 5 g of $CaCO_3$, 0.5 g of $(NH_4)_2SO_4$, 0.2 g of KCl, 1 g of $MgSO_4.7H_2O$, 5 g of yeast extract, 15 g of agar per liter of distilled water at pH 7.0 [162]. The isolated bacteria were grown in CCS agar plates. The plates were incubated for 5 days at 28 °C; clear halos around colonies indicated that the bacteria had calcite-solubilizing properties.

Bacterial strains were then spread on agar plates to analyze their urease activity. For this test, the strains were first inoculated for 24 hours with CCP media, and then 500 μl were spread equally in the urease plates to assure low concentration of bacterial cells. The medium of urease agar plates consisted of 1 g bacteriological peptone, 1 g of D-

glucose, 5 g of NaCl, 2 g of NaH_2PO_4, 20 g of urea, 12 mg of phenol red, 15 g of agar per liter, and the final pH was adjusted to 6.8 [161]. The urease activity of isolated strains was detected by urease medium agar containing 2% urea and phenol red as pH indicator [20]. Microorganisms with urease enzyme hydrolyze urea producing ammonium ions, causing color change in the agar medium from yellow to red. The change in color of the agar plates determines the relative urease activity due to the generation of ammonium and carbonate ions, which are increasing the pH of the solution, thus changing the color of phenol (λ_{max}=443 nm, pH~6.8) to red (λ_{max}=570 nm, pH~8.2) [164]. The incubation period lasted for 3 days at 28 °C.

2.3 Molecular Identification of species and Phylogenetic tree analysis.

The total DNA was extracted from 100 mL microbial cultures. The cultures were centrifuged (Eppendorf 5810R Centrifuge) at 10000 rpm for 10 min. The supernatant was discarded, and the total DNA was extracted from the biomass using the NucleoSpin Microbial DNA Kit (Macherey – Nagel, Germany), following the manufacturer's instructions. For identification of the strain of each microbial culture, 16S rRNA gene sequencing was performed (Macrogen Ltd., Amsterdam, the Netherlands). The nearest relative strains were identified by Basic Local Alignment Search Tool (BLAST) analysis against the National Center for Biotechnology Information (NCBI). The phylogenetic tree analysis was performed using the Mega11 software tool.

2.4 Microbial Growth, Precipitation and Collection

Cultures of the isolated strains were grown in 250 ml Erlenmeyer flasks with 50 ml of CCP liquid media at 30 ºC and 120 rpm in an incubator (mrc ltd). Microbial growth was monitored through optical density (OD) A densitometer is a device that measures the degree of darkness (the optical density) of a photographic or semitransparent material or of a reflecting surface. The densitometer is essentially a light source aimed at a photoelectric cell. It determines the density of a sample placed between the light source and the photoelectric cell from differences in the readings. Modern densitometers also have electronic integrated circuitry for better reading. Optical density was conducted at 600 nm (UV-Visible Spectrophotometer, JASCO V-530 PC). OD was measured regularly for 192h to monitor the bacterial growth.

For product collection, bacterial cultures were grown in 250 ml Erlenmeyer flasks with 50 ml of liquid media and incubated at 30 °C for 8 days. Subsequently, the samples were transferred to 50 ml falcon tubes and centrifuged with Eppendorf 5810R Centrifuge at 10000 rpm for 10 min resulting in the separation of the product and bacterial cell from water and ammonia. The remaining pellet was resuspended with 50 ml of phosphate-buffered saline (PBS) (NaCl 137 mM, KCl 2.7 mM, Na_2HPO_4 10 mM, KH_2PO_4 1.8 mM pH 7.4), including also 100 μl of lysozyme (Sigma-Aldrich, UK) at a final concentration of 2 mg/ml, and was treated for 1 hour at 33 °C to hydrolyze the bacteria cell wall. Centrifugation was then used to remove the cell debris, and the pellet was rinsed with sterile distilled water at pH 8.5 and centrifuged again before being air-dried at 33 °C for 48 hours. The pellet was weighed to determine the amount of $CaCO_3$ precipitated by the various strains.

2.5 Optimization of Yield and Production

Strains were grown in another four different media commonly used by the scientific community for MICP studies [1,11]. Modifications of the media were also performed to optimize the yield and observe if there is any difference of the product which would be formed. The media used were (1) B4, (2) B4+urea, (3) yeast extract+ammonium sulfate and (4) yeast extract+urea. B4 is one of the most used media for biomineralization and consists of 4g/L calcium acetate, 10g/L D+ glucose and 4g/L yeast extract. B4 with the addition of 10g/L urea aimed to provide the high yield of B4 together with the urea hydrolysis pathway. Yeast extract (YE) + ammonium sulfate (AS), which is a well-known medium to the scientific community, was mixed at 10g/L and 20g/L, respectively. Finally, in 10g/L yeast extract, 20g/L urea were added to form the fourth medium.

2.6 X-ray diffraction (XRD) and Scanning Electron Microscopy (SEM)

The XRD analysis of the extracted $CaCO_3$ was performed using a Bruker D8 Advance system with Cu Kα radiation (λ = 0.15406 nm) at 40 kV and 40 mA. The analysis was carried out with continual rotation of the sample and a step of 2°/min within the 2-70° 2θ angle range. The International Centre for Diffraction Data (ICDD) PDF 4 database was used for the qualitative identification of the $CaCO_3$ polymorphs.

The samples were also thoroughly characterized using a JEOL, JSM-6610 LV scanning electron microscope (SEM) equipped with a BRUKER type QUANTAX 200 energy dispersive X-ray spectrometer (EDS). Representative samples were used, mounted on double-sided carbon tape and sputter-coated with Au, in order to determine their morphological features.

2.7 Biological Treatment of stone

Two representative building limestones from Cyprus were used in this study (Table 1). The first stone is known with the commercial name "Petra Lympion" (LYM) and originates from the Lefkara geological formation, which belongs to the Circum Troodos Sedimentary Succession. This is a packstone quarried in the Lympia village area, which is located in the Larnaca District, at the southeast of Cyprus. The grains of this stone are almost exclusively Globigerina-type foraminifera; rarely, some well-preserved radiolaria are also visible. XRD analysis indicated that this lithology is composed almost exclusively of calcite, while traces of quartz also exist. LYM also exhibits significant intragranular porosity within the foraminifera [164].

The second stone studied was Petra Gerolakkou (GER), which is a bioclastic limestone found in the Nicosia-Athalassa geological formation. This stone was quarried in the Gerolakkos area, at the south of Pentadaktylos mountain range; the geological formation, however, stretches from Mammari to the northeast to Larnaca district, at the southwest of Cyprus. GER has been used extensively for the construction of several historic monuments in Nicosia (e.g., the Venetian fortifications of the old city - 16th century - and the Agia Sofia Cathedral - 14th century). This stone consists of relatively large biogenic and silicate grains, loosely bound together by micro-sparry and sparry calcite (Ioannou et al., 2009).

Table 1. Physical properties of the LYM and GER stones [164].

		LYM	GER
p_o, % EN 1936	*ave*	42.8	49.5
	sd	1.4	1.0
	cov	0.03	0.02
ρ_a, kgm^{-3} EN 1936	*ave*	1535	1370
	sd	41	30
	cov	0.03	0.02
Pore size, µm	*ave*	0.23	
	sd	0.14	0.05
	cov	0.63	0.14
CAC, $gm^{-2}s^{-1/2}$ EN 1925	*ave*	141.0	1001.7
	sd	30.2	77.7
	cov	0.22	0.08

Ave: average; sd: standard deviation; cov: coefficient of variance; p_o: open porosity; ρ_a: apparent density; pore size, average pore throat diameter; CAC, capillary absorption coefficient.

The dimensions of the original stone specimen were 4 x 4 x 9 cm. The biological treatment was carried out on half of the specimen (4 x 4 x 4.5 cm) for CCP medium treatment with *A. crystallopoietes* DSM 20117, while the other half served as the control.

The goal for having control and treated areas on the same specimen was to enable direct comparison of the effect of the biological treatment after its application on part of a specimen, right next to the control area, thereby avoiding any errors due to physical and mechanical inhomogeneity of the rock material itself. The sample stones were sterilized using autoclave at 121 °C, covered in aluminum foil to prevent steam from penetrating it. They were then placed in the oven at 40 °C for 3 days to dry to constant mass (final weightings conducted at 24 ± 2 h intervals differed by < 0.1%). A solution was used for the bio-treatment of the stones, which included 50% medium and 50% bacterial culture, starting from an initial optical density (OD) of 0.1 (0.1 L culture volume) at 600 nm (UV-Visible Spectrophotometer, JASCO V-530 PC). The treatment was performed with a brush, applying approximately 3-4 ml of solution every 24h for 15 days, only at the upper half of the stone specimen (Figure 5). During the aforementioned

15-day period, the specimens were stored in a small incubator at room temperature, to avoid bacteria from the atmosphere interacting with the stone.

For the optimization treatment, the stones were separated in three areas (4 x 4 x 3 cm), the control and two treatment areas for two different strains (Figure 6**)** to observe the difference between products formed by different strains. Both specimens had a control area where it was treated with sterilized B4 medium to observe if the medium alone is involved in consolidation. In both specimens, the middle area was B4 with *A. crystallopoietes* DSM 20117, whereas the third part in Specimen 1 was *A. crystallopoietes* P21 with B4; in Specimen 2, *Micrococcus sp*. DSM 105846 with B4+Urea was used for 5 days, followed by *A. crystallopoietes* P21 with B4 for another 10 days in P4 producing hydroxyapatite and then in P3 producing calcite and vaterite to observe if the hydroxyapatite for the first 5 days will make a protection layer at the top of the stone. It is also worthy to mention that the two bacteria, *Micrococcus sp*. DSM 105846 and *A. crystallopoietes* P21 were first tested for symbiotic ability.

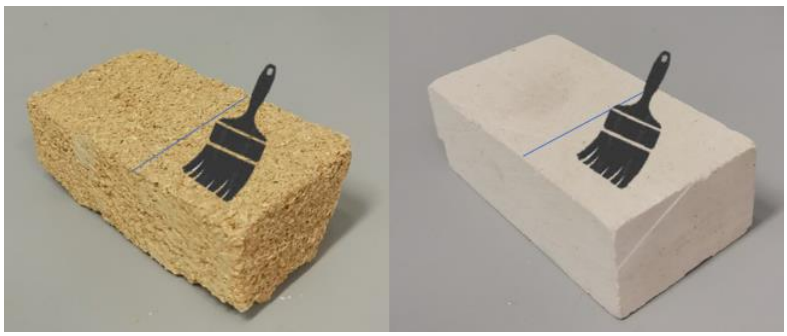

Figure 5: Treatment with brush, applying approximately 3-4 ml of solution every 24h for 15 days.

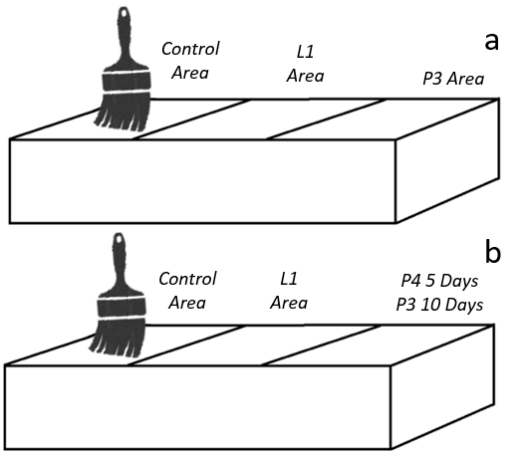

Figure 6: Optimization treatment with brush, applying approximately 3-4 ml of solution every 24h for 15 days.

2.8 Evaluation of biological treatment

2.8.1 Resistance to water penetration

2.8.1.1 Karsten Tube Tests

The Karsten Tube test [EN 16302] provides information on the volume of penetrating water under the effect of gravity, per unit surface area of the material, as a function of elapsed time. The apparatus used in the measurements comprised of a standard Karsten tube, consisting of a clear graduated pipe, welded at its lower part on a cylindrical cell with a circular brim of internal diameter D = 2 cm. During the test, the circular brim of the cell was temporarily affixed perpendicular to the top surface of the stone specimen under study, using an impermeable adhesive putty (i.e., plasticine), which also acted as a perimeter sealant. Initially, the limestone specimen was dried to constant mass. Deionized water was then added through the upper, open end of the Karsten tube, until the column reached the "0" level gradation mark. After 1 minute, the tube was refilled up to the “0” mark and timing of the test was initiated. As water gradually penetrated the porous substrate, the Karsten tube was topped up to maintain a steady pressure. The quantity of water absorbed by the material was measured directly from the graduated pipe at time intervals of 1 min for a total of 10 minutes. The % difference between the treated and control area was calculated based on the slope of the trendline of the measurements generated in each area, respectively.

2.8.1.2 Dynamic Contact Angle Measurements.

Contact angle measurements are used to examine the wettability of a surface. The shape that a drop takes on the surface under study depends on the surface tension of the fluid and the nature of the surface itself. At the boundary between the droplet and the gaseous environment, the surface tension causes a curved contour. Contact angles were hereby measured using an optical contact angle pocket goniometer (PGX+, TQC Sheen C&W Specialist Equipment, UK). The PGPlus software was used to measure the angle volume, base and height of the droplets and to create plots relative to the time. Dynamic mode was used, with 80 photos/minute. The volume of the droplet was 4 μl. A minimum of three sets of measurements were completed for each side (control/biologically

treated) of the stone specimen surface. The % difference between the treated and control area was calculated based on the average of the slope of the trendline generated by the average measurements of the three replicates in each area, respectively.

2.8.2 Drilling Resistance Measurements

The drilling resistance of the control/biologically treated sides of the stone specimen under study was measured using the Drilling Resistance Measurements System (DRMS, SINT Technology, Italy). The test adopts a non-standardized micro-destructive approach to determine the drilling resistance of a material either in the lab or *in situ*. The system is capable of measuring forces between 0 and 100 N and can penetrate to a depth of 10 mm. In this study, at least three holes with 5 mm diameter and 10 mm depth were drilled on both the control and the biologically treated sides of the stone specimen surface. The % difference between the treated and control area was calculated based on the average of the measurements of the three replicates in each area, respectively.

2.8.3 Scratch Test

The scratch tool presumes the gradual formation of a superficial groove on the surface of the material, using a rectangular diamond cutter with a width, w=10 mm, and a negative back rake angle of 15°, moving at a constant velocity of v=10 mm/s. During the scratch, tangential (Ft) and normal (Fn) forces acting on the cutter are recorded. The magnitude of the forces marks any distinctions in the depth of the material and in between the control and the treatment area. To assess the results of the test, analysis of variance (ANOVA) was used to examine whether the difference between the two areas of the stone (which are the treated and the untreated) was statistically important.

For the GER specimen, six cuts were made. The first scratch was at 0,05 mm, which was the leveling scratch, and the depth of each cut increased incrementally with step 0,05 mm until the total depth reached 1,05 mm. Similarly, for the LYM specimen, five cuts in total were made starting with 0,01 mm, which was the leveling scratch, until the total depth reached 0,05 mm.

2.8.4 Statistical analysis (ANOVA)

Regarding the scratch test, statistical analysis of variance (ANOVA) was used. The influence of the treatment and its impact on the cutting forces (Fn, Ft) for every depth of the scratch test (excluding the leveling scratch) between the two different areas (which were the treated and the untreated) was assessed for statistical importance. For this, the individual factors and interactions were determined by the ANOVA. The probability of rejecting a null hypothesis was set as P-value<0.01.

Chapter 3: Results related to MICP.

3.1 Isolation of Bacteria, Identification of Species and Phylogenetic Tree Analysis

Fourteen different colonies were able to grow in the calcium carbonate precipitation (CCP) agar plates, tentatively designated as P1-P7 (Protaras) and L1-L7 (Larnaca). The colonies were primarily white and yellow opaque coccus with a shiny and smooth texture. The only exception was L2 strain, which grew aggressively with yellow color and filamentous morphology.

The fourteen samples were partially sequenced using 16S rRNA gene analysis, and the taxonomic analysis based on nBLAST indicated that the strains are likely to be *Micrococcus* sp. (DSM 105846, 3517), *M. luteus* (PP1, PP2, PP3, PP4), *M. yunnanensis* PP1, *Arthrobacter crystallopoietes* DSM 20117, *Arthrobacter crystallopoietes* P-21, *Bacillus licheniformis* PP1 and *Staphylococcus epidermidis* PP1, as shown in Table 2. As *Staphylococcus* could be a potential pathogen [165], no further analysis and assessment was performed on P6. Phylogenetic analysis of the other sequences was performed. This showed the relevance of the isolated strains with other species of *Arthrobacter*, *Bacillus* and *Micrococcus*, respectively (Figure 7). Furthermore, *Arthrobacter crystallopoietes* P-21 and *Arthrobacter crystallopoietes* DSM 20117 seem to be closely related, but differences were observed in their properties, which were examined in the laboratory, with relation to the quantity and morphology of $CaCO_3$ precipitation and urease activity, as seen below.

Table 2. Bacteria identified using sanger sequencing and nBlast.

Samples	Name of the strain	Accession number	Reference
P1	*Micrococcus luteus* PP4	OP531859	this study
P2	*Micrococcus* sp. DSM 105846	MN537502.1	
P4			
P7			
L7			
P3	*Arthrobacter crystallopoietes* P-21	OP530235	this study
P5	*Micrococcus* sp. 3517	KP345959.1	
P6	*Staphylococcus epidermis* PP1	OP531855	this study
L1	*Arthrobacter crystallopoietes* DSM 20117	CP018863.1	
L2	*Bacillus licheniformis* PP1	OP531847	this study
L3	*Micrococcus luteus* PP1	OP531067	this study
L4	*Micrococcus luteus* PP2	OP531068	this study
L5	*Micrococcus yunnanensis* PP1	OP531840	this study
L6	*Micrococcus luteus* PP3	OP531854	this study

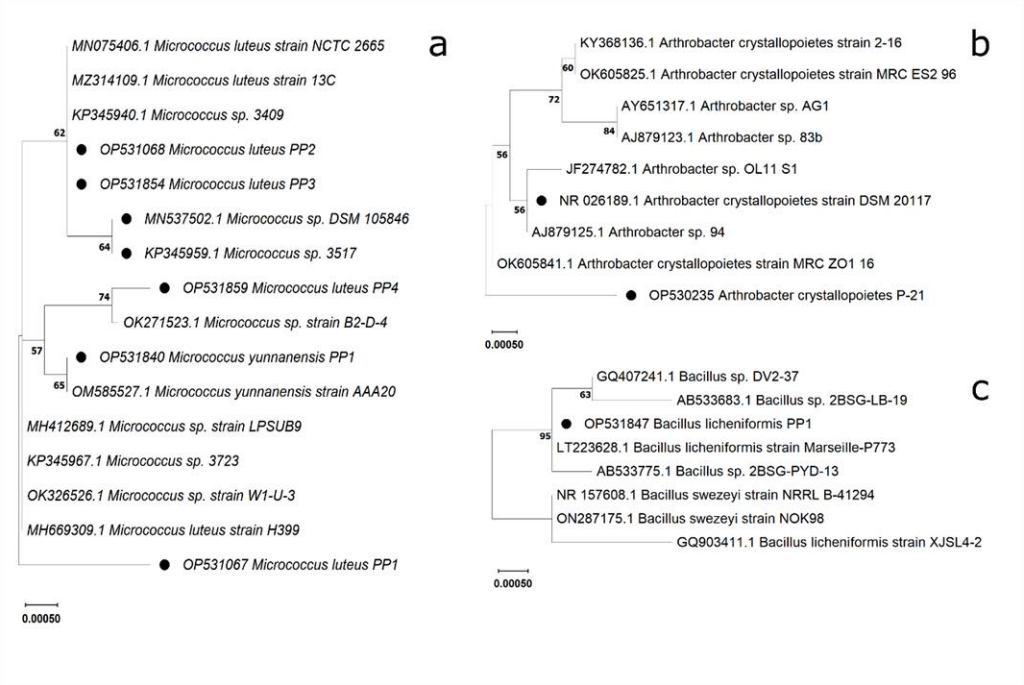

Figure 7 Phylogenetic trees of bacterial isolates from neighbour-joining analysis, showing the position of the isolated Micrococcus (A), Arthrobacter (B) and Bacillus (C) strains among similar strains. This analysis is based on partial 16S rRNA gene sequences.

3.2 Calcium Carbonate Solubilization (CCS) and Urease Activity.

CCS evaluation was performed to examine whether the $CaCO_3$ polymorph produced and precipitated by the newly isolated bacterial strains was soluble, since this could result in the deterioration of carbonate rocks when MICP would be applied *in-situ*. The aforementioned evaluation confirmed that none of the isolates have CCS properties. Consequently, the isolates were screened qualitatively for urease activity in agar plates. All strains of *Micrococcus* species were catalase positive, changing the color of the plate to pink. *B. licheniformis* PP1 (L2) showed negative urease activity by not changing the agar plates colour. *Arthrobacter crystallopoietes* P-21 (P3) was hydrolyzing urea, because it showed positive urease activity by changing the plate colour to red. Interestingly, *Arthrobacter crystallopoietes* DSM 20117 (L1) was the strain presenting the highest activity, showing change of colour to intense pink, fuchsia, which indicated pH>8.2 (Figure 8).

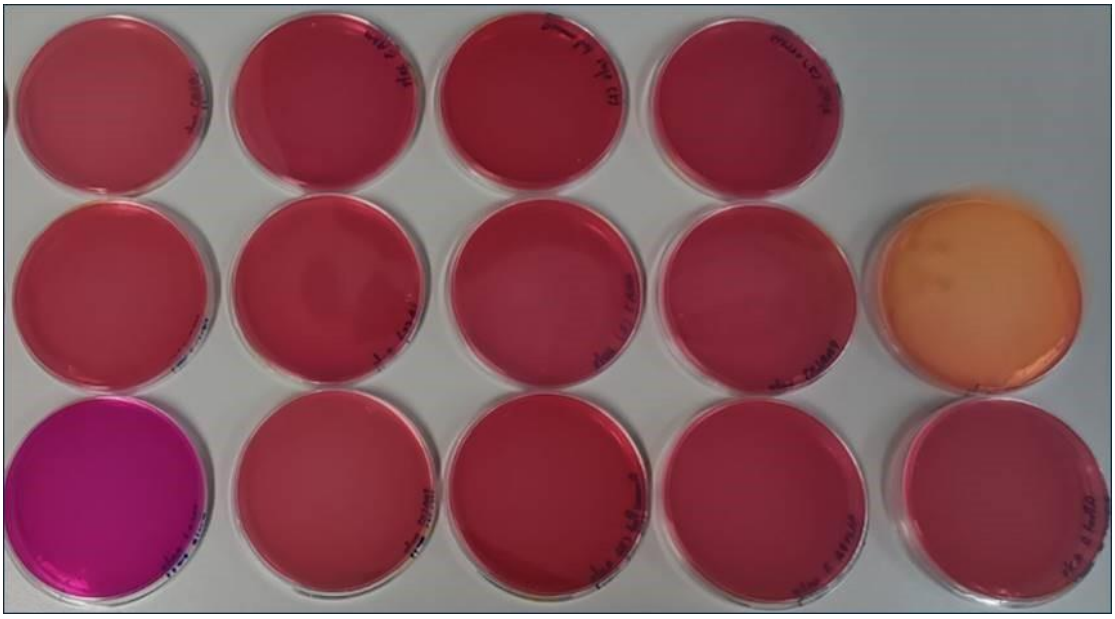

Figure 8: Plates showing urease activity after inoculation with all the isolated microbial strains.

3.3 Microbial growth kinetics of the isolated species

Microbial growth kinetics was studied to evaluate the profile of the newly isolated microbes, which induce precipitation and microbial growth. Microbial growth was regularly monitored for 192h. Figure 9 shows the growth curve of the different bacterial strains in CCP culture medium. It was observed that all micrococci grew similarly, reaching an average OD of 0.7 at the end of the exponential phase. *M. luteus* strain PP1,

PP2, PP3, and *Micrococcus* sp. 3517 had a lag phase of 24h, while *M. luteus* strain PP4 needed 48h to adapt. The exponential phase lasted for 72h. The microbial growth of micrococci was higher compared to other species. *Arthrobacter crystallopoietes* P-21 had no lag phase and for the first 24h it was growing rapidly until it reached high OD values. Following that time point, it seems that it entered the stationary phase. In contrast, *A. crystallopoietes* DSM 20117 had a lag phase which lasted at least 48h. This strain was growing until the end of the process with peak OD~0.2, which was lower compared to *Micrococcus* and *Arthrobacter crystallopoietes* P-21. It was also observed that precipitation of $CaCO_3$ started after 72h (no data shown). *B. licheniformis* PP1 strain induced precipitation of $CaCO_3$ (no data shown) in the first 48h, with gradual increase of microbial growth until OD~0.2, again much lower compared to *Micrococcus* and *Arthrobacter crystallopoietes* P-21.

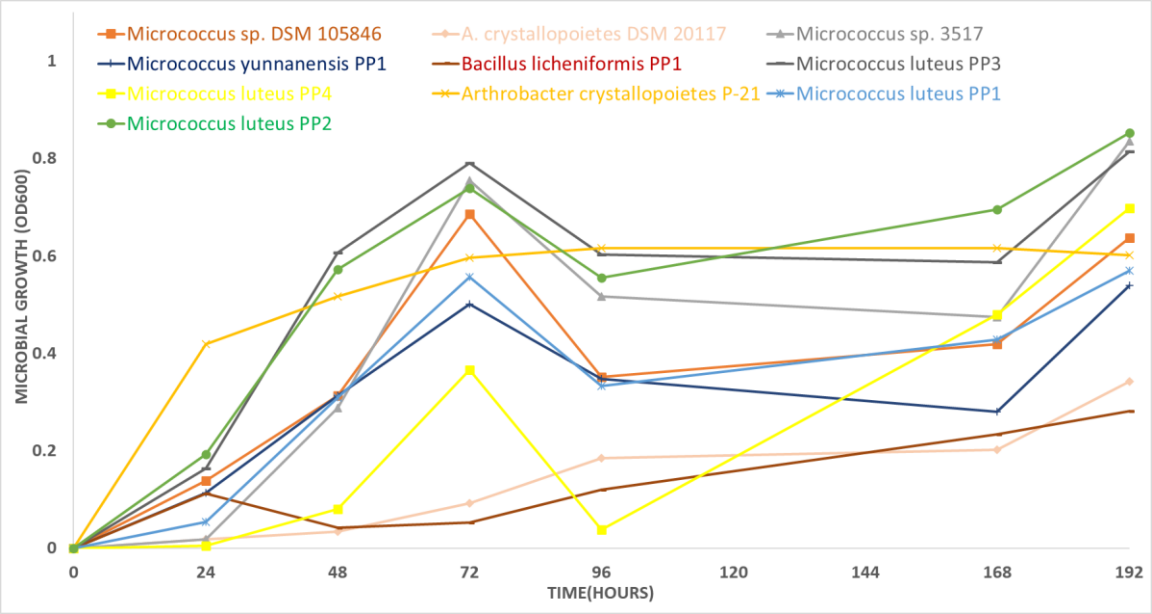

Figure 9: Microbial growth kinetics monitoring of the isolated strains, which were able to induce CaCO3 precipitation.

3.4 Quantification of Product Precipitation

After 192h of incubation, the precipitated $CaCO_3$ forms of each microorganism were collected and dried. *A. crystallopoietes* DSM 20117 (L1) produced by far the highest concentration of $CaCO_3$, reaching 2286 mg/L (Figure 10). $CaCO_3$ production from this strain significantly outperformed production from the other isolated species**.** The second highest producer was *Micrococcus* sp. DSM 105846 (P2), forming 448 mg/L of $CaCO_3$. The other strains of *Micrococcus* produced from 100-300 mg/L, while *Micrococcus yunnanensis* PP1 (L5) strain produced the most insignificant concentration of $CaCO_3$, reaching 104 mg/L. *Arthrobacter crystallopoietes* P-21 strain (P3), produced 242 mg/L and *B. licheniformis* PP1 strain (L2) induced precipitation of 226 mg/L $CaCO_3$.

As *A. crystallopoietes* DSM 20117 (L1), *Micrococcus* sp. DSM 105846 (P2), and *Arthrobacter crystallopoietes* P-21 (P3) strains seem promising when combining urease activity and $CaCO_3$ precipitation, they were chosen to grow in B4, B4+urea, YE+AS, and YE+Urea media (Figure 11). *A. crystallopoietes* DSM 20117 (L1) formed 12240 mg/L of product with B4 medium, which was the highest amount of product among the three strains using each media. Then, 6160 mg/L of product was formed with YE+AS, followed by 3110 mg/L with YE+Urea and 2460 mg/L with B4 + Urea. *Micrococcus* sp. DSM 105846 (P2) formed a product of 6405mg/L with YE+AS then 6380mg/L with B4+Urea, 5470mg/L with B4 and 3960mg/L with YE+Urea. *A. crystallopoietes* P-21 strain (P3) formed the highest amount of product when it was grown in YE+AS reaching 7930mg/L, followed by 5550 mg/L when it was grown with YE+Urea, then 4074mg/L with B4+Urea and 2645mg/L with B4. Furthermore, as noticed in Figure 11, comparing the product formed upon use of the different media by each tested strain, the amount of formed product with CCP medium was by far the lowest.

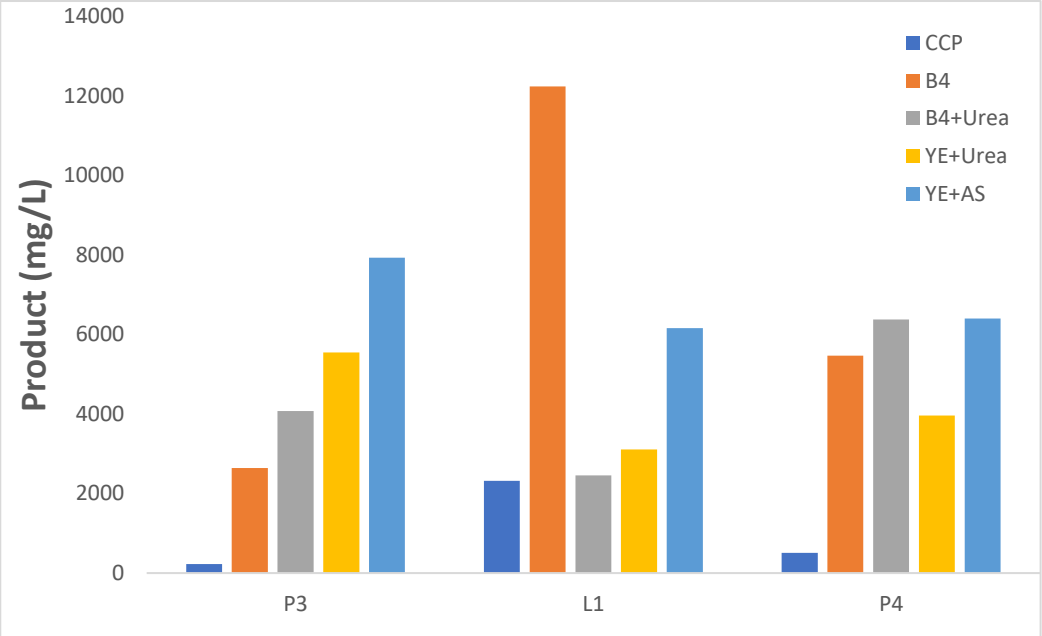

Figure 10: CaCO3 (mg/L) produced by each strain after 192h of incubation, where P1: Micrococcus luteus PP4; P2, P4, P7, L7: Micrococcus sp. DSM 105846, P3: Arthrobacter crystallopoietes P-21, P5: Micrococcus sp. 3517, L1: Arthrobacter crystallopoietes DSM 20117, L

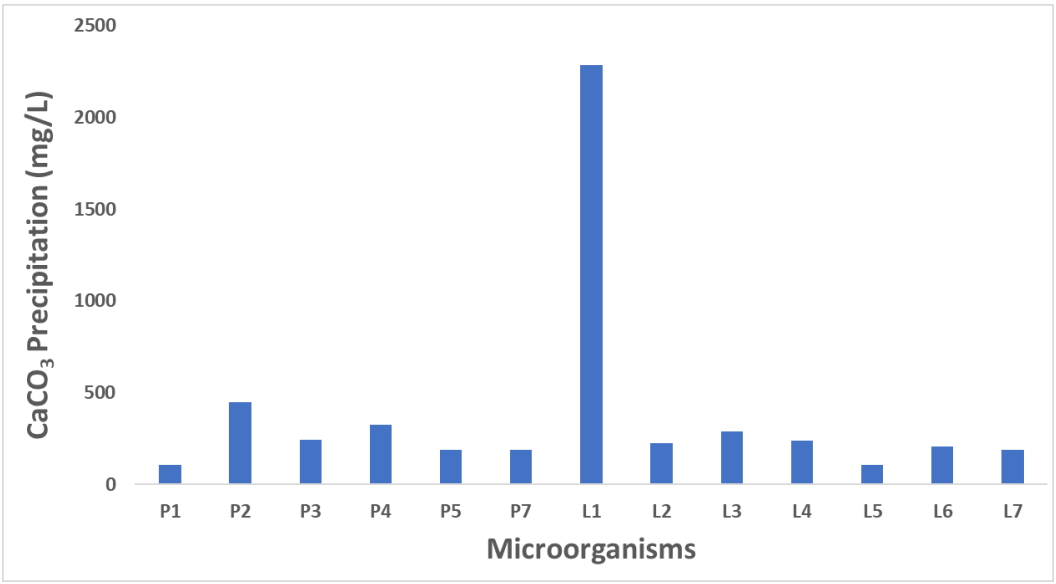

Figure 11. Product (mg/ml) produced by the different strains after 192h of incubation, where P3: Arthrobacter crystallopoietes P-21, L1: Arthrobacter crystallopoietes DSM 20117, P4: Micrococcus sp. DSM 105846.

3.5 XRD and SEM analyses

The powder XRD technique was used to identify the $CaCO_3$ polymorphs that were recovered at the end of the experiments. In particular, when CCP medium was used, XRD analysis was performed in the $CaCO_3$ precipitate extracted from *A. crystallopoietes* DSM 20117, as the most promising MICP strain, *B. licheniformis* PP1 strain, representing *Bacillus* species, and a sample of *Micrococcus* species, *Micrococcus* sp. DSM 105846 (Figure 12). The XRD patterns showed that *A. crystallopoietes* DSM 20117 induced mainly the precipitation of calcite crystals (main peaks in Figure 12a). Vaterite peaks of lower intensity were also observed, thus indicating that this specific $CaCO_3$ polymorph was precipitated in smaller amounts, compared to calcite (Figure 12a). *B. licheniformis* PP1 showed peaks of calcite and vaterite (Figure 12b). In this case, more intense vaterite peaks were detected, compared to *A. crystallopoietes* DSM 20117 (compare Figure 12a with 12b). *Micrococcus* sp. DSM 105846 produced a low amount of hydroxyapatite and a negligible amount of calcite (Figure 12c).

XRD analysis has also taken place in the optimization step in which different media were used (Figure 13). *A. crystallopoietes* P-21 (P3), *A. crystallopoietes* DSM 20117 (L1) and *Micrococcus* sp. DSM 105846 (P4) have been grown on B4, B4+Urea, YE+Urea and YE+AS. Comparing a, b and c in Figure 13, for all tested strains (*A. crystallopoietes* P-21, *A. crystallopoietes* DSM 20117,) and *Micrococcus* sp. DSM 105846), it is observed that although YE+AS ($(NH_4)_2SO_4$) had high product formation, this was mostly organic compounds, as the peaks are at low degrees of 2θ graph and are also distributed, thus suggesting the presence of biomass.

A. crystallopoietes P-21 (P3) grown in YE+Urea medium produced cancrinite (Figure 13a). Cancrinite is a complex carbonate and silicate of sodium, calcium and aluminium with the formula $Na_6Ca_2[(CO_3)_2|Al_6Si_6O_{24}]\cdot 2H_2O$ and hardness around 5-6 in Mohs scale. Furthermore, *A. crystallopoietes* P-21 grown in B4+Urea produced very clear peaks of hydroxyapatite, which was produced in the highest amount among the three strains. *A. crystallopoietes* P-21 grown in B4 media showed clear peaks of calcite ~12 times more intense than in CCP media.

The most interesting result of this experiment was the growth of *A. crystallopoietes* DSM 20117 (L1). As mentioned above, *A. crystallopoietes* DSM 20117 produced the highest amount of calcite when it was grown in CCP media. When the strain grew in

B4 media it produced ~ 5.3 times more product. That product was clear weddellite in XRD analysis (Figure 13b). This crystallizes in a tetragonal system: the classic crystal shape is the eight-face bipyramid and it has hardness 4 in Mohs scale. When *A. crystallopoietes* DSM 20117 was grown on YE+urea, low amounts of halite were observed, while growth in B4+urea resulted in very low, almost negligible, amounts of hydroxyapatite. *A. crystallopoietes* DSM 20117 grown in YE+$(NH_4)_2SO_4$ medium did not produce any precipitation that could be analyzed with XRD, showing a negative reaction of the strain in ammonium sulfate; this shows that although the strain can follow urease activity pathway to produce energy and $CaCO_3$, on the other hand, ammonium ions from ammonium sulfate cannot be incorporated into amino acids, nucleotides and other cellular components, contributing to cellular growth and energy production through metabolic pathways like the tricarboxylic acid (TCA) cycle and oxidative phosphorylation. *Micrococcus* sp. DSM 105846 (P4) strain when grown in B4+Urea medium showed high concentration of hydroxyapatite together with vaterite. Growth in YE+Urea showed no peaks, while growth in B4 media produced calcite and vaterite, which was ~11 times more than that produced when the CCP medium was used.

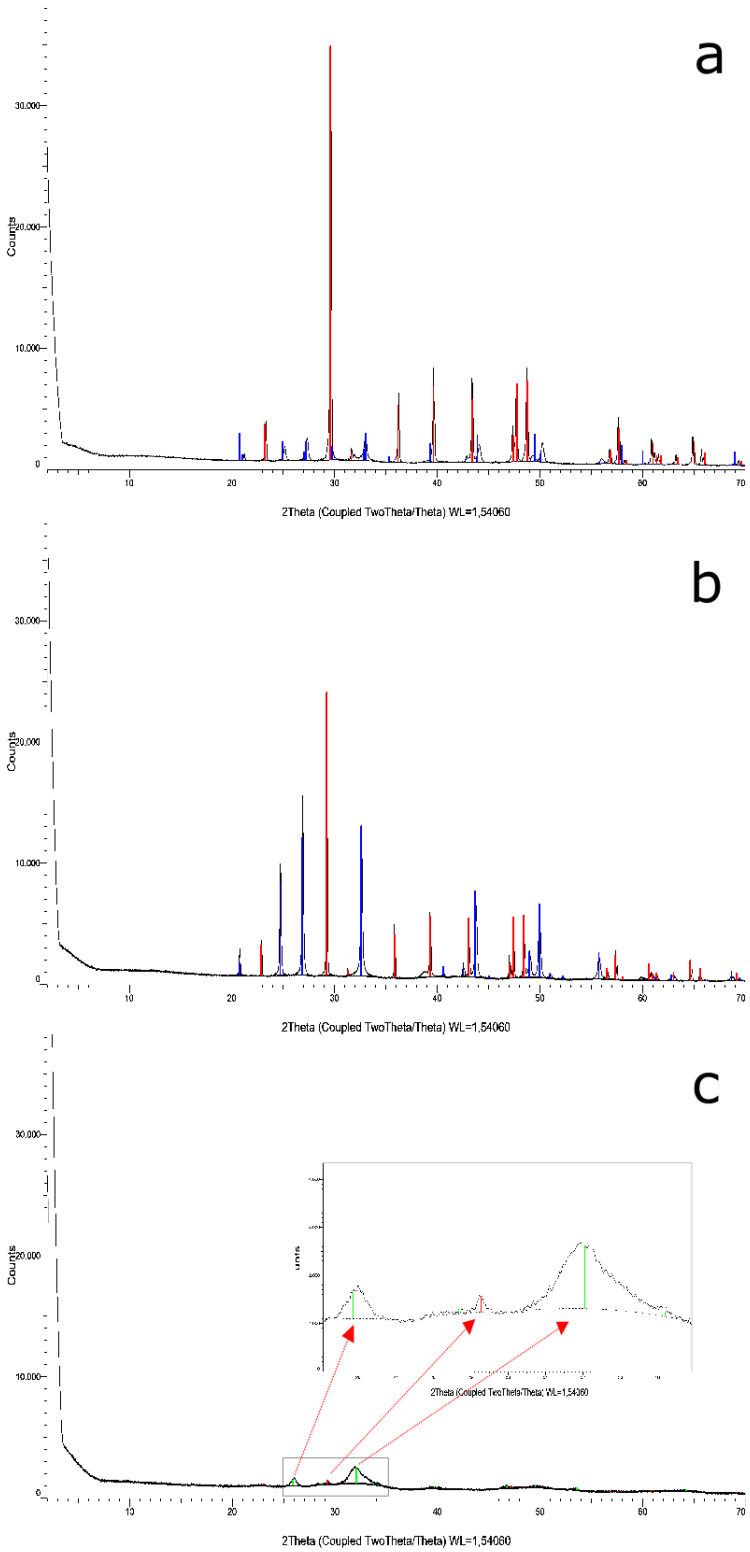

Figure 12: XRD analysis of CaCO3 product collected by A. crystallopoietes DSM 20117 (a), B. licheniformis PP1 (b) and Micrococcus sp. DSM 105846 (c). Red, blue, and green peaks represent calcite, vaterite and hydroxyapatite crystals, respectively.

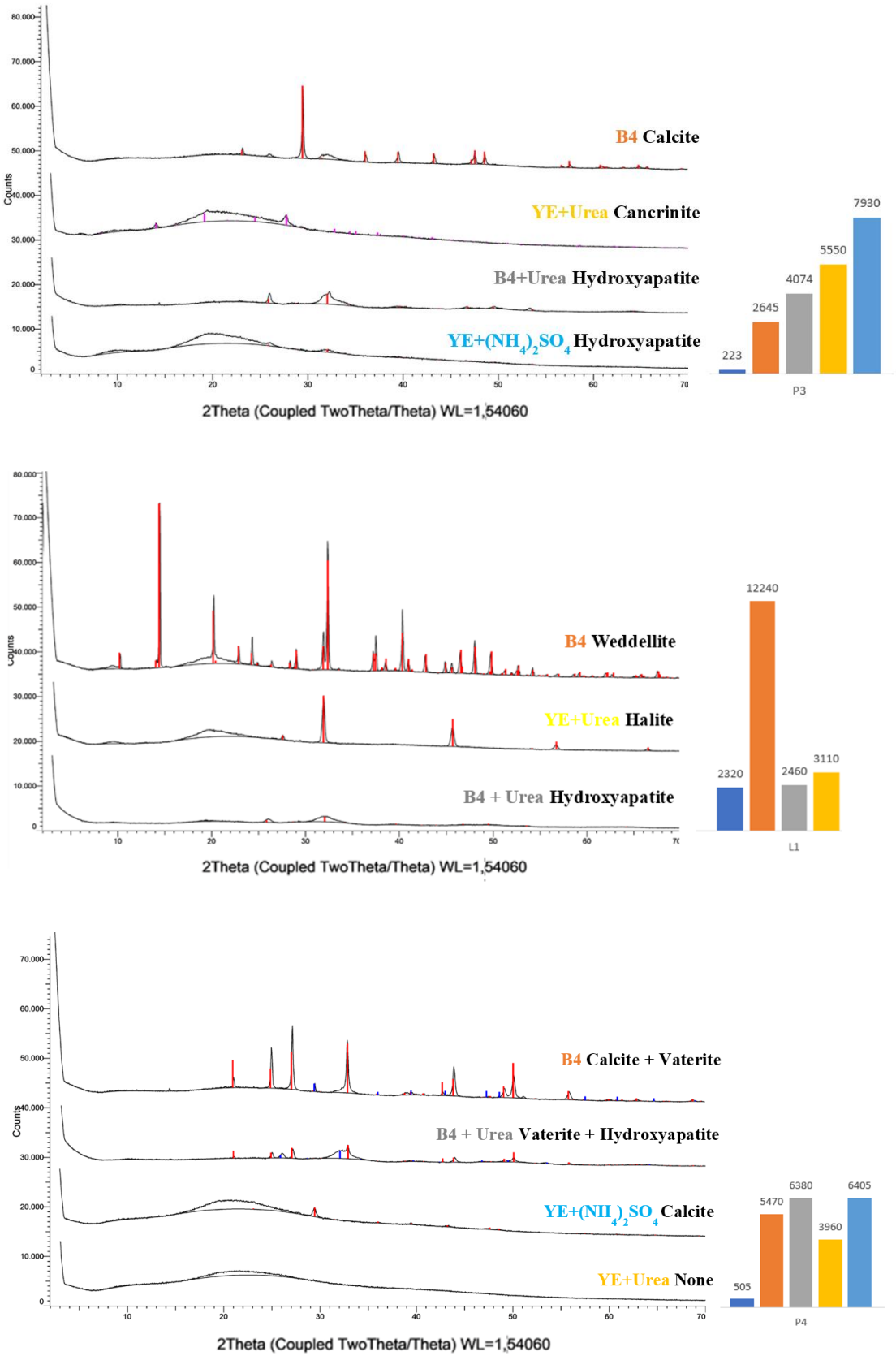

Figure 13: XRD analysis of product collected by (a) A. crystallopoietes P-21, (b) A. crystallopoietes DSM 20117 and (c) Micrococcus sp. DSM 105846. Blue, orange, gray, yellow and sky blue peaks represent product formation (mg/L) in medium CCP, B4, B4+Urea, YE+AS and YE+Urea, respectively.

When the CCP media was used, the $CaCO_3$ crystals of *A. crystallopoietes* DSM 20117 and *B. licheniformis* PP1 strain, which showed higher abundance of $CaCO_3$ polymorphs compared to *Micrococcus* sp. strain, were further investigated using SEM. The aim was to acquire valuable information on the morphological characteristics of the different polymorphs detected through XRD analysis. SEM images of the samples at various magnifications are presented in Figure 14. For *A. crystallopoietes* DSM 20117, SEM images indicated different crystal sizes of calcite and vaterite (Figure 14a & b). Calcite appears in the form of irregular, plate-like or rhombohedral crystals, while vaterite crystals show a characteristic spherical morphology. *B. licheniformis* PP1 produced similar sized crystals of calcite and vaterite (Fig. 14c & d). However, *A. crystallopoietes* DSM 20117 produced larger crystals than *B. licheniformis* PP1 strain (compare Figures 14 a,b with c,d).

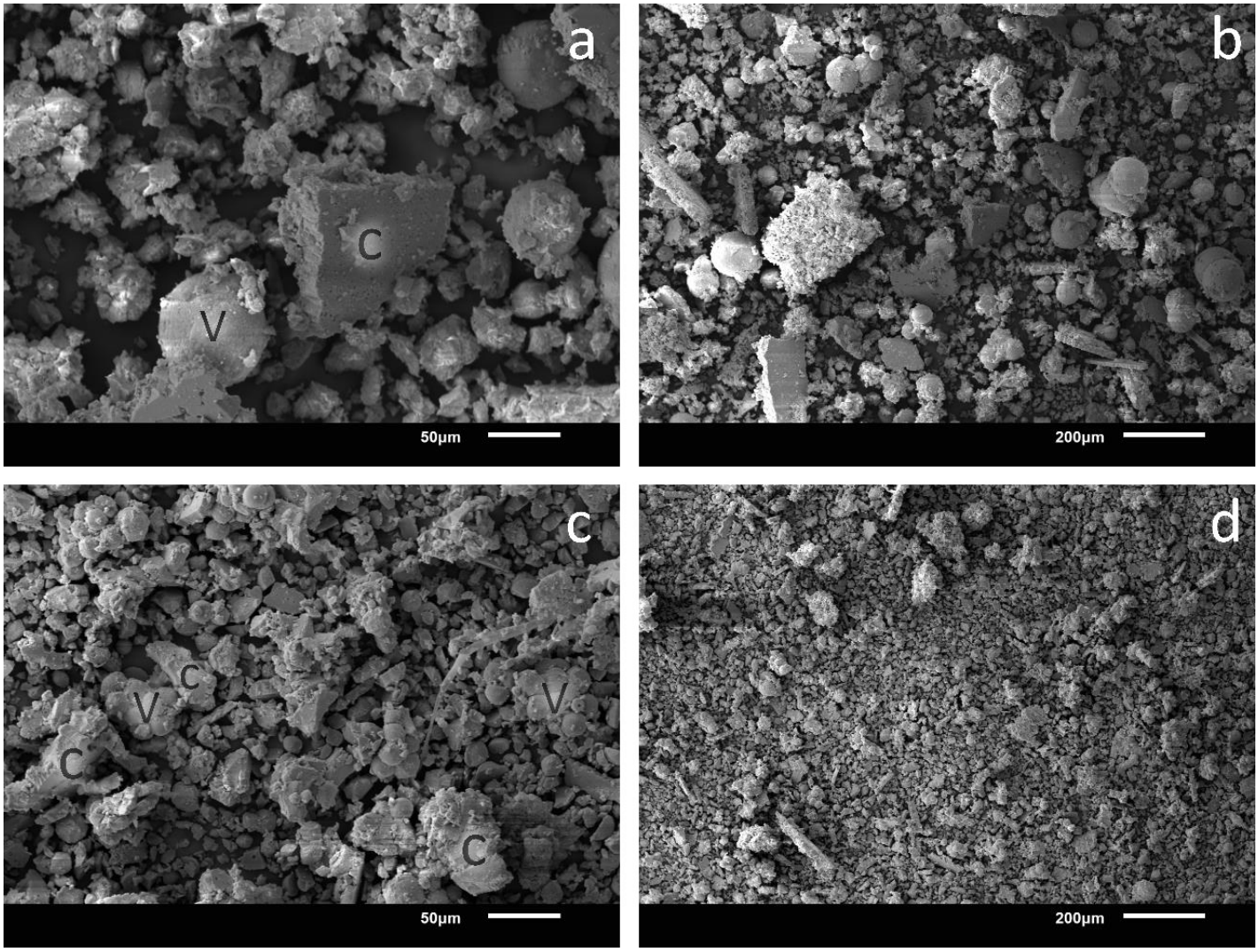

Figure 14: SEM images showing calcite and vaterite crystals produced by A. crystallopoietes DSM 20117 (a, b) and B. licheniformis PP1 (c, d) at higher (left) and lower (right) magnifications (C: calcite, V: vaterite).

3.6 Evaluation of stone biological treatment

Explanation

Two biological treatments were performed using Lympia (LYM) and Gerolakkos (GER) stones. In the first one, the *A. crystallopoietes* DSM 20117 grown in CCP medium was used, which produced the highest $CaCO_3$ amount identified as calcite. The second treatment was the optimization step following growth in different media (i.e. B4, B4+urea, YE+AS, YE+urea). The growth in different media showed promising results in terms of product quantity and quality about *A. crystallopoietes* DSM 20117 and *A. crystallopoietes* P-21 grown in B4. Furthermore, *Micrococcus sp*. DSM 105846 grown in B4+Urea was used because it produced considerable amounts of hydroxyapatite, which may be promising compound for consolidation.

In the first treatment, the specimen of each stone was separated in two areas, control and treated. In the treated area 3-4ml of *A. crystallopoietes* DSM 20117 strain grown with CCP media at OD=0,1 was brushed every 24h for 15 days.

For the optimization treatment, the specimens of each stone were separated in three areas, control and two treated. The control area was treated with sterilized B4 medium to observe if the medium alone is involved in consolidation. In both specimens, the middle area was B4 with *A. crystallopoietes* DSM 20117, whereas the third part in Specimen 1 was *A. crystallopoietes* P-21 with B4; in Specimen 2 *Micrococcus sp*. DSM 105846 with B4+Urea was used for 5 days, followed by *A. crystallopoietes* P-21 with B4 use for another 10 days.

3.6.1 Resistance to water penetration

The Karsten Tube and Contact Angle tests were performed to evaluate the water absorption resistance of the treated and un-treated (i.e. control) areas of LYM and GER stone.

3.6.1.1 Karsten Tube

3.6.1.1.1 Lympia (LYM) stone

In the first treatment, the results regarding the CCP media treatment were significant. The non-biologically treated area (LYMC) showed an absorption of 0.227 ml/min, while the biologically treated area (LYMT) had a significantly lower absorption of 0.121 ml/min. The coefficient of determination (R^2) was higher than 0.99, for both the treated and the non-treated area (Figure 15). Notably, the results showed that the absorption rate of the LYMT area was 47% lower than that of the control area.

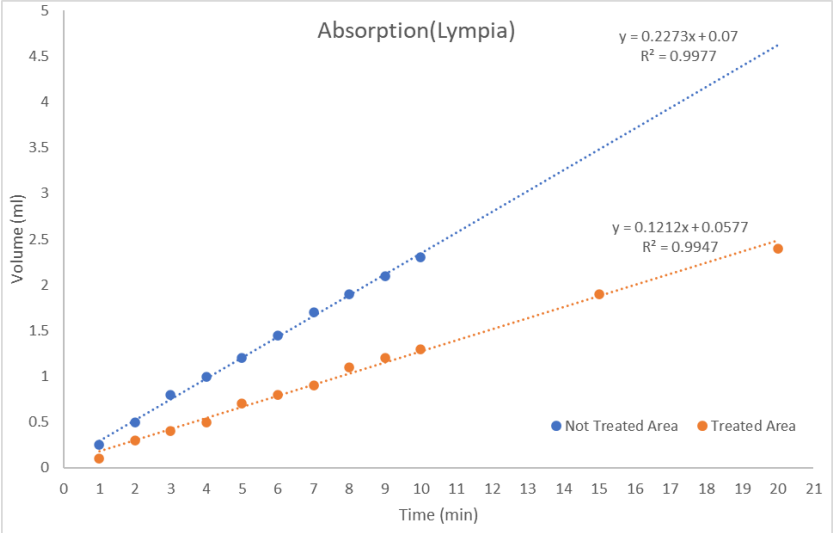

Figure 15: Karsten tube test results for the non-treated and treated areas of LYM specimen treated with CCP medium and A crystallopoietes DSM 20117.

In the optimization treatment (Figure 16), LYM specimen 1 control area tested with B4 media had an average absorption of 0.2414 ml/min and coefficient of determination (R^2) >0.99; thus, not showing any affection from B4 medium, when compared with LYMC treated with CCP media above. *A. crystallopoietes* DSM 20117 (L1) treated area had 0.0142 ml/min absorption rate and $R^2 > 0.99$. *A. crystallopoietes* P-21 (P3) treated area had 0.0071 ml/min and R^2 >0.99 (Figure 16). After the treatment, DSM 20117 (L1) and P-21 (P3) area had 1 and 2 orders of magnitude lower water absorption, compared to the control area.

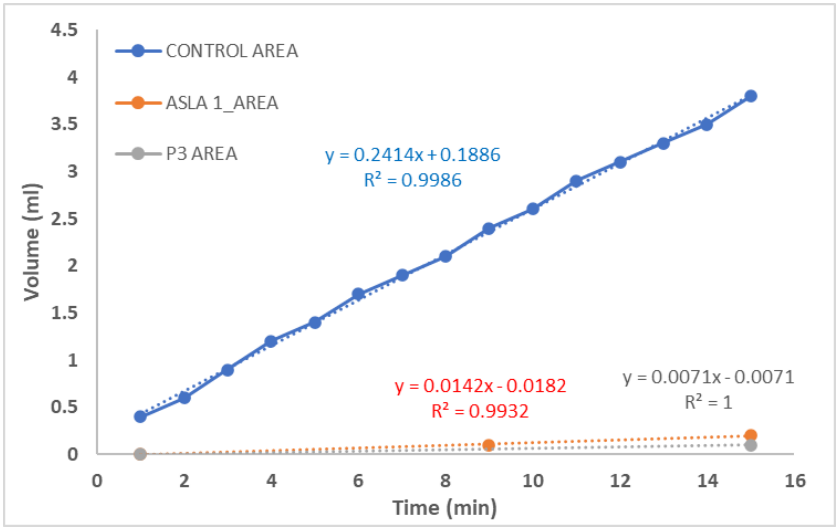

Figure 16: Karsten tube test results of LYM stonefor Specimen 1 optimization test with B4. ASLA1: A. crystallopoietes DSM 20117, P3+P4: A. crystallopoietes P-21 + Micrococcus sp. DSM 105846.

LYM specimen 2 control area brushed with B4 medium had an average absorption of 0.2211 ml/min and coefficient of determination R^2 >0.99; thus, not showing any significant affection from B4 medium, when compared with LYMC which was not treated with pure medium. *A. crystallopoietes* DSM 20117 (L1) treated area had 0.0165 ml/min absorption rate and R^2 > 0.99. *A. crystallopoietes* P-21 (P3) + *Micrococcus sp*. DSM 105846 (P4) area had 0.0319 ml/min and R^2 >0.99 (Figure 17). After the treatment, *A. crystallopoietes* DSM 20117 (L1) and *A. crystallopoietes* P-21 (P3) + *Micrococcus sp*. DSM 105846 (P4) area had one order of magnitude lower water absorption rate, compared to the control area.

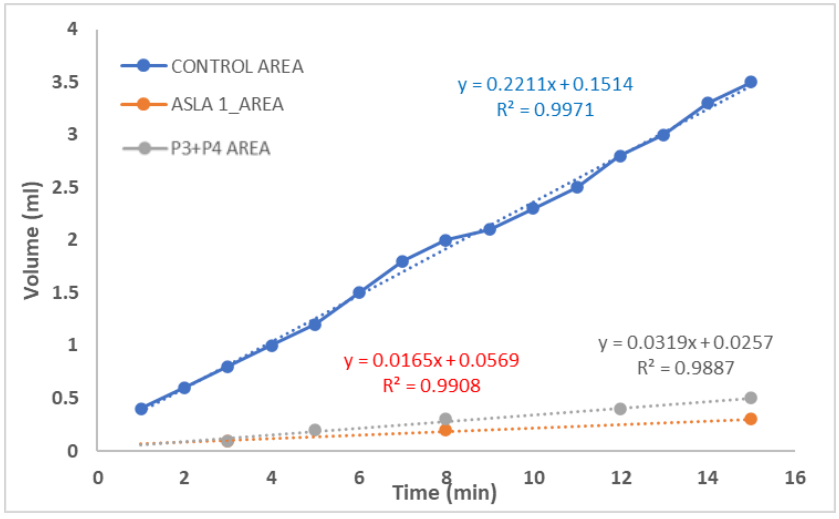

Figure 17: Karsten tube test results of LYM stone for Specimen 2 optimization test with B4. ASLA1: A. crystallopoietes DSM 20117, P3: A. crystallopoietes P-21

3.6.1.1.2 Gerolakkos (GER) stone

In the first GER stone treatment, there were no results for Karsten tube tests, because absorption was instantaneous when the sample was treated with CCP medium. On the contrary, GER stone was consolidated in the optimisation treatment, using B4 medium. GER Specimen 1 control area had an average absorption of 2.77 ml/min and coefficient of determination (R^2) >0.90. In this treatment, the absorption was not instantanous. Most probably this was due to the B4 medium treatment without strain, thus showing that the medium also affects the stone's absortion rate. *A. crystallopoietes* DSM 20117 (L1) area had 0.31ml/min absorption rate and $R^2 > 0.76$. *A. crystallopoietes* P-21 (P3) area had 0.14 ml/min and R^2 >0.85 (Figure 18). After the treatment, DSM 20117 and P-21 area had 8.9 and 19.8 times less water absorbed than the control area.

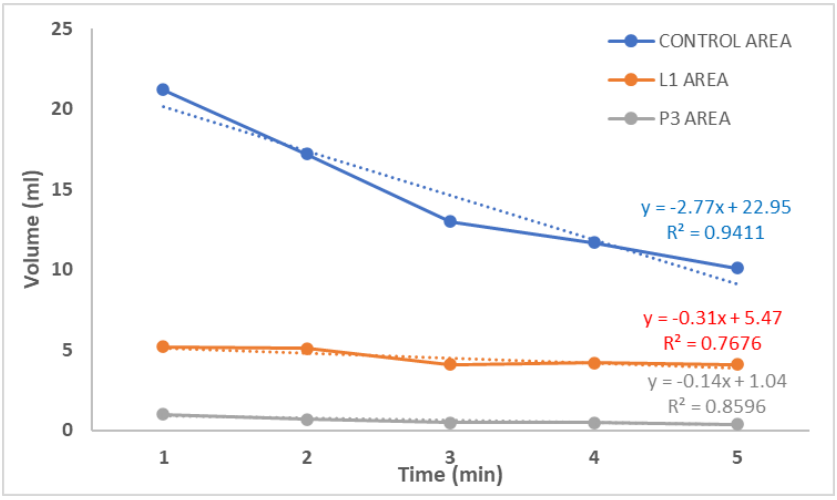

Figure 18: Karsten tube test results of GER stone for Specimen 1 optimization test with B4 medium. L1: A. crystallopoietes DSM 20117, P3: A. crystallopoietes P-21.

GER specimen 2 control area (Figure 19) had average absorption of 2.37 ml/min and a coefficient of determination (R^2) > 0.89, also showing an effect due to B4 medium. *A. crystallopoietes* DSM 20117 (L1) area had 0.37 ml/min absorption rate and $R^2 > 0.90$. *A. crystallopoietes* P-21 (P3) + *Micrococcus sp*. DSM 105846 (P4) area had 0.33 ml/min absorption and R^2 >0.94. After the treatment, *A. crystallopoietes* DSM 20117 (L1) and *A. crystallopoietes* P-21+*Micrococcus sp*. DSM 105846 (P4) area had 6.4 and 7.18 times lower water absorption rate, respectively, compared to the control area. This shows that treatment with just *A. crystallopoietes* P-21 worked better for 15 days than

together with *Micrococcus sp*. DSM 105846 (P4), when comparing treatments in specimen 1 and 2.

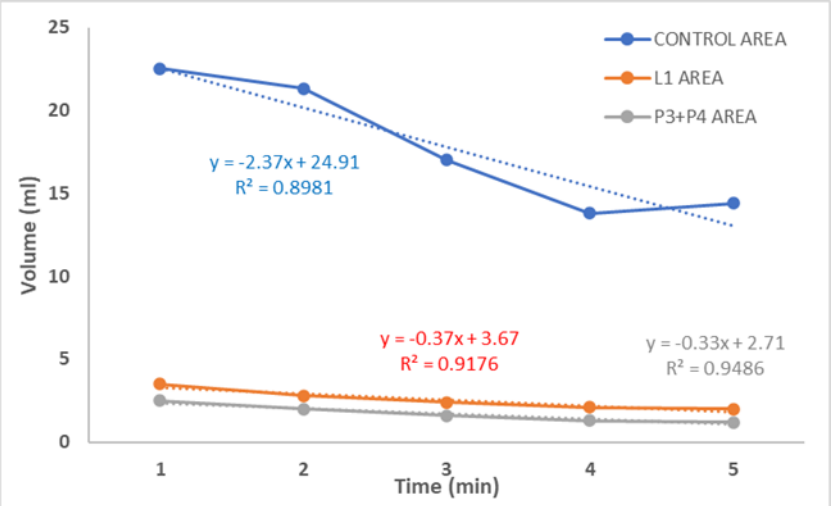

Figure 19: Karsten tube test results of LYM stone for Specimen 2 optimization with B4 medium. L1: A. crystallopoietes DSM 20117, P3+P4: A. crystallopoietes P-21 + Micrococcus sp. DSM 105846.

The above results show that, in both stones, treatment with *A. crystallopoietes* P-21 strain in B4, which produces calcite and vaterite, is the most promising (Figure 20a, b). Furthermore, comparing the first (with CCP medium) and the optimization (with B4 medium) treatment, B4 shows better results. In the case of LYM stone (Figure 20a), it was noted that the B4 medium yielded superior results across all three distinct stone areas. Particularly noteworthy was the heightened efficacy observed in the region treated with *A. crystallopoietes* P-21 (P3), followed by *A. crystallopoietes* DSM 20117 (L1), with the least favorable outcome observed in the area treated with *A. crystallopoietes* P-21 (P3) along with *Micrococcus* sp. DSM 105846 (P4).

In GER stone (Figure 20b), CCP treatment was not feasible due to its instantaneous absorption. However, with the B4 treatment, *A. crystallopoietes* P-21 (P3) exhibited the lowest absorption rate compared to the control area, followed closely by the other two treated areas (with *A. crystallopoietes* DSM 20117 (L1) and *A. crystallopoietes* P-21 (P3) + *Micrococcus* sp. DSM 105846 (P4)), whereby the results were relatively comparable.

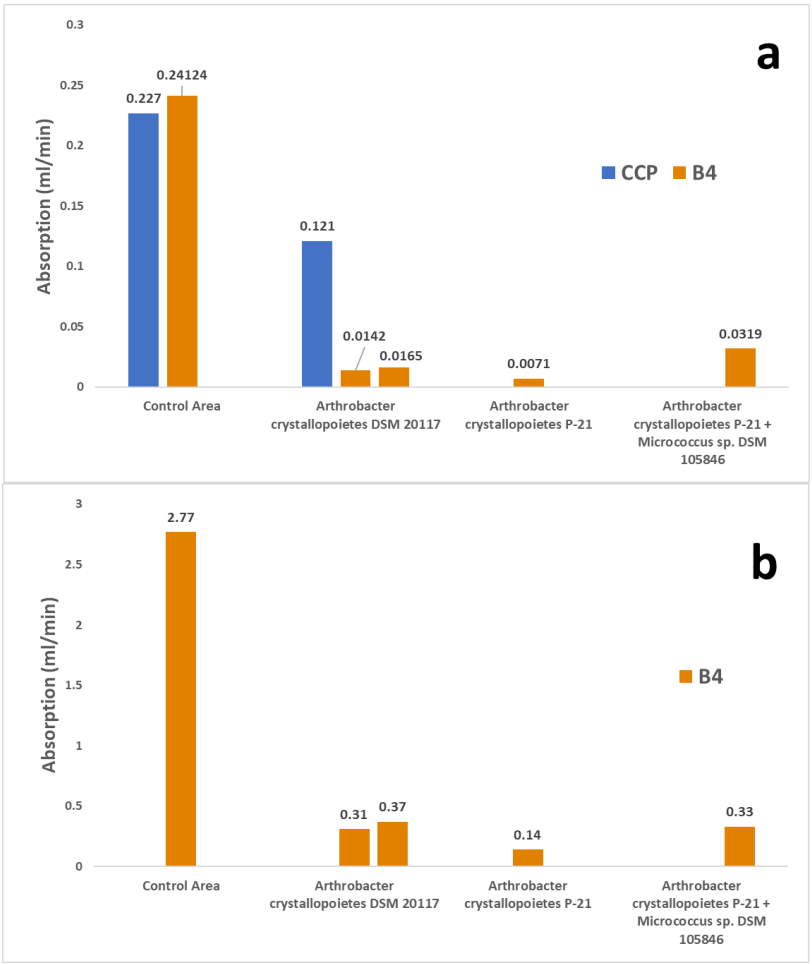

Figure 20: Karsten tube test absorption results for a) LYM stone b) GER stone with CCP and B4 medium.

3.6.1.2 Contact Angle

3.6.1.2.1 Lympia (LYM) stone

Regarding the results of the contact angle test after treatment with CCP medium and *A. crystallopoietes* DSM 20117, both LYMC and LYMT followed a linear progression of water droplet volume decrease over time (Figure 21A). However, LYMC had an initial contact angle of 50°, while LYMT initial angle was 85°. Among the triplicates tested (Appendix Figure 29B), LYMC took around 2 seconds to absorb the droplet, with an average absorption rate of 1.46 µl/sec. The average absorption rate of LYMT was 0.29 µl/sec, thus indicating an 80% reduction compared to the non-treated area. For the LYMT area, none of the droplets were fully absorbed within the first 6 seconds, which was the duration that the measurements lasted.

Among the treatment areas investigated in the optimization step with B4 medium (Figure 22), the most effective alteration in surface properties was observed in the region treated with *A. crystallopoietes* DSM20117 (L1), where the initial average contact angle increased to 80.6 degrees, accompanied by a substantial reduction in the average absorption rate to 0.062 µl/sec. Comparatively, this represents a remarkable decrease in absorption compared to the control area, with the treatment exhibiting approximately 28 times lower absorption. The other treatment areas also demonstrated notable improvements, such as *A. crystallopoietes* P-21 (P3) with a 76.4 degrees initial average contact angle and an average absorption rate of 0.166 µl/sec, with 2.7 times higher absorption rate, compared to the *A. crystallopoietes* DSM20117 (L1) treatment. Furthermore, the combined treatment area with *A. crystallopoietes* P-21 (P3) and *Micrococcus* sp. DSM 105846 (P4), showing an average contact angle of 76.5 degrees and an average absorption rate of 0.072 µl/sec, still exhibited 1.13 times higher absorption rates compared to the *A. crystallopoietes* DSM20117 (L1) treatment. These findings highlight the superior efficacy of the *A. crystallopoietes* DSM20117 (L1) treatment with B4 medium in reducing absorption and modifying the surface properties of LYM stone.

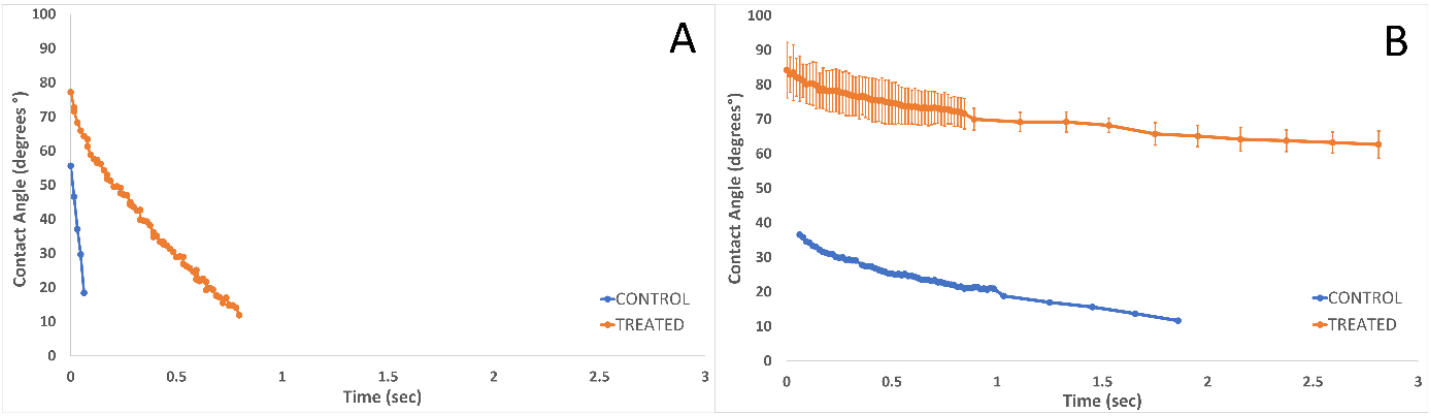

Figure 21: Contact angle test results comparing the control and the biologically treated areas of GER and LYM stones. The test was conducted in three replicates and standard deviation was determined for both the control and the treated area.

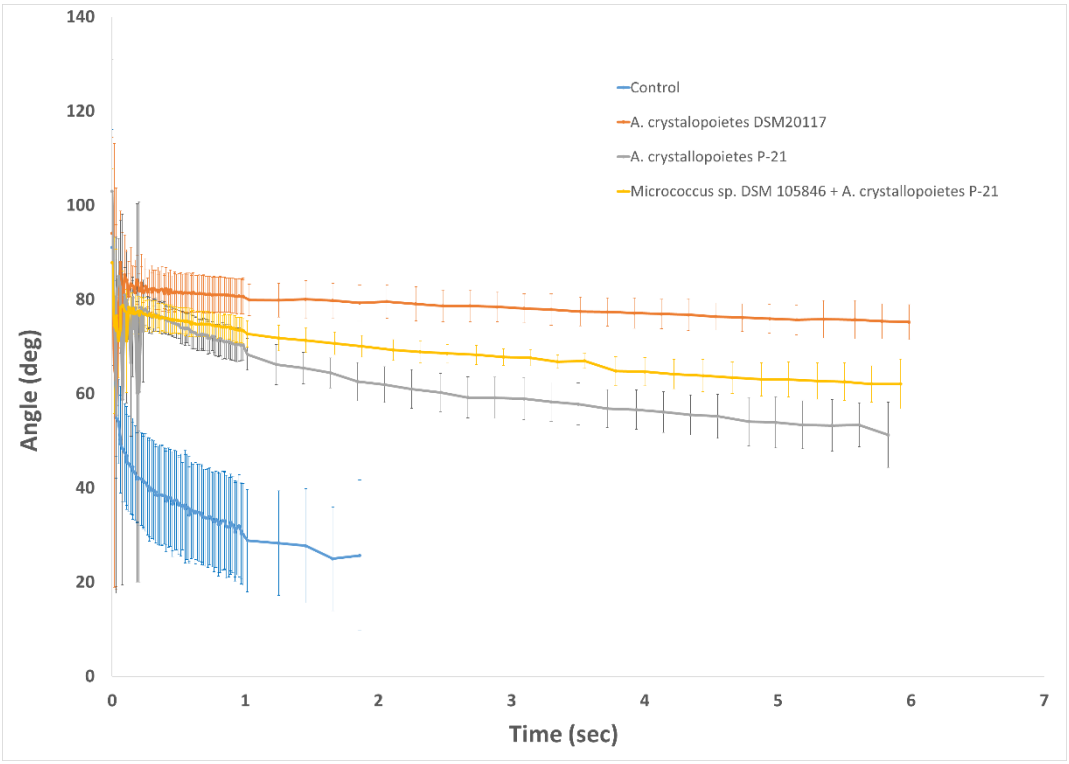

Figure 22: Contact angle test results for B4 medium comparing the control and the biologically treated areas of LYM stone. The test was conducted in three replicates and standard deviation was determined for both the control and the treated area.

3.6.1.2.2 Gerolakkos (GER) stone

Regarding the results of contact angle tests in GER stone treated with CCP medium and *A. crystallopoietes* DSM 20117, among the triplicates tested with the optical contact angle goniometer (Figure 21A and Appendix Figure 29), the control area of GER stone (GERC) showed a hydrophilic behavior, absorbing the 4 μl droplet in around 0.10 sec, with an average absorption rate of 34.74 μl/sec. The absorption rate of the biologically treated GER specimen area (GERT) was on average 5.14 μl/sec; this is 85% slower compared to the non-treated area. The contact angle had an initial value around 55 º and 75 º for GERC and GERT, respectively.

Following the optimization, the results of contact angle tests on the samples treated with B4 medium (Figure 23 and Appendix Figure 30), showed again hydrophilic behaviour for the control area of GERC with absorption of one droplet in around 0.10 sec, with an average absorption rate of 34.74 μl/sec, the same as the GERT treated with CCP medium (compare Figure 21B and 23). Thus, GER was not affected by the pure B4 treatment used in the control area.

In Figure 23, the absorption rate of the *A. crystallopoietes* DSM 20117 (L1) biologically treated area showed an increase from an initial value of 50-60 º up to 90 º. Also, the water absorption rate dropped at an average to 1.12 μl/sec, which is 34 times less than the average of the control area. For *A. crystallopoietes* P-21(P3) treated with B4, the initial contact angle of an average 55 º increased to an average 80 º and the water absorption rate of the droplet decreased to an average of 0.80 μl/sec, which is 43 times lower than the control area and 1.4 times lower than *A. crystallopoietes* DSM 20117 (L1) area.

In Specimen 2, *A.crystallopoietes* P-21 + *Micrococcus* sp. DSM 105846 showed a water absorption rate of the droplet of 1.81 μl/sec (Figure 23), which is 19 times less than that of the control area and 1.6 times more than *A. crystallopoietes* P-21 (P3) area. This confirms that treatment with sole *A. crystallopoietes* P-21 (P3) is more efficient compared to the combination of microorganisms. The initial contact angle of an average 55º increased to an average 80º.

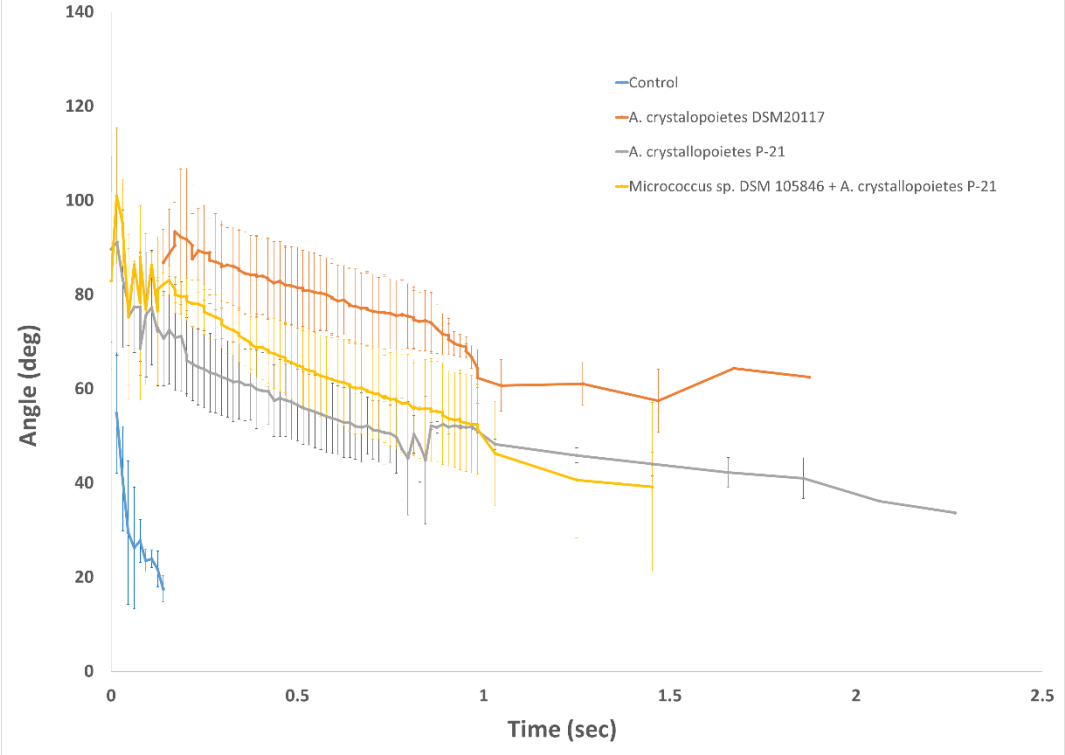

Figure 23: Contact angle test results in B4 medium comparing the control and the biologically treated areas of GER stone. The test was conducted in three replicates and standard deviation was determined for both the control and the treated area.

3.6.2 Drilling Resistance Measurements

The drilling resistance test was performed to evaluate the effectiveness and depth of the MICP in the first and optimization treatment, for both stones. The location of the drilling holes was selected to be as far as possible from the centre of the specimen, where there was a higher possibility of the medium penetrating from the treated area to the control area due to capillary movement (Figure 24).

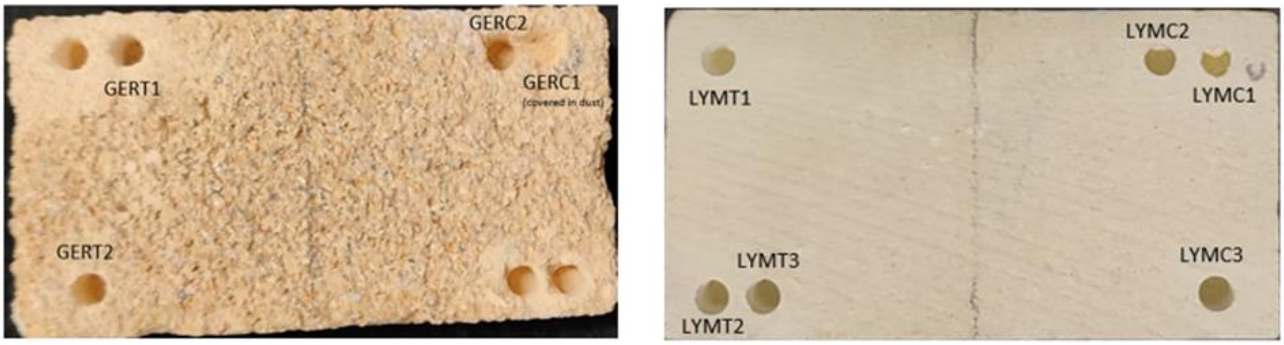

Figure 24: DRMS test holes positions for GER (left) and LYM (right) stones. The dimensions of treated (T) and control (C) area is 4x4x4.5cm, respectively.

3.6.2.1 Gerolakkos (GER) stone

For GER stone, a total of four holes were drilled in the GERC area; however, only two of them were deemed representative of the sample (Figure 24), In the first treatment, the GERC area had an average drilling resistance of 0.87 N. The GERT area showed a noticeable increase in the drilling resistance, reaching an average of 1.48 N, which suggests a 58.8% increase compared to the non-treated area (Figure 25A). Due to the inherent inhomogeneity of the GER stone, which often results in misleading drilling resistances (e.g., when the drilling head encounters quartz grains, which are significantly harder compared to the other constituent minerals), an unrealistically high drilling resistance could be reported. Thus, further optimization experiments are deemed necessary.

For the optimization treatment with B4 medium, GERC had an average drilling resistance of 0.60N (Figure 26). *A. crystallopoietes* DSM 20117 (L1), *A. crystallopoietes* P-21 (P3) and *A.crystallopoietes* P-21 (P3) + *Micrococcus* sp. DSM 105846 (P4) strain treatment area led to drilling resistances of 1.32 N, 1.13 N and 1.30 N, respectively. The percentage of increase in drilling resistance for *A. crystallopoietes* DSM 20117 (L1), *A. crystallopoietes* P21(P3) and *A. crystallopoietes* P21(P3) + *Micrococcus* sp. DSM 105846 (P4), compared to the average control area, was 122%, 90% and 118%, respectively.

In terms of GER drilling resistance, the difference in the results between the different strains and strain combinations is not significant, although treatment with *A. crystallopoietes* DSM 20117 (L1) seems to accomplish higher drilling resistance compared to the other two.

Compared to the CCP media treatment in GER stone, treatment with B4 showed more significant increase but, to be absolute, the two GER stones cannot directly be compared because, as aforementioned, this stone consists of relatively large biogenic and silicate grains, loosely bound together by micro-sparry and sparry calcite and dispersed quartz deposits which can differentiate the drilling resistance and the compressive strength.

3.6.2.2 Lympia (LYM) stone

Three holes were drilled on each side of the LYM limestone specimen (Figure 24). In the first treatment, LYMC had an average overall drilling resistance of 1.43 N, while

the respective average value of LYMT was 1.60 N, thus presenting an increase of 11.89% (Figure 25). Interestingly, Figure 25B shows a much more notable increase in drilling resistance within the first 0-500 μm of depth, where the average of the three holes was 1.13 N and 1.86 N for the LYMC and the LYMT area respectively, showing a significant localized increase of 64.89% in the treated area.

In our investigation, LYM stone treated with the B4 medium displayed notable results, as illustrated in Figure 27. The control area treated with pure B4 medium exhibited an average drilling resistance of 2.50 N. Meanwhile, the *A. crystallopoietes* DSM 20117 (L1) area showed an average drilling resistance of 2.54 N, while the *A. crystallopoietes* P-21 (P3) area recorded an average of 2.47 N. Additionally, the combined treatment area of *A. crystallopoietes* P-21 (P3) and *Micrococcus* sp. DSM 105846 (P4) displayed an average drilling resistance of 2.49 N. Notably, the overall average drilling resistance across the three treatment areas was similar. However, distinct variations emerged when considering the depth within the first 0-500 μm.

In this context, the *A. crystallopoietes* DSM 20117 (L1) area exhibited a notable increase in drilling resistance to 3.1 N, compared to the control area. Similarly, the *A. crystallopoietes* P-21 (P3) area displayed a drilling resistance of 2.64 N, while the combined treatment area showed a resistance of 2.85 N. These values signify percentage increases of 72%, 46%, and 58%, respectively, compared to the average drilling resistance of the control area within the first 0-500 μm. These findings underscore the significant impact of treatment on drilling resistance within LYM stone, particularly evident at shallow depths, thereby highlighting the efficacy of tailored treatments in modifying surface properties.

In terms of LYM drilling resistance, the difference in the results between the different strains and strain combinations shows higher drilling resistance when *A. crystallopoietes* DSM 20117 (L1) with B4 is used for treatment compared to the other two strains.

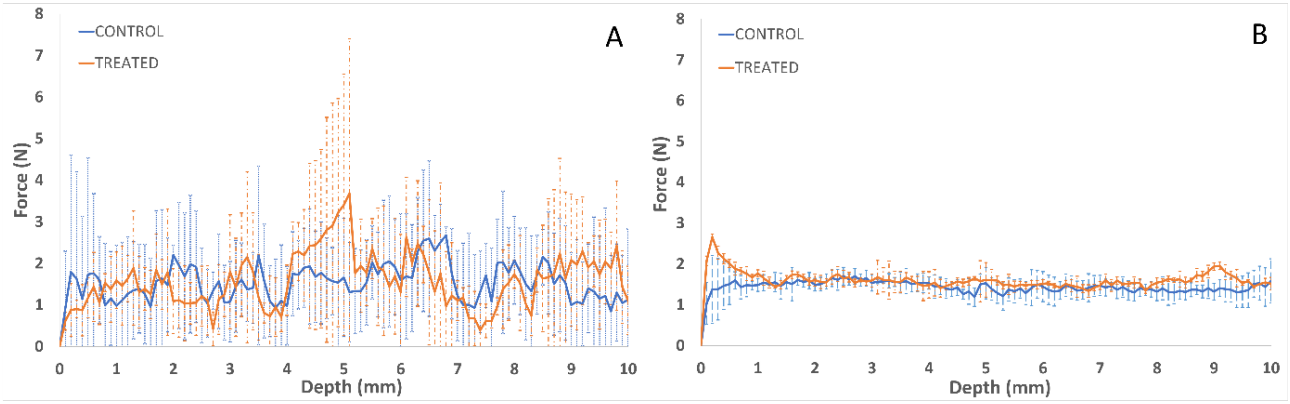

.

Figure 5: DRMS results comparing the control and the biologically treated areas with CCP medium of GER (A) and LYM (B) stone

.

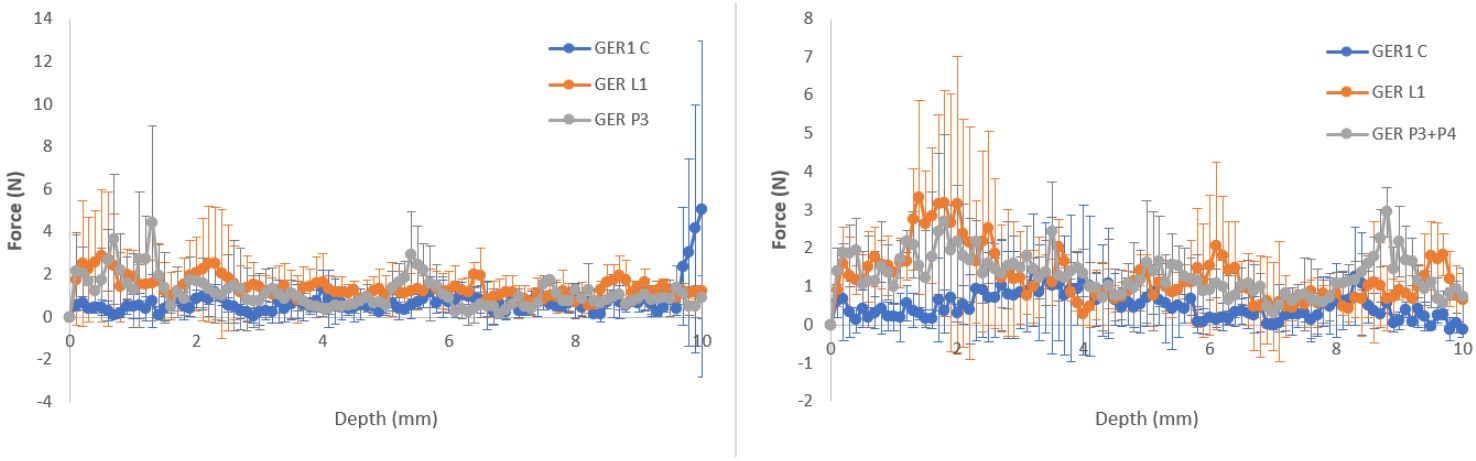

Figure 266: DRMS results comparing the control and the biologically treated areas with B4 medium of GER specimen 1 (left) and GER specimen 2 (right). L1: A. crystallopoietes DSM 20117, P3+P4: A. crystallopoietes P-21 + Micrococcus sp. DSM 105846.

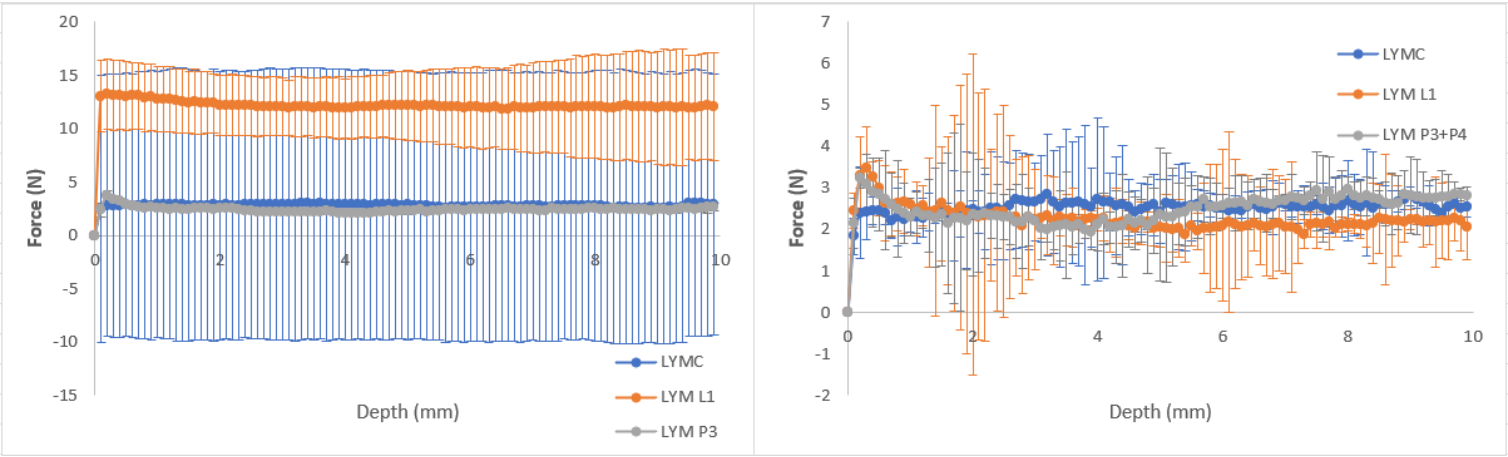

Figure 277: DRMS results comparing the control and the biologically treated areas with B4 medium of LYM specimen 1 (left) and LYM specimen 2 (right). L1: A. crystallopoietes DSM 20117, P3+P4: A. crystallopoietes P-21 + Micrococcus sp. DSM 105846

3.6.3 Scratch Test

The Scratch test served as a complement to the DRMS test for estimating the treatment depth. In this test, the specimen was scratched across both the control and treated areas, aiming to reveal increased forces indicative of stone consolidation by microbial products. Tangential (Ft) and normal (Fn) forces acting on the cutter were recorded, with only Fn utilized for analysis.

3.6.3.1 Gerolakkos (GER) stone

In the first treatment, (Figure 32) in the case of GER stone, characterized by quartz and large biogenic and silicate grains loosely bound together, variations in results between the two areas were insignificant. Therefore, ANOVA analysis was employed to ascertain the treatment's significant impact on the stone.

The statistical analysis revealed a significant difference in Fn between the GERC and GERT areas (P-value < 0.01) at depths of 0.5 and 0.75 mm. The most substantial increase occurred at 0.75 mm, with average Fn 21.5% increase than the GERC area in the same depth, with P-value less than $1x10^{-7}$.

During the optimization treatment, (Figure 34) all test depths (0.05, 0.15, 0.3, 0.5, 0.75, 1.05 mm) were statistically significant (P-value < 0.01). Treatment with *A. crystallopoietes* P-21 + *Micrococcus* sp. DSM 105846 showed the most significant improvement at 0.05 mm, followed by depths of 0.15 mm, 0.3 mm, and 0.5 mm, with increases in depth of 0.05 mm being 403%, 184%, 134%, and 84%, respectively. Improvement was observed up to a depth of 1.05 mm, indicating more uniform treatment throughout the stone.

3.6.3.2 Lympia (LYM) stone

In the first treatment for LYM stone, (Figure 33) evaluation revealed a significant increase at depths of 0.02 and 0.03 mm between the LYMC and LYMT areas, particularly notable at 0.02 mm with Fn increases of 34.1%. This confirms the treated area increased resistance near the surface, as indicated by DRMS.

During the optimization treatment (Figure 35), all test depths (0.05, 0.15, 0.3, 0.5, 0.75, 1.05 mm) were statistically significant (P-value < 0.01). *A. crystallopoietes* P-21 exhibited approximately 16% increase across all scratch depths. *A. crystallopoietes* P-21 + *Micrococcus* sp. DSM 105846 showed increases across all depths except for 0.05 mm, with a 6% decrease and a 19% increase for all the other depths. Notably, *A. crystallopoietes* DSM 20117 displayed decreases in all areas except at a depth of 1.05 mm, which increased by 1%, with a mean increase of 3% for all the other depths.

Lympia stone results are deemed more stable and valid due to the stone's homogeneous structure. These findings affirm *A.crystallopoietes* P-21 + *Micrococcus* sp. DSM 105846 as the most effective treatment for the entire stone area.

3.6.4 SEM following biological treatment

The LYM limestone specimen under study was further characterized by SEM following biological treatment with *A. crystallopoietes* DSM 20117 when treated with CCP medium (Figure 28a, b, c). SEM was performed on representative samples taken from the top dimension of the control and biologically treated areas, as well as on a sample taken along the cross-section of the treated area. The goal was to examine the effectiveness and depth of the treatment induced by *A. crystallopoietes* DSM 20117.

The upper part of the treated area showed an evidently denser microstructure, compared to the upper part of the control area, which seemed to be more porous (compare Figure 28a with b). Thorough observations revealed that the pores were filled with calcite crystals induced by *A. crystallopoietes* DSM 20117 (see arrows in Figure 28b). In line with this finding, the cross-section of the treated specimen further confirmed a consolidation (i.e., reduction in porosity) due to the biological treatment applied; this was observed within the first ca. 350 µm from the surface of the specimen (Figure 28c), in line with the localized increase in drilling resistance noted in the DRMS results.

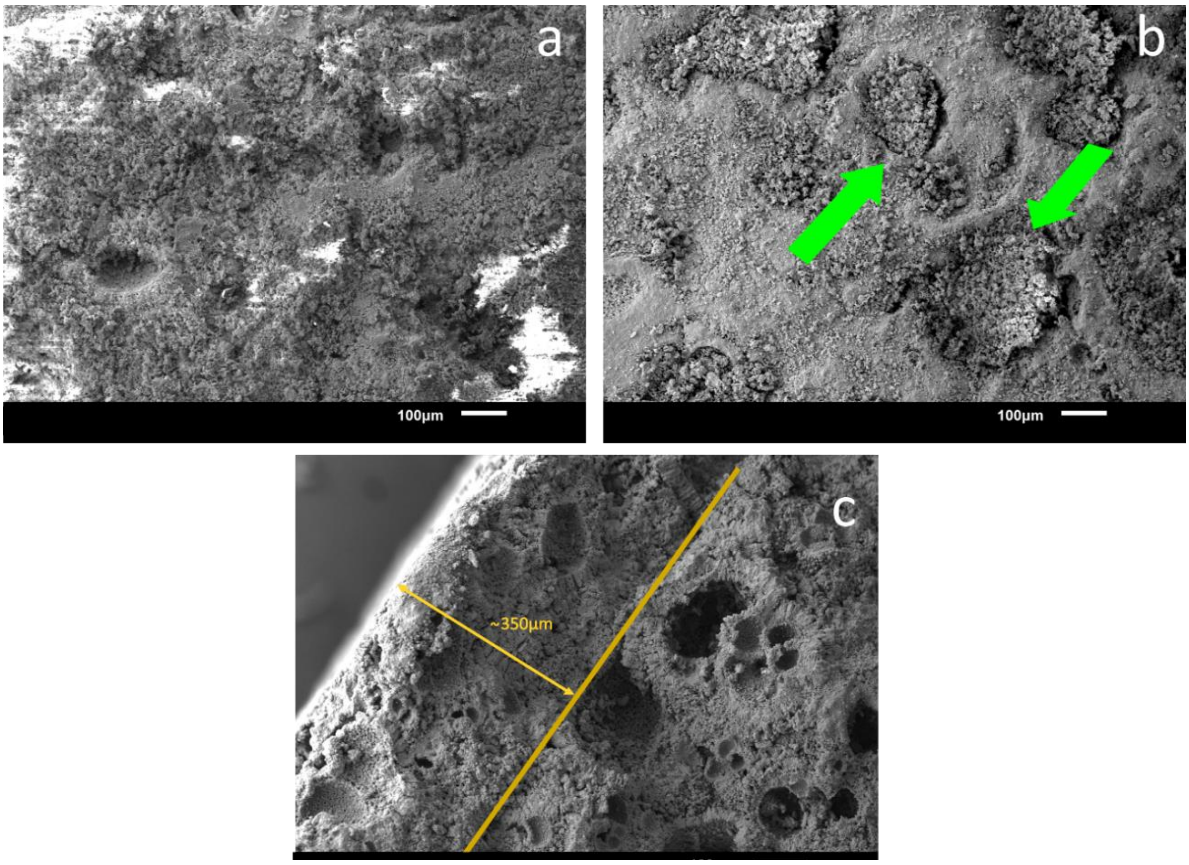

Figure 28: SEM images showing the microstructure on the top of the (a) non-treated (LYMC), and (b) treated (LYMT) area, as well as (c) along the cross-section of the treated area (LYMT).

Chapter 4: Cost Analysis

Cost analysis is shown in Tables 3 and 4. In Table 3, the cost of the medium per liter, depending on the chemical compounds of each medium, was analyzed. In Table 4, the product precipitation of the strains among the different media used for biological treatment in the current thesis were analysed and correlated with the liters of media used to precipitate 1 kg of product.

Among the five different media that have been tested, B4 is the cheapest (€2.418/Liter), while YE+Urea is the most expensive (€6.86/Liter) medium. For production of calcite + vaterite, which has shown significant result in terms of consolidation, *A. crystallopoietes* DSM 20117 (L1) in CCP media needs 431 L to produce 1 kg of $CaCO_3$ which costs €2335.5. *A. crystallopoietes* P-21 (P3) produces $CaCO_3$ in the form of calcite in B4 media requiring 378 L/kg, which costs €950. This is exactly 246% less than DSM 20117 strain. *Micrococcus* sp. DSM 105846 (P4) produces calcite with YE+AS needing 156.13 L of medium/1 kg which costs €1033.6. But from the XRD it was observed that it produced both calcite and a lot of biomass, thus this assumption is not very reliable. The most inexpensive is hydroxyapatite production/1 kg by *A. crystallopoietes* P-21 (P3) in B4+Urea, taking into consideration the purity of XRD; this is priced at €965/kg.

Table 3: Cost analysis of medium/precipitation (in euro)

Medium	Ingredients	Code Number (Sigmaaldrich)	Cost 1kg	g/500ml	g/L	Cost g/L	Cost/L of Media
CCP	Urea	U5378-1KG	142	10	20	2.84	5.418416
	Sodium Carbonate	222321-1KG	89.8	1.06	2.12	0.190376	
	Ammonium Chloride	213330-1KG	101	5	10	1.01	
	Nutrient broth	N7519-1KG	347	1.5	3	1.041	
	Calcium Carbonate dihydrate	223506-500G	76.6	2.2	4.4	0.33704	
B4	Calcium Acetate	C1000-500G	268	1.25	2.5	0.67	2.513
	Glucose	G8270-1KG	75.5	5	10	0.755	
	Yeast Extract	Y1625-1KG	272	2	4	1.088	
B4_Urea	Calcium Acetate	C1000-500G	268	1.25	2.5	0.67	3.933
	Glucose	G8270-1KG	75.5	5	10	0.755	
	Yeast Extract	Y1625-1KG	272	2	4	1.088	
YE_Urea	Urea	U5378-1KG	142	5	10	1.42	6.86
	Yeast Extract	Y1625-1KG	272	10	20	5.44	
YE_Amm.Sulfate	Urea	U5378-1KG	142	5	10	1.42	6.62
	Yeast Extract	Y1625-1KG	272	10	20	5.44	
	Ammonium Sulfate	A4915-1KG	118	5	10	1.18	

Table 4: Cost of Medium/Liter Analysis (in euro)

Microorganism	Medium	Precipitation	Amount(g/50ml)	g/ml	g/L	Liters for 1g precipitation	Liters for 1kg precipitation	Cost/1kg Product
L1	CCP	Calcite+Vaterite	0.116	0.0023	2.320	0.431	431.034	2335.524
	B4	Weddellite	0.612	0.0122	12.240	0.082	81.699	205.310
	B4_Urea	Hydroxyapatite	0.123	0.0025	2.460	0.407	406.504	1598.780
	YE_Urea	Halite	0.156	0.0031	3.110	0.322	321.543	2205.788
	YE_Amm.Sulfate	UNNONE	0.308	0.0062	6.160	0.162	162.338	1074.675
P3	CCP	Hydroxyapatite	0.011	0.0002	0.223	4.484	4484.305	24297.830
	B4	Calcite	0.132	0.0026	2.645	0.378	378.072	950.095
	B4_Urea	Hydroxyapatite	0.204	0.0041	4.074	0.245	245.459	965.390
	YE_Urea	Cancrinite	0.278	0.0056	5.550	0.180	180.180	1236.036
	YE_Amm.Sulfate	Hydroxyapatite	0.397	0.0079	7.930	0.126	126.103	834.805
P4	CCP	Hydroxyapatite	0.025	0.0005	0.505	1.980	1980.198	10729.537
	B4	Calcite+Vaterite	0.274	0.0055	5.470	0.183	182.815	459.415
	B4_Urea	Vaterite+Hydroxyapatite	0.319	0.0064	6.380	0.157	156.740	616.458
	YE_Urea	UNNONE	0.198	0.0040	3.960	0.253	252.525	1732.323
	YE_Amm.Sulfate	Calcite	0.320	0.0064	6.405	0.156	156.128	1033.568

In conclusion, the most inexpensive, pure and viable product that was produced with *A. crystallopoietes* DSM 20117 (L1) using B4 medium was weddellite. This strain can produce 1 kg of product using just 81 L of B4 medium at a cost of €205. These volumes and costs are much lower compared to the liters and production costs of the other media used for growth of the same or other strains; thus, comparing also the amount of $CaCO_3$ produced, the XRD results, and the results from the biological treatments, *A. crystallopoietes* DSM 20117 (L1) is the most efficient among the strains under investigation.

Chapter 5: Discussion

In this study, MICP was evaluated using bacterial strains isolated from Cypriot marine sediments. Marine sediments are natural habitats of microorganisms inducing calcium carbonate precipitation [23]. Calcite, aragonite and vaterite are among the main biomineral polymorphs with different crystal habits, such as rhombohedral, orthorhombic and hexagonal [29]. Among the bacterial strains isolated in the present work, *A. crystallopoietes* DSM 20117 was by far the most efficient in precipitating $CaCO_3$ in the form of calcite, followed by *A. crystallopoietes* P-21, comparing the concentration produced, the efficiency of the biological treatments and the cost of production.

Regarding *A. crystallopoietes*, it grows as spheres in glucose-mineral salt media and as rods in the presence of specific morphogenesis, inducing compounds or complex mixtures of amino acids [168]. It has been isolated from calcareous stones, soil samples and concrete structures [169-172]. It has also been reported to have high ability to form $CaCO_3$ [168,171], similarly to the present study, and to significantly improve concrete properties [169]. In line with the experimental results hereby obtained, Jroundi et al. [171] reported that a high amount of $CaCO_3$ was produced and consolidation occurred in stones when *A. crystallopoietes* was used. However, the same authors also reported that consolidation was better when the biological treatment was combined with *Myxococcus xanthus*.

Both *Micrococcus* sp. and *A. crystallopoietes* species, which were isolated in the current study, are Gram-positive obligate aerobe bacteria. *Micrococcus* sp. is a high G+C content bacterium [166], and it is well suited for long-term survival in extreme

environments. It has been isolated from tap water by Liu et al. [167] and showed the ability to precipitate $CaCO_3$, in the form of calcium phosphate, in B4 medium. This is in agreement with the results of the present study, which also showed the ability of *Micrococcus* sp. to precipitate $CaCO_3$ hydrate in the form of hydroxyapatite.

B. licheniformis is a species which was also isolated in the present study. Based on Vahabi et al. [173], *B. licheniformis* AK01, inoculated for 7 days at 32 °C, produced more than 1000 mg/L of $CaCO_3$. This is in contrast with the results of the current study, in which *B. licheniformis* PP1 produced only 226 mg/L. However, B4 medium was used in [161], while in the current study CCP medium was used, which could have a negative effect on $CaCO_3$ formation.

In this study, *A. crystallopoietes* DSM 20117 has shown high urease activity, in line with that reported for *S. pasteurii* [34,35]. Nevertheless, in contrast to *S. pasteurii*, *A. crystallopoietes* is one of the less employed bacteria for MICP, albeit very promising. *Arthrobacter* has also been reported to be an ureolytic bacterium in calcite precipitation in several applications [170,175,176]. In fact, it has been reported that highly ureolytic bacteria are the major microbial strains employed in MICP-treatment for the conservation of architectural heritage [32]. These previous findings are strongly supported by the experimental results hereby obtained, which demonstrate the vital role of urease activity in the $CaCO_3$ precipitation process when CCP media is used. Specifically, the results of the present work further confirm that highly ureolytic bacteria, such as *A. crystallopoietes* DSM 20117, induce increased $CaCO_3$ production, thus indicating their suitability for biomineralization. Emphasis should be placed on the fact that *A. crystallopoietes* has the ability to survive starvation, as well as extreme desiccated conditions, for unusually long periods of time [168,177]. This behaviour could potentially make it a suitable bacterium for stone consolidation applications in a great variety of climatic conditions.

XRD and SEM analyses conducted in this study, when CCP medium was used, indicated that the newly isolated bacterial species induced calcite, vaterite and hydroxyapatite precipitation. Calcite, which was the main mineral phase precipitated by *A. crystallopoietes*, is the most stable and least soluble polymorph of $CaCO_3$ under ambient conditions [178]. Vaterite, which was produced by *B. licheniformis* PP1, is a metastable $CaCO_3$ polymorph at Earth surface conditions [179] and thus rare in natural environments, as it gradually transforms into calcite. Accordingly, vaterite shows

higher solubility than calcite, and it is more likely to dissolve in the presence of water. However, the microbially induced vaterite achieves comparable levels of stability with calcite upon incorporation with organic molecules [20,33]. Another *Bacillus* species, the *megaterium*, can produce vaterite [185]. Hydroxyapatite, which was formed by *Micrococcus* sp., is a bio-composite with a stoichiometry of $Ca_{10}(PO_4)_6(OH)_2$ and it is the principal mineral constituent of bone and teeth. According to Weiner and Dove [180], hydroxyapatite, also called dahllite, is one of the most abundant biogenic phosphate types. Hydroxyapatite was found to be produced also by *M. xanthus* [181] and *Sphingobium limneticum* S2 [167].

XRD analysis when B4, B4+urea, YE+urea and YE+AS were used as media for growth of the two *A. crystallopoietes* strains and *Micrococcus* sp., revealed that *A. crystallopoietes* DSM 20117 can produce weddellite. Weddellite or calcium oxalate dihydrate ($CaC_2O_4 \cdot 2H_2O$) is a hydrated oxalate of calcium, found naturally in plant tissues, in sediments as a mineral of organic origin, and in urinary stones. About 70 percent (70%) of human urinary stones contain whewellite and/or weddellite, either solely or mixed with other components, mostly phosphates, uric acids, or urates [1]. It crystallizes in a tetragonal system: the classic crystal shape is the eight-face bipyramid and it has hardness 4 in the Mohs scale. The growth of *A. crystallopoietes* DSM 20117 in YE+urea showed halite production. Halite is a mineral form of sodium chloride (NaCl), commonly known as rock salt or table salt.

The metabolic process leading to a specific polymorph in microorganisms inducing $CaCO_3$ precipitation is not completely understood [182]. Until now, the most reasonable explanation is the type of microorganism employed, the urease activity and structure [183], and/or the microbial growth rate [184]. It has also been suggested that in *Bacillus megaterium* species, EPS production enhanced vaterite production [185]. In addition, the media used and the Ca source added play a key role in the morphology of $CaCO_3$ [186]. However, polymorph formation can also be affected by factors such as chemical composition, pH and ionic strength of the surrounding environment. *In the present study, it was also noticed that the medium composition not only played a key role in polymorph formation but also in the amount of the polymorph formed.*

In the present study, MICP treatment of LYM limestone by *A. crystallopoietes* DSM 20117 with CCP medium led to bio-consolidation close to the surface (within the first 500 μm) of the specimen under study, as indicated by SEM analysis and drilling

resistance measurements on both the treated and control areas. This is attributed to the pore structure of LYM limestone the effects of MICP treatment in stones with such small pores are expected to appear close to the surface, since the superficial precipitation of $CaCO_3$ leads to pore clogging, thus obstructing further absorption inside the material. In addition, the bacteria size of *A. crystallopoietes* is approximately 0.8 x 1.0-1.5 μm [187], which is bigger than the predominant pore throat diameter of LYM stone. This could also partially obstruct the absorption of the solution deeper into the stone.

Superficial pore clogging following the MICP treatment also seemed to significantly reduce the water resistance of the LYM stone in both CCP and B4 media, as confirmed by water penetration and contact angle measurements. This is certainly desirable, since water is behind several limestone weathering mechanisms.

In the optimization treatment of LYM stone, strains treated with B4 medium exhibited superior results compared to those treated with CCP medium. Karsten tube analysis indicated lower absorption for *A. crystallopoietes* DSM 20117, *A. crytallopoietes* P-21, and *A. crystallopoietes* P-21 + *Micrococcus* sp. DSM 105846, with *A. crystallopoietes* P-21 showing the most significant reduction in absorption, having 19.8 and 34 times lower absorption, respectively, compared to the initial control area.

In the contact angle test, the most significant increase was observed in the *A. crystallopoietes* P-21 (P3) area treated with B4 medium. The initial contact angle of approximately 55° increased to an average of 80°, while the water absorption rate decreased to an average of 0.80 μl/sec, representing in a 43-fold reduction, compared to the control area and 1.4 times less than the *A. crystallopoietes* DSM 20117 (L1) area.

Drilling resistance test (DRMS) results indicated that CCP treatment led to better outcomes for GER stone, with *A. crystallopoietes* DSM 20117 (L1), increasing the drilling resistance by 58.8% from the control area, compared to a 22% increase with B4 treatment. Conversely, B4 treatment yielded better results for LYM stone, with *A. crystallopoietes* DSM 20117 (L1), increasing the drilling resistance by 72% within the first 500 μm. The aforementioned findings are also in agreement with other works that reported reduced water absorption, along with increased drilling resistance, in carbonate rocks (i.e., limestones, dolomites) following biomineralization [188,189].

The varying effectiveness of strains observed in the Karsten tube and contact angle tests carried out in the framework of this study can be attributed to differences in the test characteristics. The Karsten tube provides a broader assessment of stone absorption over time due to the larger water volume, reflecting changes in the stone matrix resulting from void blockage. Conversely, the contact angle test offers instantaneous results of stone absorption and droplet angle, focusing on surface material interaction with water.

In the scratch test, GER stone exhibited a 403% increase at a depth of 0.05 mm compared to the control area, with a P-value > 0.01. *A. crystallopoietes* P-21 showed improved scratch resistance with B4 medium at a depth of 0.05 mm, followed by *A.crystallopoietes* P-21 + *Micrococcus* sp. DSM 105846 with a 24% increase at a depth of 0.75 mm.

Combining the findings from the scratch test with those of the Karsten tube and contact angle tests, it is suggested that *A. crystallopoietes* P-21 and *A. crystallopoietes* P-21 + *Micrococcus* sp. DSM 105846 in B4 medium, along with *A. crystallopoietes* DSM 20117 (L1) in CCP medium, can penetrate deeper into both stones pore structure. It is also suggested that in the case of LYM stone, due to its smaller pore structure and surface treatment method, microorganisms may not have sufficient time to penetrate the stone, leading to surface clogging and treatment.

It was observed that the efficacy of the biological treatment varied depending on the composition of the stone. Notably, LYM stone, primarily composed of pure calcium carbonate, exhibited more favorable outcomes compared to GER stone, characterized by biogenic and silicate grains bound together by calcite. This discrepancy can be attributed to the differential absorption rates of the treatment into the respective stones.

In LYM stone, the treatment exhibited a slower absorption rate, allowing it to gradually infiltrate the stone and fill its pores, consequently leading to pore clogging on the surface. Conversely, GER stone demonstrated rapid absorption of the treatment, resulting in less effective penetration into the surface area. However, despite this disparity in surface treatment, the overall efficacy of the treatment was found to be superior in GER stone due to its uniform treatment throughout the stone volume.

Conclusion and future work

Conclusion

Among the strains isolated from Cypriot marine sediments (*Arthrobacter*, *Micrococcus* and *Bacillus* species), which are natural microbial $CaCO_3$ producers, *A. crystallopoietes* DSM 20117 was distinguished for its $CaCO_3$ non-solubilizing characteristics, high ureolytic activity and highest $CaCO_3$ precipitation efficiency, even when different media were used for its growth. The $CaCO_3$ polymorph mainly precipitated by this strain was calcite, which is the most stable one in nature. Vaterite and hydroxyapatite were precipitated by *B. licheniformis PP1* and *Micrococcus* sp. DSM 105846, respectively, upon use of CCP medium. It is worth noting that *A. crystallopoietes* DSM 20117 is a species and strain less studied in MICP applications; thus, it is certainly worth further investigation.

MICP by *A. crystallopoietes* DSM 20117 was applied to two Cypriot limestones, namely Gerolakkos (GER) and Lympia (LYM), in order to get an insight of the technological potential of the process in the field of cultural heritage. The results were very promising, since following the biological treatment, the water absorption of both stones was evidently reduced. Drilling resistance measurements of LYM stone revealed superficial consolidation, also confirmed by SEM observations. Drilling resistance measurements of GER also revealed consolidation. However, these results are not completely reliable due to non-regular porosity and grains in GER stone.

Following that, in order to optimize the MICP, four (4) different media such as B4, B4+Urea, YE+Urea, and YE+Ammonium sulfate were used for *A. crystallopoietes* DSM 20117 (L1), *A. crystallopoietes* P-21 (P3) and *Micrococcus* sp. DSM 105846 (P4) growth. The use of different media in each strain resulted in different polymorphs of the precipitant. However, the amount of precipitant produced by these strains using the 4 media was much higher compared to the one produced upon CCP use. These findings underscore the significant role of the medium and its ingredients in defining the resulting products. Different media lead to activation of different metabolic pathways resulting in different end products formed with completely different structures, even if the same strain was used.

In the optimization treatment, *A. crystallopoietes* P-21 (P3) proved most effective in reducing water absorption rates in both stones compared to the other strains. Moreover,

in the DRMS test, the area treated with *A. crystallopoietes* DSM 20117 (L1) demonstrated superior effectiveness compared to the other strains. The overall results demonstrated the potential of *A. crystallopoietes* DSM 20117 and *A. crystallopoietes* P-21 with B4 medium to be used as an alternative environmental-friendly means for the conservation of architectural stone heritage. At the same time, the aforementioned strains show significant potential for application in other fields, as well, such as in the bioremediation and self-healing of concrete, due to their high urease activity and production of calcite and vaterite when the appropriate medium is used.

Future work

For future research, it is essential to assess the breathability of the treated stones. Further research is deemed necessary to investigate the drying behavior of the sample before and after treatment. Also accelerated weathering tests for example freezing and thawing and salt crystallization to investigate the durability of the treated stones in relation with the non-treated.In case the latter has been negatively affected, optimization of the biological treatment may be needed to enhance the precipitation of $CaCO_3$ and its penetration deeper into the inner matrix of the stone under investigation.

Last but not least, studying the metabolic pathways, such as urea hydrolysis, when different media are used is necessary in order to understand the effect of different media in product formation and composition.

References

[1] M.I. Daskalakis, A. Magoulas, G. Kotoulas, I. Catsikis, A. Bakolas, A.P. Karageorgis, A. Mavridou, D. Doulia, F. Rigas, Pseudomonas, Pantoea and Cupriavidus isolates induce calcium carbonate precipitation for biorestoration of ornamental stone, J. Appl. Microbiol. 115 (2013) 409–423. https://doi.org/10.1111/jam.12234.

[2] P. Tiano, L. Biagiotti, G. Mastromei, Bacterial bio-mediated calcite precipitation for monumental stones conservation: Methods of evaluation, J. Microbiol. Methods. 36 (1999) 139–145. https://doi.org/10.1016/S0167-7012(99)00019-6.

[3] M. Andreolli, S. Lampis, P. Bernardi, S. Calò, G. Vallini, Bacteria from black crusts on stone monuments can precipitate CaCO3 allowing the development of a new bio-consolidation protocol for ornamental stone, Int. Biodeterior. Biodegrad. 153 (2020) 105031. https://doi.org/10.1016/j.ibiod.2020.105031.

[4] C. Jimenez-Lopez, C. Rodriguez-Navarro, G. Piñar, F.J. Carrillo-Rosúa, M. Rodriguez-Gallego, M.T. Gonzalez-Muñoz, Consolidation of degraded ornamental porous limestone stone by calcium carbonate precipitation induced by the microbiota inhabiting the stone, Chemosphere. 68 (2007) 1929–1936. https://doi.org/10.1016/j.chemosphere.2007.02.044.

[5] F. Jroundi, M. Schiro, E. Ruiz-Agudo, K. Elert, I. Martín-Sánchez, M.T. González-Muñoz, C. Rodriguez-Navarro, Protection and consolidation of stone heritage by self-inoculation with indigenous carbonatogenic bacterial communities, Nat. Commun. 8 (2017) 1–12. https://doi.org/10.1038/s41467-017-00372-3.

[6] H. Bai, D. Liu, W. Zheng, L. Ma, S. Yang, J. Cao, X. Lu, H. Wang, N. Mehta, Microbially-induced calcium carbonate precipitation by a halophilic ureolytic bacterium and its potential for remediation of heavy metal-contaminated saline environments, Int. Biodeterior. Biodegrad. 165 (2021) 105311. https://doi.org/10.1016/j.ibiod.2021.105311.

[7] W. Mwandira, K. Nakashima, S. Kawasaki, Bioremediation of lead-contaminated mine waste by Pararhodobacter sp. based on the microbially induced calcium carbonate precipitation technique and its effects on strength of coarse and fine grained sand, Ecol. Eng. 109 (2017) 57–64. https://doi.org/10.1016/j.ecoleng.2017.09.011.

[8] X. Zhu, W. Li, L. Zhan, M. Huang, Q. Zhang, V. Achal, The large-scale process of microbial carbonate precipitation for nickel remediation from an industrial soil, Environ. Pollut. 219 (2016) 149–155. https://doi.org/10.1016/j.envpol.2016.10.047.

[9] A.M. Sharaky, N.S. Mohamed, M.E. Elmashad, N.M. Shredah, Application of microbial biocementation to improve the physico-mechanical properties of sandy soil, Constr. Build. Mater. 190 (2018) 861–869. https://doi.org/10.1016/j.conbuildmat.2018.09.159.

[10] D. Mujah, M.A. Shahin, L. Cheng, State-of-the-Art Review of Biocementation by Microbially Induced Calcite Precipitation (MICP) for Soil Stabilization, Geomicrobiol. J. 34 (2017) 524–537. https://doi.org/10.1080/01490451.2016.1225866.

[11] C. Konstantinou, G. Biscontin, N.J. Jiang, K. Soga, Application of microbially induced carbonate precipitation to form bio-cemented artificial sandstone, J. Rock Mech. Geotech. Eng. 13 (2021) 579–592. https://doi.org/10.1016/j.jrmge.2021.01.010.

[12] J. Wu, X. Bin Wang, H.F. Wang, R.J. Zeng, Microbially induced calcium carbonate precipitation driven by ureolysis to enhance oil recovery, RSC Adv. 7 (2017) 37382–37391. https://doi.org/10.1039/c7ra05748b.

[13] C. Song, D. Elsworth, Microbially Induced Calcium Carbonate Plugging for Enhanced Oil Recovery, Geofluids. 2020 (2020). https://doi.org/10.1155/2020/5921789.

[14] W. Yun, S. Chang, D.A. Cogswell, S.L. Eichmann, A. Gizzatov, G. Thomas, N. Al-Hazza, A. Abdel-Fattah, W. Wang, Toward Reservoir-on-a-Chip: Rapid Performance Evaluation of Enhanced Oil Recovery Surfactants for Carbonate Reservoirs Using a Calcite-Coated Micromodel, Sci. Rep. 10 (2020) 1–12. https://doi.org/10.1038/s41598-020-57485-x.

[15] X. Wang, Y. Feng, J. Liu, H. Lee, C. Li, N. Li, N. Ren, Sequestration of CO2 discharged from anode by algal cathode in microbial carbon capture cells (MCCs), Biosens. Bioelectron. 25 (2010) 2639–2643. https://doi.org/10.1016/j.bios.2010.04.036.

[16] G. Hu, Y. Li, C. Ye, L. Liu, X. Chen, Engineering Microorganisms for Enhanced CO 2 Sequestration, Trends Biotechnol. 37 (2019) 532–547. https://doi.org/10.1016/j.tibtech.2018.10.008.

[17] P. Ronan, O. Kroukamp, S.N. Liss, G. Wolfaardt, A novel system for real-time, in situ monitoring of CO2 sequestration in photoautotrophic biofilms, Microorganisms. 8 (2020) 1–14. https://doi.org/10.3390/microorganisms8081163.

[18] H.M. Jonkers, Bacteria-based self-healing concrete, Heron. 56 (2011) 1–5.

[19] A. Al-Tabbaa, C. Litina, P. Giannaros, A. Kanellopoulos, L. Souza, First UK field application and performance of microcapsule-based self-healing concrete, Constr. Build. Mater. 208 (2019) 669–685. https://doi.org/10.1016/j.conbuildmat.2019.02.178.

[20] P. Cacchio, M. Del Gallo, A novel approach to isolation and screening of calcifying bacteria for biotechnological applications, Geosci. 9 (2019) 32–34. https://doi.org/10.3390/geosciences9110479.

[21] D. Zhuang, H. Yan, M.E. Tucker, H. Zhao, Z. Han, Y. Zhao, B. Sun, D. Li, J. Pan, Y. Zhao, R. Meng, G. Shan, X. Zhang, R. Tang, Calcite precipitation induced by Bacillus cereus MRR2 cultured at different Ca2+ concentrations: Further insights into biotic and abiotic calcite, Chem. Geol. 500 (2018) 64–87. https://doi.org/10.1016/j.chemgeo.2018.09.018.

[22] S. Castanier, G. Le Métayer-Levrel, J.P. Perthuisot, Ca-carbonates precipitation and limestone genesis - the microbiogeologist point of view, Sediment. Geol. 126 (1999) 9–23. https://doi.org/10.1016/S0037-0738(99)00028-7.

[23] M.J. Castro-Alonso, L.E. Montañez-Hernandez, M.A. Sanchez-Muñoz, M.R. Macias Franco, R. Narayanasamy, N. Balagurusamy, Microbially induced calcium carbonate precipitation (MICP) and its potential in bioconcrete: Microbiological and molecular concepts, Front. Mater. 6 (2019) 1–15. https://doi.org/10.3389/fmats.2019.00126.

[24] F. Hammes, W. Verstraete, Key roles of pH and calcium metabolism in microbial carbonate precipitation, Re/Views Environ. Sci. Bio/Technology. 1 (2002) 3–7.

[25] C. Konstantinou, Y. Wang, G. Biscontin, K. Soga, The role of bacterial urease activity on the uniformity of carbonate precipitation profiles of bio-treated coarse sand specimens, Sci. Rep. 11 (2021) 1–17. https://doi.org/10.1038/s41598-021-85712-6.

[26] A.F. Alshalif, M.I. Juki, H.A. Tajarudin, N. Othman, A.A. Al-Gheethi, S. Shamsudin, W. Altowayti, S.A. Sabah, Optimisation of self-healing of bio-foamed concrete bricks pores using Bacillus tequilensis under different temperature and CO2 curing conditions, Sci. Rep. 12 (2022) 1–19. https://doi.org/10.1038/s41598-022-05659-0.

[27] J. Ettenauer, G. Piñar, K. Sterflinger, M.T. Gonzalez-Muñoz, F. Jroundi, Molecular monitoring of the microbial dynamics occurring on historical limestone buildings during and after the in situ application of different bio-consolidation treatments, Sci. Total Environ. 409 (2011) 5337–5352. https://doi.org/10.1016/j.scitotenv.2011.08.063.

[28] S. Liu, X. Gao, Evaluation of the Anti-Erosion Characteristics of an MICP Coating on the Surface of Tabia, J. Mater. Civ. Eng. 32 (2020) 04020304. https://doi.org/10.1061/(asce)mt.1943-5533.0003408.

[29] S. Mann, Biomineralization: principles and concepts in bioinorganic materials chemistry, New York: Oxford University Press, Inc., 2001.

[30] E.E. Coleyshaw, G. Crump, W.P. Griffith, Vibrational spectra of the hydrated carbonate minerals ikaite, monohydrocalcite, lansfordite and nesquehonite, Spectrochim. Acta - Part A Mol. Biomol. Spectrosc. 59 (2003) 2231–2239. https://doi.org/10.1016/S1386-1425(03)00067-2.

[31] K.D. Mutitu, M.O. Munyao, M.J. Wachira, K.J. Thiong, M.J. Marangu, Effects of biocementation on some properties of cement-based materials incorporating Bacillus Species bacteria – a review, J. Sustain. Cem. Mater. 8 (2019) 309–325. https://doi.org/10.1080/21650373.2019.1640141.

[32] E. Ortega-Villamagua, M. Gudiño-Gomezjurado, A. Palma-Cando, Microbiologically induced carbonate precipitation in the restoration and conservation of cultural heritage materials, Molecules. 25 (2020). https://doi.org/10.3390/molecules25235499.

[33] C. Rodriguez-Navarro, M. Rodriguez-Gallego, K. Ben Chekroun, M.T. Gonzalez-Muñoz, Conservation of ornamental stone by Myxococcus xanthus-induced carbonate biomineralization, Appl. Environ. Microbiol. 69 (2003) 2182–2193. https://doi.org/10.1128/AEM.69.4.2182-2193.2003.

[34] M.M. Rahman, R.N. Hora, I. Ahenkorah, S. Beecham, M.R. Karim, A. Iqbal, State-of-the-art review of microbial-induced calcite precipitation and its sustainability in engineering applications, Sustain. 12 (2020). https://doi.org/10.3390/SU12156281.

[35] L. Ma, A.P. Pang, Y. Luo, X. Lu, F. Lin, Beneficial factors for biomineralization by ureolytic bacterium Sporosarcina pasteurii, Microb. Cell Fact. 19 (2020) 1–12. https://doi.org/10.1186/s12934-020-1281-z.

[36] S. Liu, R. Wang, J. Yu, X. Peng, Y. Cai, B. Tu, Effectiveness of the anti-erosion of an MICP coating on the surfaces of ancient clay roof tiles, Constr. Build. Mater. 243 (2020) 118202. https://doi.org/10.1016/j.conbuildmat.2020.118202.

[37] Cary SC, McDonald IR, Barrett JE et al. On the rocks: the microbiology of Antarctic dry valley soils. Nat Rev Microbiol 2010; 8: 129–38. 10.1038/nrmicro2281

[38] Dong HL, Rech JA, Jiang HC et al. Endolithic cyanobacteria in soil gypsum: occurrences in Atacama (Chile), Mojave (United States), and Al-Jafr Basin (Jordan) deserts. J Geophys Res 2007; 112: G000385. 10.1029/2006JG000385

[39] Gautron, Joël, et al. "Avian eggshell biomineralization: an update on its structure, mineralogy and protein tool kit." BMC Molecular and Cell Biology 22.1 (2021): 1-17.

[40] Ardau, Carla, David W. Blowes, and Carol J. Ptacek. "Comparison of laboratory testing protocols to field observations of the weathering of sulfide-bearing mine tailings." Journal of Geochemical Exploration 100.2-3 (2009): 182-191.

[41] Jones, Aaron A., and Philip C. Bennett. "Mineral ecology: surface specific colonization and geochemical drivers of biofilm accumulation, composition, and phylogeny." Frontiers in microbiology 8 (2017): 491.

[42] Zhao, Linduo, et al. "Biological redox cycling of iron in nontronite and its potential application in nitrate removal." Environmental science & technology 49.9 (2015): 5493-5501.

[43] Nordstrom, D. Kirk, David W. Blowes, and Carol J. Ptacek. "Hydrogeochemistry and microbiology of mine drainage: An update." Applied Geochemistry 57 (2015): 3-16.

[44] Wang, Xuan, et al. "Anaerobic microbial manganese oxidation and reduction: a critical review." Science of The Total Environment 822 (2022): 153513.

[45] Shi L, Dong H, Reguera Get al.. Extracellular electron transfer mechanisms between microorganisms and minerals. Nat Rev Microbiol 2016; 14: 651–62. 10.1038/nrmicro.2016.93

[46] Lovley, Derek R. "Syntrophy goes electric: direct interspecies electron transfer." Annual review of microbiology 71 (2017): 643-664.

[47] Seifan, Mostafa, and Aydin Berenjian. "Microbially induced calcium carbonate precipitation: a widespread phenomenon in the biological world." Applied microbiology and biotechnology 103 (2019): 4693-4708.

[48] Schepers, James Stuart, and William Raun, eds. Nitrogen in agricultural systems. No. 49. Asa-CSSA-Sssa, 2008.

[49] Van Der Star, Wouter RL, et al. "Use of waste streams and microbes for in situ transformation of sand into sandstone." International Symposium on Ground Improvement Technologies and Case Histories, ISGI'09. 2010.

[50] Kavazanjian Jr, Edward, and Ismail Karatas. "Microbiological improvement of the physical properties of soil." Proc. 6th Int. Conf. on Case Histories in Geotech. Engng, Rolla, MO (CD-ROM). 2008.

[51] Ferguson, Stuart J., David J. Richardson, and Rob JM Van Spanning. "Biochemistry and molecular biology of nitrification." Biology of the nitrogen cycle. Elsevier, 2007. 209-222.

[52] Bonnefoy, Violaine, and John A. Demoss. "Nitrate reductases in Escherichia coli." Antonie Van Leeuwenhoek 66 (1994): 47-56.

[53] Fernández, Emilio, Ángel Llamas, and Aurora Galván. "Nitrogen assimilation and its regulation." The Chlamydomonas sourcebook. Academic Press, 2009. 69-113.

[54] Jain, Surabhi, Chaolin Fang, and Varenyam Achal. "A critical review on microbial carbonate precipitation via denitrification process in building materials." Bioengineered 12.1 (2021): 7529-7551.

[55] Hino, Tomoya, et al. "Structural basis of biological N2O generation by bacterial nitric oxide reductase." Science 330.6011 (2010): 1666-1670.

[56] Hamdan, Nasser, et al. "Carbonate mineral precipitation for soil improvement through microbial denitrification." Geomicrobiology journal 34.2 (2017): 139-146.

[57] Kavazanjian, Edward, Sean T. O'Donnell, and Nasser Hamdan. "Biogeotechnical mitigation of earthquake-induced soil liquefaction by denitrification: a two-stage process." Proceedings of 6th International Conference on Earthquake Geotechnical Engineering, Christchurch, New Zealand. 2015.

[58] Almeida, J. S., et al. "Nitrite inhibition of denitrification by Pseudomonas fluorescens." Biotechnology and bioengineering 46.3 (1995): 194-201.

[59] Chung, Y-C., and M-S. Chung. "BNP test to evaluate the influence of C/N ratio on N2O production in biological denitrification." Water Science and Technology 42.3-4 (2000): 23-27.

[60] Hanaki, K., Z. Hong, and T. Matsuo. "Production of nitrous oxide gas during denitrification of wastewater." Water Science and Technology 26.5-6 (1992): 1027-1036.

[61] Zhu, Tingting, and Maria Dittrich. "Carbonate precipitation through microbial activities in natural environment, and their potential in biotechnology: a review." Frontiers in bioengineering and biotechnology 4 (2016): 4.

[62] Finster, Kai. "Microbiological disproportionation of inorganic sulfur compounds." Journal of Sulfur Chemistry 29.3-4 (2008): 281-292.

[63] Grein, Fabian, et al. "Unifying concepts in anaerobic respiration: insights from dissimilatory sulfur metabolism." Biochimica et Biophysica Acta (BBA)-Bioenergetics 1827.2 (2013): 145-160.

[64] Jørgensen, Bo Barker. "Mineralization of organic matter in the sea bed—the role of sulphate reduction." Nature 296.5858 (1982): 643-645.

[65] Leavitt, William D., et al. "Sulfur isotope effects of dissimilatory sulfite reductase." Frontiers in Microbiology 6 (2015): 1392.

[66] Loy, Alexander, et al. "Reverse dissimilatory sulfite reductase as phylogenetic marker for a subgroup of sulfur-oxidizing prokaryotes." Environmental microbiology 11.2 (2009): 289-299.

[67] Simon, Jörg, and Peter MH Kroneck. "Microbial sulfite respiration." Advances in microbial physiology. Vol. 62. Academic Press, 2013. 45-117.

[68] Thorup, Casper, et al. "Disguised as a sulfate reducer: growth of the deltaproteobacterium Desulfurivibrio alkaliphilus by sulfide oxidation with nitrate." MBio 8.4 (2017): e00671-17.

[69] Wagner, Michael, et al. "Phylogeny of dissimilatory sulfite reductases supports an early origin of sulfate respiration." Journal of bacteriology 180.11 (1998): 2975-2982.

[70] Müller, Albert Leopold, et al. "Phylogenetic and environmental diversity of DsrAB-type dissimilatory (bi) sulfite reductases." The ISME journal 9.5 (2015): 1152-1165.

[71] Hermann, Bianca, et al. "The octahaem MccA is a haem c–copper sulfite reductase." Nature 520.7549 (2015): 706-709.

[72] Shirodkar, Sheetal, et al. "The octahaem SirA catalyses dissimilatory sulfite reduction in Shewanella oneidensis MR-1." Environmental microbiology 13.1 (2011): 108-115.

[73] Anantharaman, Karthik, et al. "Expanded diversity of microbial groups that shape the dissimilatry sulfur cycle." The ISME journal 12.7 (2018): 1715-1728.

[74] Krause, Stefan, et al. "Marine ammonification and carbonic anhydrase activity induce rapid calcium carbonate precipitation." Geochimica et Cosmochimica Acta 243 (2018): 116-132.

[75] Erşan, Yusuf Çağatay, Nele De Belie, and Nico Boon. "Microbially induced CaCO3 precipitation through denitrification: an optimization study in minimal nutrient environment." Biochemical Engineering Journal 101 (2015): 108-118.

[76] Boquet, E., A. Boronat, and A. Ramos-Cormenzana. "Production of calcite (calcium carbonate) crystals by soil bacteria is a general phenomenon." Nature 246.5434 (1973): 527-529.

[77] Fischer, Alfred G. "Fossils, early life, and atmospheric history." (1965): 1205-1215.

[78] Lochte, K., and C. M. Turley. "Bacteria and cyanobacteria associated with phytodetritus in the deep sea." Nature 333 (1988): 67-69.

[79] Castanier, Sabine, Gaële Le Métayer-Levrel, and Jean-Pierre Perthuisot. "Ca-carbonates precipitation and limestone genesis—the microbiogeologist point of view." Sedimentary geology 126.1-4 (1999): 9-23.

[80] Altermann, W., et al. "Cyanobacterial calcification and its rock-building potential during 3.5 billion years of Earth history." Geobiology 4.3 (2006): 147-166.

[81] Seifan, Mostafa, Ali Khajeh Samani, and Aydin Berenjian. "Bioconcrete: next generation of self-healing concrete." Applied microbiology and biotechnology 100 (2016): 2591-2602.

[82] Lowenstam, H. A. "Mineralization processes in monerans and protoctists." Biomineralization in lower plants and animals 30 (1986): 1-17.

[83] Coleman, John R. "Carbonic anhydrase and its role in photosynthesis." Photosynthesis: Physiology and metabolism (2000): 353-367.

[84] Konstantinou, Charalampos, et al. "The role of bacterial urease activity on the uniformity of carbonate precipitation profiles of bio-treated coarse sand specimens." Scientific reports 11.1 (2021): 1-17.

[85] Castanier, Sabine, Gaële Le Métayer-Levrel, and Jean-Pierre Perthuisot. "Ca-carbonates precipitation and limestone genesis—the microbiogeologist point of view." Sedimentary geology 126.1-4 (1999): 9-23.

[86] Dodor, Daniel, and M. Tabatabai. "Alkaline hydrolyzable organic nitrogen as an index of nitrogen mineralization in soils: Relationship with activities of arylamidase and amidohydrolases." Communications in Soil Science and Plant Analysis 51.13 (2020): 1757-1766.

[87] Blakeley, Robert L., and Burt Zerner. "Jack bean urease: the first nickel enzyme." Journal of molecular catalysis 23.2-3 (1984): 263-292.

[88] Characterization of Urease and Carbonic Anhydrase Producing Bacteria and Their Role in Calcite Precipitation

[89] Smith, Kerry S., and James G. Ferry. "Prokaryotic carbonic anhydrases." FEMS microbiology reviews 24.4 (2000): 335-366.

[90] Sriwanthana, B. U. S. A. R. A. W. A. N., and H. L. Mobley. "Proteus mirabilis urease: histidine 320 of UreC is essential for urea hydrolysis and nickel ion binding within the native enzyme." Infection and immunity 61.6 (1993): 2570-2577.

[91] Petry, Thomas M., and Dallas N. Little. "Review of stabilization of clays and expansive soils in pavements and lightly loaded structures—history, practice, and future." Journal of materials in civil engineering 14.6 (2002): 447-460.

[92] Steinberg, M. L. Geomembranes and the Control of Expansive Soils in Construction (McGraw-Hill, 1998)

[93] Mitchell, James K., and J. Carlos Santamarina. "Biological considerations in geotechnical engineering." Journal of geotechnical and geoenvironmental engineering 131.10 (2005): 1222-1233.

[94] J. Chu, V. Ivanov, M. Naeimi, et al., Optimization of calcium-based bioclogging and biocementation of sand, Acta Geotech 9 (2014) 277–285, https://doi.org/10. 1007/s11440-013-0278-8

[95] Scholl, Martha A., et al. "The influence of mineralogy and solution chemistry on the attachment of bacteria to representative aquifer materials." Journal of Contaminant Hydrology 6.4 (1990): 321-336.

[96] Phillips, Adrienne J., et al. "Engineered applications of ureolytic biomineralization: a review." Biofouling 29.6 (2013): 715-733.

[97] Rahman, Md Mizanur, et al. "State-of-the-art review of microbial-induced calcite precipitation and its sustainability in engineering applications." Sustainability 12.15 (2020): 6281.

[98] Almajed, Abdullah, et al. "State-of-the-art review of the applicability and challenges of microbial-induced calcite precipitation (MICP) and enzyme-induced calcite precipitation (EICP) techniques for geotechnical and geoenvironmental applications." Crystals 11.4 (2021): 370.

[99] Sharaky, Abbas M., et al. "Application of microbial biocementation to improve the physico-mechanical properties of sandy soil." Construction and Building Materials 190 (2018): 861-869.

[100] Zhao, Xiao, et al. "An overview of preparation and applications of stabilized zero-valent iron nanoparticles for soil and groundwater remediation." Water research 100 (2016): 245-266.

[101] Chen, Xindi, et al. "The effect of cyclic variation of shear stress on non-cohesive sediment stabilization by microbial biofilms: the role of 'biofilm precursors'." Earth Surface Processes and Landforms 44.7 (2019): 1471-1481.

[102] Achal, V., & Kawasaki, S. (2016). Biogrout: A novel binding material for soil improvement and concrete repair. Frontiers in microbiology, 7, 314.

[103] Wang, Yang, et al. "Study on low-strength biocemented sands using a temperature-controlled MICP (microbially induced calcite precipitation) method." New Prospects in Geotechnical Engineering Aspects of Civil Infrastructures: Proceedings of the 5th GeoChina International Conference 2018–Civil Infrastructures Confronting Severe Weathers and Climate Changes: From Failure to Sustainability, held on July 23 to 25, 2018 in HangZhou, China. Springer International Publishing, 2019.

[104] Jiang, Ning-Jun, et al. "Bio-mediated soil improvement: An introspection into processes, materials, characterization and applications." Soil Use and Management 38.1 (2022): 68-93.

[105] San Pablo, Alexandra CM, et al. "Meter-scale biocementation experiments to advance process control and reduce impacts: Examining spatial control, ammonium by-product removal, and chemical reductions." Journal of Geotechnical and Geoenvironmental Engineering 146.11 (2020): 04020125.

[106] Hamdan, N., and E. Kavazanjian Jr. "Enzyme-induced carbonate mineral precipitation for fugitive dust control." Géotechnique 66.7 (2016): 546-555.

[107] DeJong, J. T., et al. Upscaling of bio-mediated soil improvement. No. INL/CON-09-15487. Idaho National Lab.(INL), Idaho Falls, ID (United States), 2009.

[108] Mahawish, Aamir, Abdelmalek Bouazza, and Will P. Gates. "Improvement of coarse sand engineering properties by microbially induced calcite precipitation." Geomicrobiology Journal 35.10 (2018): 887-897.

[109] Mujah, Donovan, Mohamed A. Shahin, and Liang Cheng. "State-of-the-art review of biocementation by microbially induced calcite precipitation (MICP) for soil stabilization." Geomicrobiology Journal 34.6 (2017): 524-537.

[110] Rowshanbakht, Karim, et al. "Effect of injected bacterial suspension volume and relative density on carbonate precipitation resulting from microbial treatment." Ecological engineering 89 (2016): 49-55.

[111] Cheng, Liang, and Mohamed A. Shahin. "Microbially induced calcite precipitation (MICP) for soil stabilization." Ecological wisdom inspired restoration engineering (2019): 47-68.

[112] Almajed, Abdullah, Hamed Khodadadi Tirkolaei, and Edward Kavazanjian Jr. "Baseline investigation on enzyme-induced calcium carbonate precipitation." Journal of Geotechnical and Geoenvironmental Engineering 144.11 (2018): 04018081.

[113] Cheng, Liang, M. A. Shahin, and R. Cord-Ruwisch. "Bio-cementation of sandy soil using microbially induced carbonate precipitation for marine environments." Géotechnique 64.12 (2014): 1010-1013.

[114] Cheng, Liang, Mohamed A. Shahin, and Ralf Cord-Ruwisch. "Surface percolation for soil improvement by biocementation utilizing in situ enriched indigenous aerobic and anaerobic ureolytic soil microorganisms." Geomicrobiology journal 34.6 (2017): 546-556.

[115] Omoregie, Armstrong I., Enzo A. Palombo, and Peter M. Nissom. "Bioprecipitation of calcium carbonate mediated by ureolysis: A review." Environmental Engineering Research 26.6 (2021).

[116] Mitchell, Andrew C., et al. "Microbially enhanced carbon capture and storage by mineral-trapping and solubility-trapping." Environmental science & technology 44.13 (2010): 5270-5276.

[117] Dupraz, Sébastien, et al. "Experimental and numerical modeling of bacterially induced pH increase and calcite precipitation in saline aquifers." Chemical Geology 265.1-2 (2009): 44-53.

[118] Phillips, Adrienne J., et al. "Potential CO2 leakage reduction through biofilm-induced calcium carbonate precipitation." Environmental science & technology 47.1 (2013): 142-149.

[119] Mitchell, Andrew C., et al. "Microbially enhanced carbonate mineralization and the geologic containment of CO2." (2008).

[120] Krajewska, Barbara, Rudi van Eldik, and Małgorzata Brindell. "Temperature-and pressure-dependent stopped-flow kinetic studies of jack bean urease. Implications for the catalytic mechanism." JBIC Journal of Biological Inorganic Chemistry 17 (2012): 1123-1134.

[121] Nemati, M., and G. Voordouw. "Modification of porous media permeability, using calcium carbonate produced enzymatically in situ." Enzyme and microbial technology 33.5 (2003): 635-642.

[122] Nemati, M., E. A. Greene, and G. Voordouw. "Permeability profile modification using bacterially formed calcium carbonate: comparison with enzymic option." Process Biochemistry 40.2 (2005): 925-933.

[123] Qu, Jianhua, et al. "Utilization of rice husks functionalized with xanthates as cost-effective biosorbents for optimal Cd (II) removal from aqueous solution via response surface methodology." Bioresource technology 241 (2017): 1036-1042.

[124] Krajewska, Barbara. "Urease-aided calcium carbonate mineralization for engineering applications: A review." Journal of Advanced Research 13 (2018): 59-67.

[125] Gowthaman, K., et al. "Design and synthesis of TiO2/ZnO nanocomposite with enhanced oxygen vacancy: Better photocatalytic removal of MB dye under visible light-driven condition." Inorganic Chemistry Communications 146 (2022): 110197.

[126] Kang, Chang-Ho, Yoon-Jung Kwon, and Jae-Seong So. "Bioremediation of heavy metals by using bacterial mixtures." Ecological Engineering 89 (2016): 64-69.

[127] Kim, Kyeongmin, et al. "In situ electrochemical remediation of brackish river sediment rich in aromatic organic matter using steel-slag-combined sediment microbial fuel cells." Journal of Cleaner Production 315 (2021): 128206.

[128] Castro-Alonso, María José, et al. "Microbially induced calcium carbonate precipitation (MICP) and its potential in bioconcrete: microbiological and molecular concepts." Frontiers in Materials 6 (2019): 126.

[129] Kang, Chang-Ho, et al. "Bioremediation of lead by ureolytic bacteria isolated from soil at abandoned metal mines in South Korea." Ecological Engineering 74 (2015): 402-407.

[130] Xia, Shaopan, et al. "A critical review on bioremediation technologies for Cr (VI)-contaminated soils and wastewater." Critical reviews in environmental science and technology 49.12 (2019): 1027-1078.

[131] Kumari, Babita, and D. P. Singh. "A review on multifaceted application of nanoparticles in the field of bioremediation of petroleum hydrocarbons." Ecological Engineering 97 (2016): 98-105.

[132] Rajasekar, Adharsh, Charles KS Moy, and Stephen Wilkinson. "MICP and advances towards eco-friendly and economical applications." IOP Conference Series: Earth and Environmental Science. Vol. 78. No. 1. IOP Publishing, 2017.

[133] Gomaa, Mohamed, et al. "Coupling phenol bioremediation and biodiesel production by Tetradesmus obliquus: Optimization of phenol removal, biomass productivity and lipid content." South African Journal of Botany 151 (2022): 604-613.

[134] Pirveysian, Mahtab, and Mehran Ghiaci. "Synthesis and characterization of sulfur functionalized graphene oxide nanosheets as efficient sorbent for removal of Pb2+, Cd2+, Ni2+ and Zn2+ ions from aqueous solution: a combined thermodynamic and kinetic studies." Applied Surface Science 428 (2018): 98-109.

[135] Song, Lichao, et al. "Effect of biochar-immobilized Sphingomonas sp. PJ2 on bioremediation of PAHs and bacterial community composition in saline soil." Chemosphere 279 (2021): 130427.

[136] Wei, Yanchen, et al. "Bioremediation of the petroleum contaminated desert steppe soil with Rhodococcus erythropolis KB1 and its effect on the bacterial communities of the soils." Geomicrobiology Journal 38.10 (2021): 842-849.

[137] Li, Zhaolin, et al. "A strategy for bioremediation of nuclear contaminants in the environment." Environmental Pollution (2022): 120964.

[138] Song, Lichao, et al. "Effect of biochar-immobilized Sphingomonas sp. PJ2 on bioremediation of PAHs and bacterial community composition in saline soil." Chemosphere 279 (2021): 130427.

[139] Teir, S., Eloneva, S., Fogelholm, C. J., & Zevenhoven, R. (2006). Stability of calcium carbonate and magnesium carbonate in rainwater and nitric acid solutions. Energy Conversion and Management, 47(18-19), 3059-3068.

[140] Huo, M., Sun, Q., Bai, Y., Li, J., Xie, P., Liu, Z., & Wang, X. (2012). Influence of airborne particles on the acidity of rainwater during wash-out process. Atmospheric environment, 59, 192-201.

[141] Benavente, D., et al. "Quantification of salt weathering in porous stones using an experimental continuous partial immersion method." Engineering geology 59.3-4 (2001): 313-325.

[142] Benavente, David, et al. "Durability estimation of porous building stones from pore structure and strength." Engineering geology 74.1-2 (2004): 113-127.J.Crystal Growth 204 (1999) 168.

[143] Rodriguez-Navarro, C., & Doehne, E. (1999). Salt weathering: influence of evaporation rate, supersaturation and crystallization pattern. Earth Surface Processes and Landforms: The Journal of the British Geomorphological Research Group, 24(3), 191-209.

[144] Bartoli, F., Municchia, A. C., Futagami, Y., Kashiwadani, H., Moon, K. H., & Caneva, G. (2014). Biological colonization patterns on the ruins of Angkor temples (Cambodia) in the biodeterioration vs bioprotection debate. International Biodeterioration & Biodegradation, 96, 157-165.

[145] Valentini, F., Diamanti, A., Carbone, M., Bauer, E. M., & Palleschi, G. (2012). New cleaning strategies based on carbon nanomaterials applied to the deteriorated marble surfaces: A comparative study with enzyme based treatments. Applied Surface Science, 258(16), 5965-5980.

[146] Princi, E. (2014). Handbook of polymers in stone conservation. Smithers Rapra.

[147] Doehne, E. F., & Price, C. A. (2010). Getty Conservation Institute. Stone conservation: an overview of current research, 158.

[148] Sadat-Shojai, M., & Ershad-Langroudi, A. (2009). Polymeric coatings for protection of historic monuments: Opportunities and challenges. Journal of Applied Polymer Science, 112(4), 2535-2551.

[149] Scherer, G. W., & Wheeler, G. S. (2009). Silicate consolidants for stone. Key Engineering Materials, 391, 1-25.

[150] Le Metayer-Levrel, G., Castanier, S., Orial, G., Loubière, J. F., & Perthuisot, J. P. (1999). Applications of bacterial carbonatogenesis to the protection and regeneration of limestones in buildings and historic patrimony. Sedimentary geology, 126(1-4), 25-34.

[151] Minto, J. M., Tan, Q., Lunn, R. J., El Mountassir, G., Guo, H., & Cheng, X. (2018). 'Microbial mortar'-restoration of degraded marble structures with microbially induced carbonate precipitation. Construction and Building Materials, 180, 44-54.

[152] Mu, B., Gui, Z., Lu, F., Petropoulos, E., & Yu, Y. (2021). Microbial-induced carbonate precipitation improves physical and structural properties of nanjing ancient city walls. Materials, 14(19), 5665.

[153] Liu, S., Yu, J., Peng, X., Cai, Y., & Tu, B. (2020). Preliminary study on repairing tabia cracks by using microbially induced carbonate precipitation. Construction and building materials, 248, 118611.

[154] Fernandes, P. (2006). Applied microbiology and biotechnology in the conservation of stone cultural heritage materials. Applied microbiology and biotechnology, 73, 291-296.

[155] Yang, Y., Ruan, S., Wu, S., Chu, J., Unluer, C., Liu, H., & Cheng, L. (2021). Biocarbonation of reactive magnesia for soil improvement. Acta Geotechnica, 16, 1113-1125.

[156] Chen, Z., Fang, X., Long, K., Shen, C., Yang, Y., & Liu, J. (2021). Using the biocarbonization of reactive magnesia to cure electrolytic manganese residue. Geomicrobiology Journal, 38(8), 709-718.

[157] Wang, R., Tang, C. S., Pan, X. H., Wang, D. L., Dong, Z. H., & Shi, B. (2023). Stabilization of dredged sludge using bio-carbonation of reactive magnesia cement method. Acta Geotechnica, 18(3), 1529-1541.

[158] Dong, Z. H., Pan, X. H., Tang, C. S., Wang, D. L., Wang, R., & Shi, B. (2023). An efficient microbial sealing of rock weathering cracks using bio-carbonation of reactive magnesia cement. Construction and Building Materials, 366, 130038.

[159] Wang, D. L., Tang, C. S., Pan, X. H., Wang, R., Li, J. W., Dong, Z. H., & Shi, B. (2022). Construction and demolition waste stabilization through a bio-carbonation of reactive magnesia cement for underwater engineering. Construction and Building Materials, 335, 127458.

[160] Y. Nir, THE COASTS OF CYPRUS, (1993).

[161] S. Wei, H. Cui, Z. Jiang, H. Liu, H. He, N. Fang, Biomineralization processes of calcite induced by bacteria isolated from marine sediments, Brazilian J. Microbiol. 46 (2015) 455–464. https://doi.org/10.1590/S1517-838246220140533.

[162] G. Rana, T. Mandal, N.K. Mandal, D. Sakha, B.C. Meikap, Calcite Solubilization by Bacteria: A Novel Method of Environment Pollution Control, Geomicrobiol. J. 32 (2015) 846–852. https://doi.org/10.1080/01490451.2015.1010755.

[163] D. Chang, K. Tram, B. Li, Q. Feng, Z. Shen, C.H. Lee, J. Bruno, Detection of DNA Amplicons of Polymerase Chain Reaction Using Litmus Test, (2017) 1–8. https://doi.org/10.1038/s41598-017-03009-z.

[164] S. Modestou, M. Theodoridou, R. Fournari, I. Ioannou, Physico-mechanical properties and durability performance of natural building and decorative carbonate stones from Cyprus, Geol. Soc. Spec. Publ. 416 (2016) 145–162. https://doi.org/10.1144/SP416.3.

[165] M. Otto, Staphylococcus epidermidis – the “accidental” pathogen, Nat Rev Microbiol. 7 (2008) 555–567. https://doi.org/10.1038/nrmicro2182.Staphylococcus.

[166] C.L. Greenblatt, J. Baum, B.Y. Klein, S. Nachshon, V. Koltunov, R.J. Cano, Micrococcus luteus - Survival in amber, Microb. Ecol. 48 (2004) 120–127. https://doi.org/10.1007/s00248-003-2016-5.

[167] X. Liu, G. Zarfel, R. Van Der Weijden, W. Loiskandl, B. Bitschnau, I.J.T. Dinkla, E.C. Fuchs, A.H. Paulitsch-fuchs, Density-dependent microbial calcium carbonate precipitation by drinking water bacteria via amino acid metabolism and biosorption, Water Res. 202 (2021) 117444. https://doi.org/10.1016/j.watres.2021.117444.

[168] J.C. Ensign, Long-term starvation survival of rod and spherical cells of Arthrobacter crystallopoietes., J. Bacteriol. 103 (1970) 569–577. https://doi.org/10.1128/jb.103.3.569-577.1970.

[169] S.J. Park, Y.M. Park, W.Y. Chun, W.J. Kim, S.Y. Ghim, Calcite-forming bacteria for compressive strength improvement in mortar, J. Microbiol. Biotechnol. 20 (2010) 782–788. https://doi.org/10.4014/jmb.0911.11015.

[170] S.M. Montaño-Salazar, J. Lizarazo-Marriaga, P.F.B. Brandão, Isolation and Potential Biocementation of Calcite Precipitation Inducing Bacteria from Colombian Buildings, Curr. Microbiol. 75 (2018) 256–265. https://doi.org/10.1007/s00284-017-1373-0.

[171] F. Jroundi, P. Gómez-Suaga, C. Jimenez-Lopez, M.T. González-Muñoz, M.A. Fernandez-Vivas, Stone-isolated carbonatogenic bacteria as inoculants in bioconsolidation treatments for historical limestone, Sci. Total Environ. 425 (2012) 89–98. https://doi.org/10.1016/j.scitotenv.2012.02.059.

[172] F.A.O. Camargo, F.M. Bento, B.C. Okeke, W.T. Frankenberger, Hexavalent chromium reduction by an actinomycete, Arthrobacter crystallopoietes ES 32, Biol. Trace Elem. Res. 97 (2004) 183–194. https://doi.org/10.1385/BTER:97:2:183.

[173] A. Vahabi, A.A. Ramezanianpour, H. Sharafi, H.S. Zahiri, H. Vali, K.A. Noghabi, Calcium carbonate precipitation by strain Bacillus licheniformis AK01, newly isolated from loamy soil: A promising alternative for sealing cement-based materials, J. Basic Microbiol. 55 (2015) 105–111. https://doi.org/10.1002/jobm.201300560.

[174] M. Seifan, A.K. Samani, A. Berenjian, Induced calcium carbonate precipitation using Bacillus species, Appl. Microbiol. Biotechnol. 100 (2016) 9895–9906. https://doi.org/10.1007/s00253-016-7701-7.

[175] R. Ramesh, M. Aarthy, M.K. Gowthaman, Screening and production of a potent extracellular Arthrobacter creatinolyticus urease for determination of heavy metal ions, (2014) 285–295. https://doi.org/10.1002/jobm.201200561.

[176] J. Schneider, H. Kaltwasser, I. Stadtwald, Hicroldology, (1984) 355–360.

[177] C.W. Boylen, Survival of Arthrobacter crystallopoietes during prolonged periods of extreme desiccation., J. Bacteriol. 113 (1973) 33–37. https://doi.org/10.1128/jb.113.1.33-37.1973.

[178] F. Heberling, T. Klačić, P. Raiteri, J.D. Gale, P.J. Eng, J.E. Stubbs, T. Gil-Díaz, T. Begović, J. Lützenkirchen, Structure and Surface Complexation at the Calcite(104)-Water Interface, Environ. Sci. Technol. 55 (2021) 12403–12413. https://doi.org/10.1021/acs.est.1c03578.

[179] G.T. Zhou, J.C. Yu, X.C. Wang, L.Z. Zhang, Sonochemical synthesis of aragonite-type calcium carbonate with different morphologies, New J. Chem. 28 (2004) 1027–1031. https://doi.org/10.1039/b315198k.

[180] S. Weiner, P.M. Dove, An Overview of Biomineralization Processes and the Problem of the Vital Effect, Rev. Mineral. Geochemistry. 54 (2003) 1–29.

[181] M.T. González-Muñoz, C. Rodriguez-Navarro, F. Martínez-Ruiz, J.M. Arias, M.L. Merroun, M. Rodriguez-Gallego, Bacterial biomineralization: New insights from Myxococcus-induced mineral precipitation, Geol. Soc. Spec. Publ. 336 (2010) 31–50. https://doi.org/10.1144/SP336.3.

[182] K. Sarayu, N.R. Iyer, A.R. Murthy, Exploration on the biotechnological aspect of the ureolytic bacteria for the production of the cementitious materials - A review, Appl. Biochem. Biotechnol. 172 (2014) 2308–2323. https://doi.org/10.1007/s12010-013-0686-0.

[183] I. Sondi, B. Salopek-Sondi, Influence of the primary structure of enzymes on the formation of CaCO 3 polymorphs: A comparison of plant (Canavalia ensiformis) and bacterial (Bacillus pasteurii) ureases, Langmuir. 21 (2005) 8876–8882. https://doi.org/10.1021/la051129v.

[184] N. Kaur, M.S. Reddy, A. Mukherjee, Biomineralization of calcium carbonate polymorphs by the bacterial strains isolated from calcareous sites, J. Microbiol. Biotechnol. 23 (2013) 707–714. https://doi.org/10.4014/jmb.1212.11087.

[185] B. Lian, Q. Hu, J. Chen, J. Ji, H.H. Teng, Carbonate biomineralization induced by soil bacterium Bacillus megaterium, Geochim. Cosmochim. Acta. 70 (2006) 5522–5535. https://doi.org/10.1016/j.gca.2006.08.044.

[186] Y. Zhang, H.X. Guo, X.H. Cheng, Role of calcium sources in the strength and microstructure of microbial mortar, Constr. Build. Mater. 77 (2015) 160–167. https://doi.org/10.1016/j.conbuildmat.2014.12.040.

[187] Y. Sekiguchi, H. Makita, A. Yamamura, A Thermostable Histamine Oxidase from Arthrobacter crystallopoietes KAIT-B-007, 97 (2004) 104–110.

[188] B. Perito, M. Marvasi, C. Barabesi, G. Mastromei, S. Bracci, M. Vendrell, P. Tiano, A Bacillus subtilis cell fraction (BCF) inducing calcium carbonate precipitation: Biotechnological perspectives for monumental stone reinforcement, J. Cult. Herit. 15 (2014) 345–351. https://doi.org/10.1016/j.culher.2013.10.001.

[189] J. Delgado Rodrigues, A.P. Ferreira Pinto, Stone consolidation by biomineralisation. Contribution for a new conceptual and practical approach to consolidate soft decayed limestones, J. Cult. Herit. 39 (2019) 82–92. https://doi.org/10.1016/j.culher.2019.04.022.

Appendix

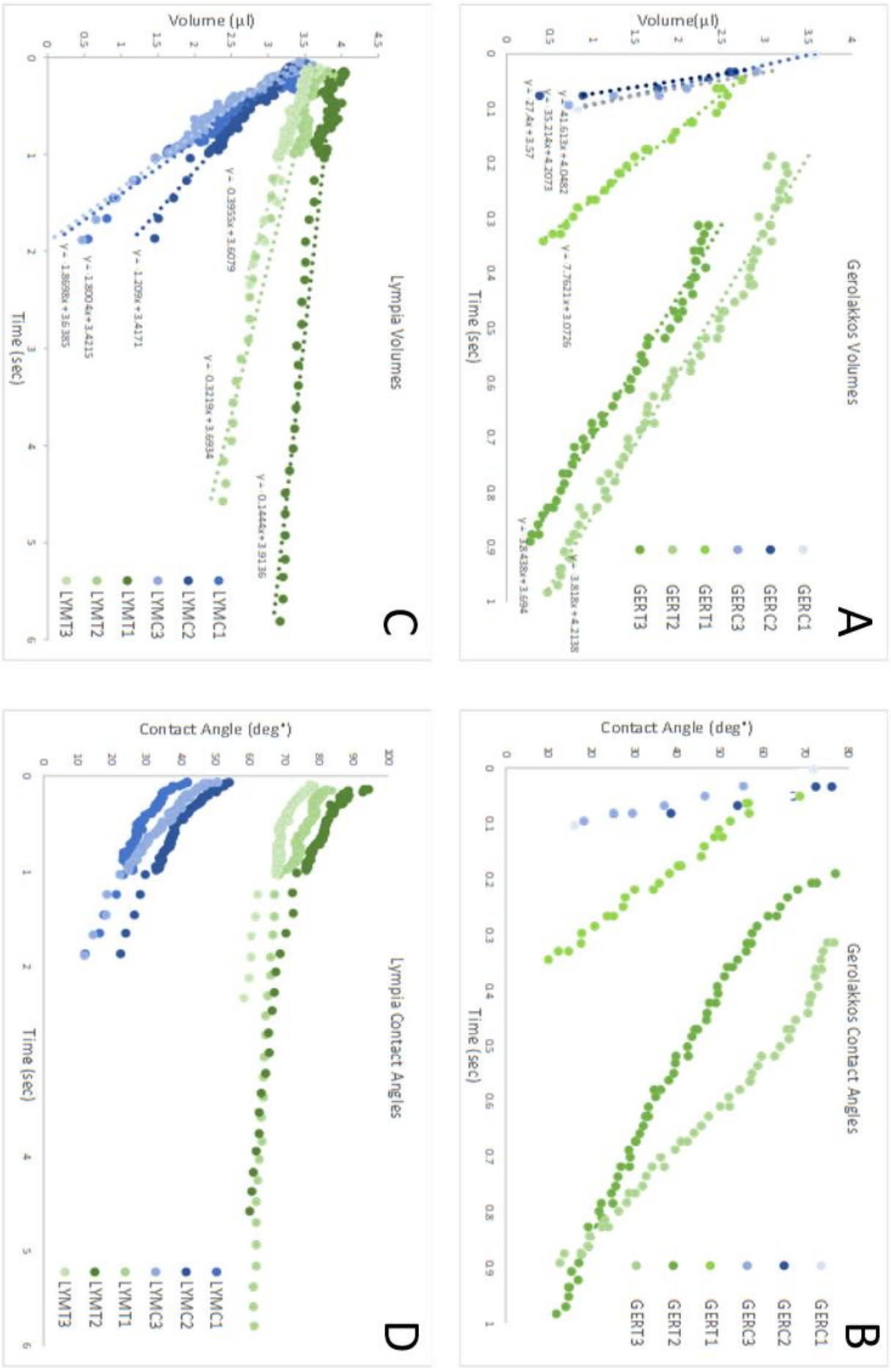

Figure29: Contact angle test results for GER (A, B) and LYM (C, D)

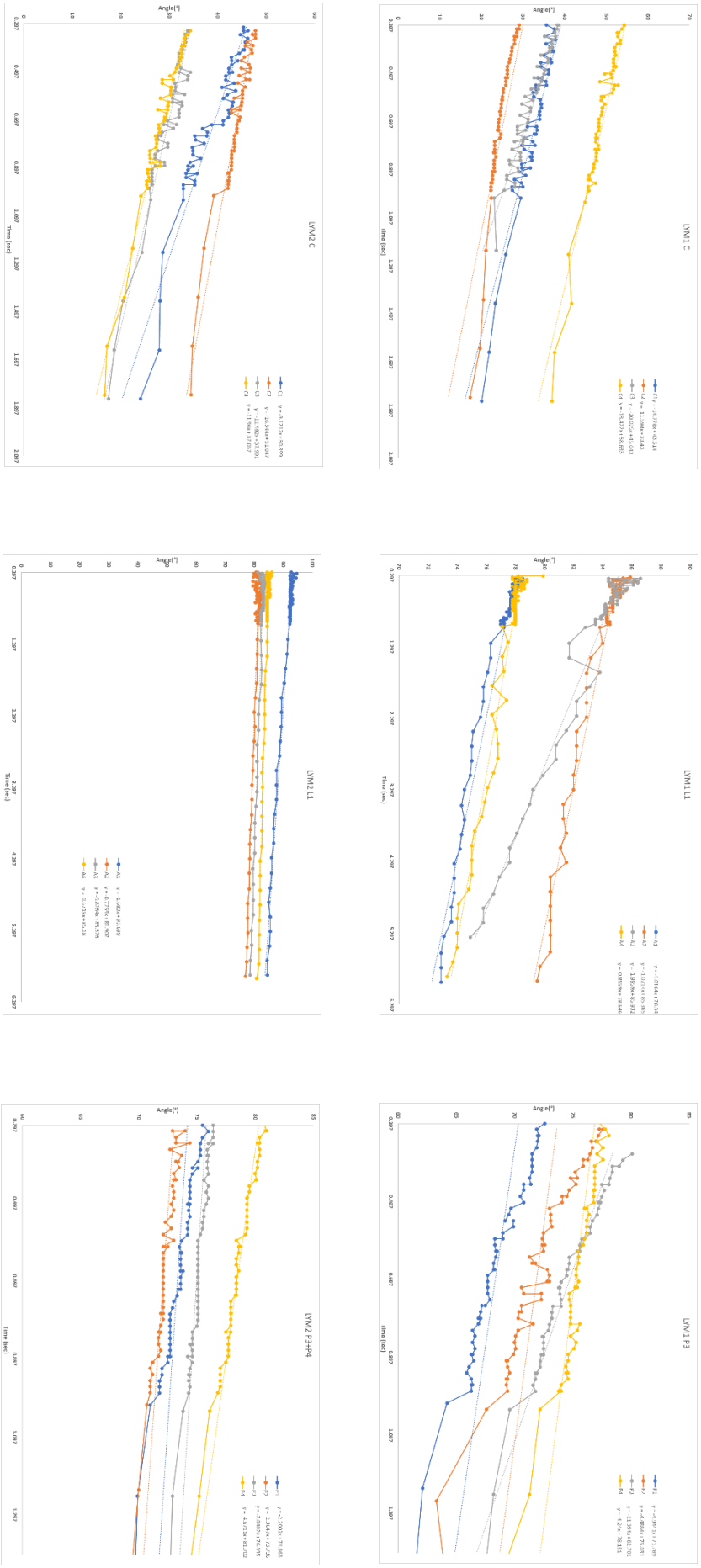

Figure 30: Contact angle test results for GER Specimen 1.2 B4 treatment

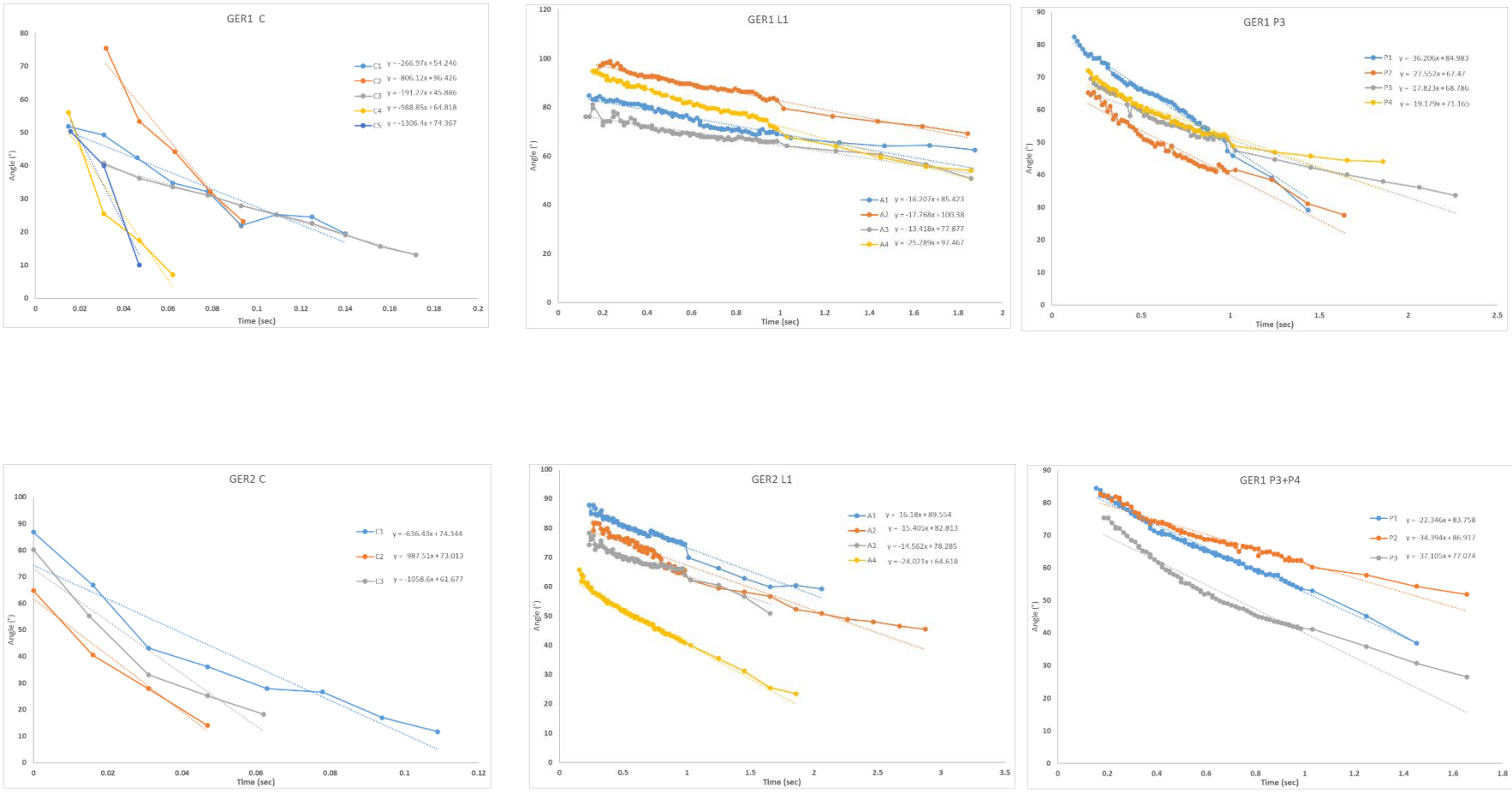

Figure 31: Contact angle test results for LYM Specimen 1,2 B4 treatment

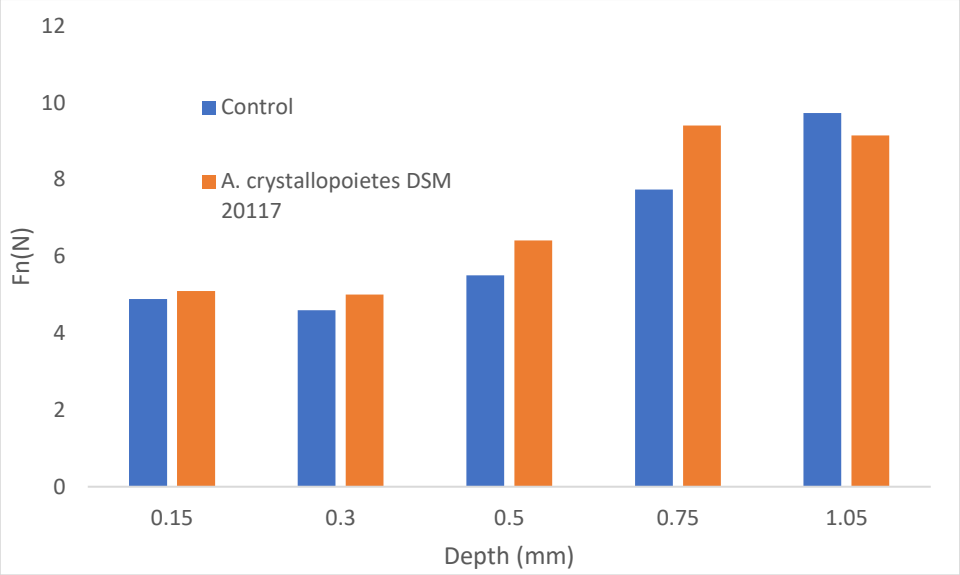

Figure 32: Scratch Test GER Stone Evaluation treatment with CCP medium

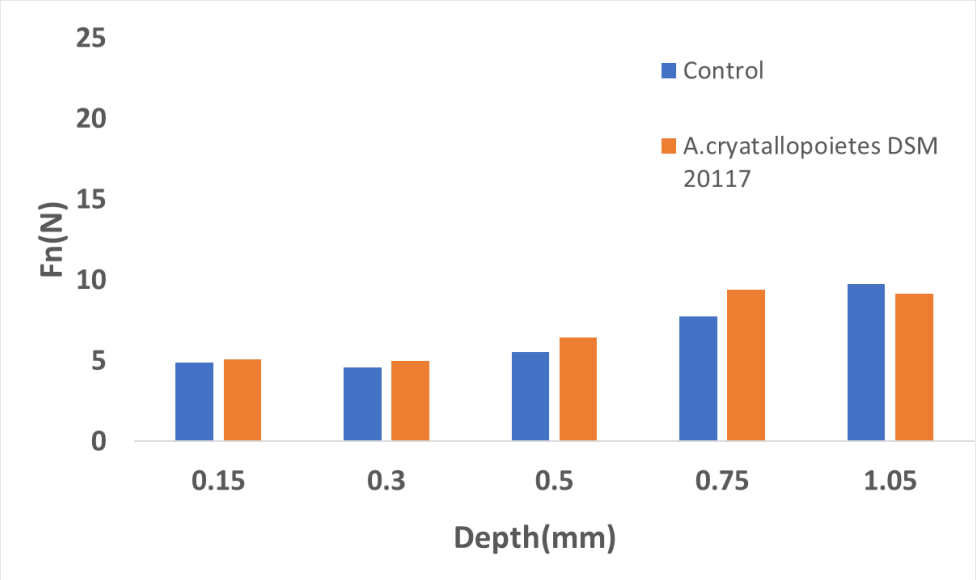

Figure 33: Scratch Test LYM Stone Evaluation treatment with CCP medium

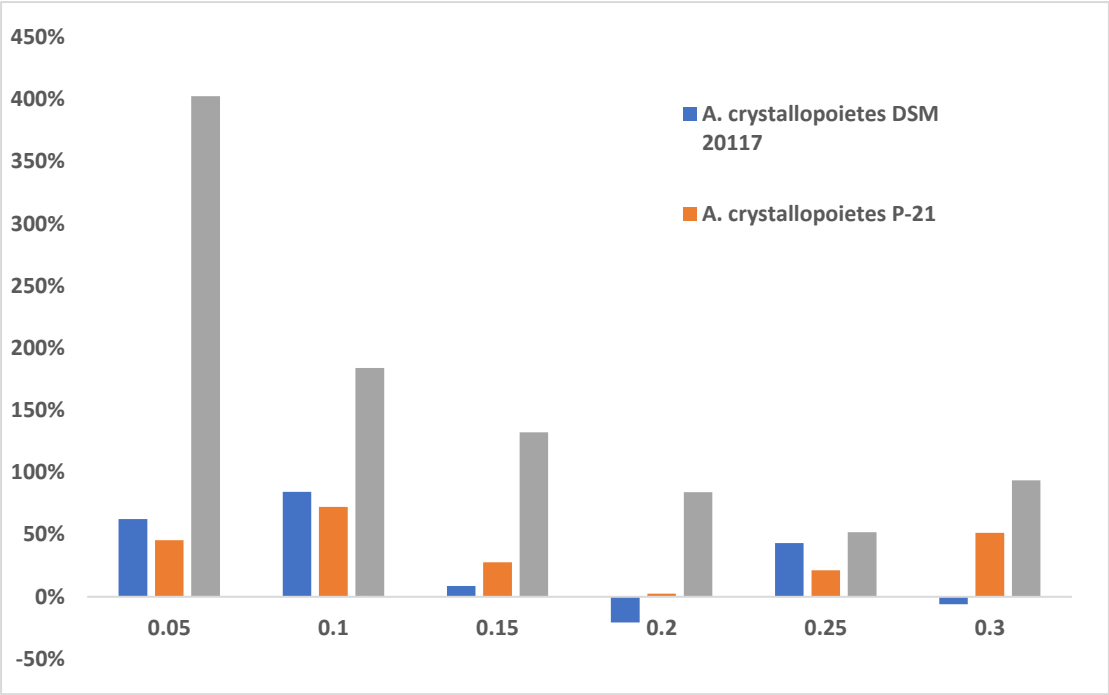

Figure 34: Scratch Test GER Stone Optimization treatment with B4 medium

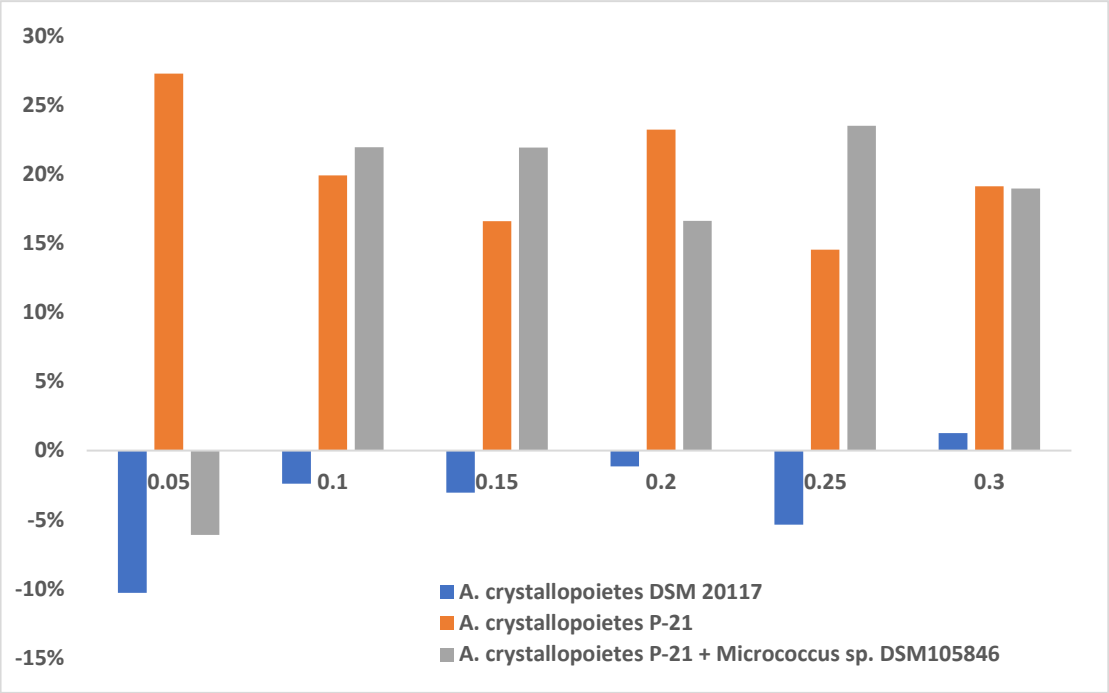

Figure 35: Scratch Test LYM Stone Optimization treatment with B4 medium